A surface-charge model for mudstones and the application to Pore Pressure Prediction

Traugott, Martin Olson

A Surface-Charge Model for Mudstones and the Application to Pore Pressure Prediction

by
Martin Olson Traugott

A thesis submitted in partial fulfilment of the requirements for the degree of Doctor of Philosophy

Department of Geological Sciences

University of Durham

April 2005

Table of Contents

Abstract

New geologic concepts have been developed that illuminate the critical role of bound water in the generation and prediction of overpressures in mudstones. The concept is based on new understanding of the surface-charge effects on water adsorbed on solid surfaces and comes in part from molecular modelling, atomic force measurements, and high-beam neutron diffraction studies reported in the literature.

The picture that is emerging is as follows. Bound water on clay surfaces can support a lithostatic load. The bound water fraction increases with compaction, as free water is expelled, with a concomitant decrease in permeability. Overpressures commence at a threshold depth, the retention depth, where the rate of fluid loss is not sufficient to establish pressure equilibrium with the surface. With deeper burial there is a second threshold depth, a gating depth, where bound water condenses to a high-density phase. Below this gating depth, fluid expansion or other effects are responsible for secondary pressure anomalies.

Knowledge of bound water effects accounts for discrepancies observed in laboratory measurements of mudstone properties. For instance, mercury intrusion and surface-area measurements depend strongly on how much (hygroscopic) bound water has been absorbed or adsorbed on a sample before measurements.

Surface charge effects tend to increase with compaction due, in part, to reduction of iron and beidellitization. A large data set for mudstones is used to show that the fraction of bound water tends to reach a maximum of almost 100 percent at a depth of 2 to 3 km.

An important part of this research is the development of the empirical equation $BW = 0.734\ CEC\ (1-\Phi)/\Phi$, where BW is bound water (fraction of total pore volume), Φ is porosity and CEC is cation-exchange capacity (expressed in meq/gm). Porosity and CEC are borehole derived using resistivity and acoustic methods described here. As an adjunct part of this research a software package (called P3) has been written that puts the concepts and relationships into practice.

Acknowledgements

This work was supported by financial grants from BP and was supervised by Dr. Richard Swarbrick at Durham. I gratefully acknowledge Dr. Swarbrick. He was a key advisor and a critical reviewer, and his experience as coordinator of **Geo**science **P**roject into **O**ver**P**ressure (GeoPoP) enabled him to be a wonderful source of information such as a provider of key publications.

Appreciation is expressed to Professor Arthur Rowe (University of Nottingham) and Dr. Francois Renard (Université Joseph Fourier) for providing key references. A special note of thanks is given to Dr. Anthony Mallon, Professor Roger Searle, Professor Neil Goulty, and Dr. Hugh Powell at Durham. Dr. Mallon collaborated on laboratory tests of bound water procedures developed here. Professor Searle energised this research with his enthusiastic support as department head. Professor Goulty provided a most helpful review of the dimensionless gradient component of this work before publication. And, Dr. Powell helped with questions about clay chemistry and surface effects.

Thanks go too to my brother Dr. William Traugott and his wife Shelby for editorial comments and to my wife Loyce and, son Adam, for tolerating life away from home and country for three years.

Gratitude is given to Jay Patchett for ideas shared on mudstones while we worked as team members 15 years ago at the Amoco Research Centre and thanks to him for publishing a large and unique data set on shales, all incorporated into this work. Appreciation is given to Philip Heppard with whom I shared the role of principal pore pressure specialist for ten years at Amoco. Thanks to Wayne Cox for providing a data set from Canada and to Dr. Peter Flemings (Penn State) and Dr. John Smith (Louisiana State University) for recommending me for this research post.

I acknowledge the efforts of Wolfgang Schollnberger, Jonathan Holt and Mark Alberty at BP. Wolfgang made my educational leave (from BP) possible. Jonathan was instrumental in demonstrating that an incrementally small improvement in pressure-prediction technology would translate into a large cost savings for BP. Mark was a mentor, a colleague, and a facilitator who provided, among other things, a computer.

I also acknowledge Jim Sheeler at Shell (my manager 35 years ago) who insisted that, when writing a report, I take the time to make it short - a point I was mindful of while writing this thesis. Jim liked to quote Mark Twain: “I would have written you a short letter (instead of this long one) but I didn’t have the time”.

I recognize the association and helpful debates with other pore pressure specialists, e.g., Dave Powley, John Bradley, Glenn Bowers, Jamaal Hoesni, Fred Gyllenhammar, and Ernie Onyia. And last, I recognize the ideas and suggestions provided by participants in pressure prediction courses I have given for ChevronTexaco, Veritas, the European Association of Geologists and Engineers, and the Society of Exploration Geophysicists. One participant, Tad Smith, is especially acknowledged for his suggestions that lead to the development of the P3 software.

I also express gratitude to the examiners for their careful and thoughtful criticism: Professor Neil Goulty (Durham) and Professor David Manning (Newcastle).

Declaration

The content of this thesis is the original work of the author (other people's work, where included, is acknowledged by reference). It has not been previously submitted for a degree at this or any other university.

M.O. Traugott
Durham
April 2005

Copyright

Chapter 1: Introduction

It is not uncommon to encounter abnormally high overpressures during oil and gas exploration in sedimentary basins worldwide. Fluid pressure in porous rocks (i.e. pore pressure) can be up to 2.5 times higher than normal hydrostatic pressure (Jones, 1967). This is a serious concern for drilling engineers, who are mindful of the 508 pressure-related blowouts in the Gulf of Mexico (GOM) and Continental Shelf of the United States in the last 40 years (Wojtanowicz et al., 2000). According to Adams and Young (2004) the ten most serious blowouts worldwide resulted in a cost of £3 billion.

Pore pressure prediction is a critical component of exploration risk analysis. It is a critical component for the petroleum geologist who must determine the potential for trapped hydrocarbons, for a given pore pressure, and a critical component for the drilling engineer who must develop a safe drilling plan. But pore pressure predictions are notoriously uncertain and improvements are needed. It has been estimated at BP that a modest improvement in prediction methods would save an estimated £10 million per well in the overpressured regions in the North Sea (J. Holt, personal communication).

As a route to improved pore pressure prediction, this research (funded by BP) examines the surface charge effects on mudstones. It is based on the hypothesis that the thickness of charge-bound water sorbed on clay surfaces is a function of effective stress (Renard and Ortoleva, 1997). It is also based on an idea that bound water reduces the permeability in mudstones, which allows for the entrapment of overpressures.

Key information for this research comes from medical, food, agriculture, and electronic industries. Green and Lu (1995), for example, observed that fluid flow in biological systems is gated on and off by surface charge variations. Toney et al. (1994, 1995) at IBM laboratories observed that bound water in a thin film on a charged surface has a density double that of ordinary water based on X-ray scattering experiments. The IBM work, now verified by Nakamura et al. (2002), leads to evidence for the notion of condensed, immobile bound water in sediments at deep burial depths.

The main conclusion from this research is that the bound water fraction in mudstones increases with compaction, as free water is expelled, with a concomitant decrease in permeability. Overpressures commence at a threshold depth, the retention depth, where the rate of fluid loss is not sufficient to establish pressure equilibrium with the surface. With deeper burial there is sometimes a second threshold depth, a gating

depth, where bound water condenses to a high-density phase. Below this gating depth, fluid expansion, or other effects, are responsible for secondary pressure anomalies.

1.01 Purpose and Scope

The purpose of this research is to examine surface-charge induced bound water in mudstones and to determine the effect on the magnitude of trapped overpressures. A special interest is the way in which bound water fraction affects acoustic and resistivity derived pore pressure prediction methods. An adjunct aim is the development of software for testing and for putting the developed concepts to practice. An important component is the development of simple procedures for determining bound water content from wellbore data.

The scope includes an investigation of bound water data from the biomedical, soil mechanics, food, sanitation, agricultural, physics, chemistry, petrophysical, and electrical engineering industries. These data include molecular modelling of sorbed water (Spohr, 2002), atomic force microscopy on thin water films (Teschke et al., 2002), and high beam neutron diffraction on interlayer water in clays (Skipper et al., 2000). The scope does not include a description of the effect of lateral pressure transfer or hydrocarbon buoyancy on pore pressure. It does include a discussion of the uncertainties in measurement of mudstone properties that directly affect predictions.

1.02 Background Information

Methods for predicting pore pressure in the subsurface have been known for a long time. Ham (1966a) defined a depth of sealing (retention depth) below which pore pressure increases linearly at a rate of 22.6 kPa/m (1psi/ft). Eaton (1976) developed a seismic-derived method that relates pressure gradient to $(V/V_n)^3$ where V is interval velocity, V_n is velocity for normal hydrostatic pressure and 3 is an empirical coefficient with unknown physical meaning. Bredehoeft and Hanshaw (1968) developed basin model methods that relate the magnitude of overpressures to sediment burial rate and sediment permeability.

But the methods have not been applied without problems. There is a depth in some basins below which the Ham, Eaton and basin model methods grossly underestimate pore pressure. Bowers (2001) worked this underestimation problem and patented an unloading solution. Scott and Thomsen (1993) proposed and patented an irreversible compaction model that also potentially corrects for underestimation. But

both have been debated and neither offer workable or stable solutions. Basin model pressure prediction methods avoid the problem but require difficult-to-obtain knowledge of mudstone permeability. Carstens and Dypvik (1981) and Teige et al. (1999) articulated clearly the problems associated with conventional pore pressure prediction methods. Lahann et al. (2001) linked the problems to a clay diagenetic effect, pointing more to issues that are discussed here.

1.03 Units

SI units are used throughout, but nanodarcy (nD) and gram per cubic centimetre (g/cc) are retained as practical units for permeability and density. Two useful conversions are: 1 nD = 0.9869 x 10^{-21} m^2; and 1 g/cc = 1000 $kg/m^{3.}$ The adoption of SI leads to unfamiliar units for length, i.e., the nanometre (nm) where 1 nm is 10^{-9} metres (10 ångströms). In addition, drilling fluid density (mud weight) is expressed as either dimensionless specific gravity (SG) or pounds per gallon (lbs/gal) where 1 SG equals 8.335 lbs/gal.

1.04 Terminology and Key Definitions

Terms that might be ambiguous or obscure to the reader are described below. To build context for what follows, the items are listed in logical order, not alphabetical. Note that in this text the terms mudstone and shale are used interchangeably. Also note that the general term sorption (or sorbed) is used to describe the hydrophilic gathering of water on a solid surface by either absorption or adsorption, or a combination of the two.

Mudstone is a compacted clay-silica rich sediment with large surface area. A key mudstone property is a high negative surface charge that occurs because of isomorphic substitution in the clay crystal structure, or hydroxyl dissociation on silica surfaces. A fully charged surface is about two electron charges per nm^2 for clay (Israelachvili, 1991) and 4.7 electron charges per nm^2 for silica surfaces (Meziani et al., 2001).

Counter-Ions are cations (usually sodium) that attach to the charged surfaces and provide electrical neutrality. There is one positive cation per negative charge site (Giese and Oss, 2002). The concentration of the counter-ion layer that condenses on clay and silica surfaces is between 7 and 25 molar (Porter and Zinn, 1993; Bolt, 1956), i.e., up to 50 times higher than cation concentration in sea water. Skipper, Soper, and McConnell

(1991) examined the cation layer in clays using neutron diffraction and found 2 to 5 water molecules per counter-ion.

Cation-Exchange Capacity (CEC) is the number of counter-ions per gram of dry sediment expressed in milliequivalents (meq) where 1 meq is 6.02×10^{20} ions. It will be seen in Chapter 2 that CEC measurement is a core part of mudstone and soil analysis. It is important to note that CEC is often reported as meq/100 g in the literature.

Water Content (W) is the weight of water per gram of dry sample. W is directly related to pore space: e.g., porosity equals $W\rho_{grain}/(1+W\rho_{grain})$ where ρ_{grain} is grain density. As a reference, porosity is 0.395 (39.5 percent) if W is 0.24 g/g and ρ_{grain} is 2.72 g/cc, typical values for clays. Note that the relation is for 100 percent water saturation with a specific gravity of 1.0. Also note that W is often reported as g/100 grams (a convention avoided in this document).

Hydrogen Bonding (H-bond) is the atomic bonding that forms the open tetrahedral structure of water and ice (Franks, 1975). The specific gravity of water would be 1.84 (1.84 times more dense) if no hydrogen bonding existed (Mitchell, 1993). One or two layers of water are H-bonded to clay and silica surface with some of the hydrogen interpenetrating the clay surface (Skipper et al., 2000). The definition of H-bonding is an inter-oxygen distance less than 0.35 nm and a O-HO angle less than 30° (Hensen et al., 2001). There are suggestions that H-bonds are broken at elevated temperature at great burial depths (Uffindell et al., 2000)

Anion exclusion describes the phenomenon that, when dry crushed sediment containing clay is mixed in a saltwater solution, the chlorides content of the solution increases. The increase in salinity is due to the repulsion of anions from the vicinity of charged surfaces (Schofield, 1947). As will be seen later, Hill et al. (1979) used anion exclusion measurements to calculate the weight of bound water on clay rich sandstones.

Bound Water (BW) is a term coined in 1940 (cited in Palmer et al., 1952) to describe immobile water that is attached to charged solid surfaces. To follow common practice, bound water is defined as the anion-free volume (Juhasz, 1979; Truman, et al., 1989) as illustrated in Figure 1.1. It does not include the diffuse zone noted in the

primitive double-layer model (Tang et al., 1992). The thickness of the bound water layer is about 1 nm (Bocker et al., 1966) and represents a pore space of about 14 percent for a mudstone with a surface area of 100 m^2/g. Bound water is used interchangeably in the literature with hygroscopic water or water of absorption or adsorption, or more accurately, as water of sorption. Bound water is a 2-dimensional, layered structure as illustrated Figure 1.2.

Suction (hygroscopic suction) expresses how strongly water sorbs on dry samples (Cui et al., 2002). Suction measurements are simple. A dry sample is put in a desiccator (a vessel with a lid) on a tray above a solution of a given compound, e.g., a saturated sodium bromide solution. According to the vapour-pressure properties of the solution, a given relative humidity is imposed within the desiccator. After equilibrium (which may take days), water content (W) is determined by gravimetric methods using a simple balance. Figure 1.3 shows an example for a clay sample from Delage et al. (1998). The data in Figure 1.3, if extrapolated to zero water content, give a value of about 1000 MPa (145,000 psi). It can be argued that it would require a stress of about 1000 MPa to remove all bound water from this sample.

Free Water describes the mobile fraction of water in pores. It includes the diffuse layer, which can have a thickness of 60 nm as measured with atomic force apparatus (de Souza et al., 2001). Free water has a suppressed freezing temperature, the magnitude of which is related to pore size (Overloop and Van Gerven, 1993). Except for a suppressed freezing point, free water in confined pores has the same properties as bulk water.

C_o-C_w refers to a laboratory technique for calculating the electrical conductivity of bound water. Bulk conductivity (C_o) is measured on a saturated sample at several different values of water conductivity (C_w). The data are plotted and extrapolated to zero C_w to give bound water conductivity as illustrated in Figure 1.4. The data are used later to infer that only bound water remains at deep burial depths.

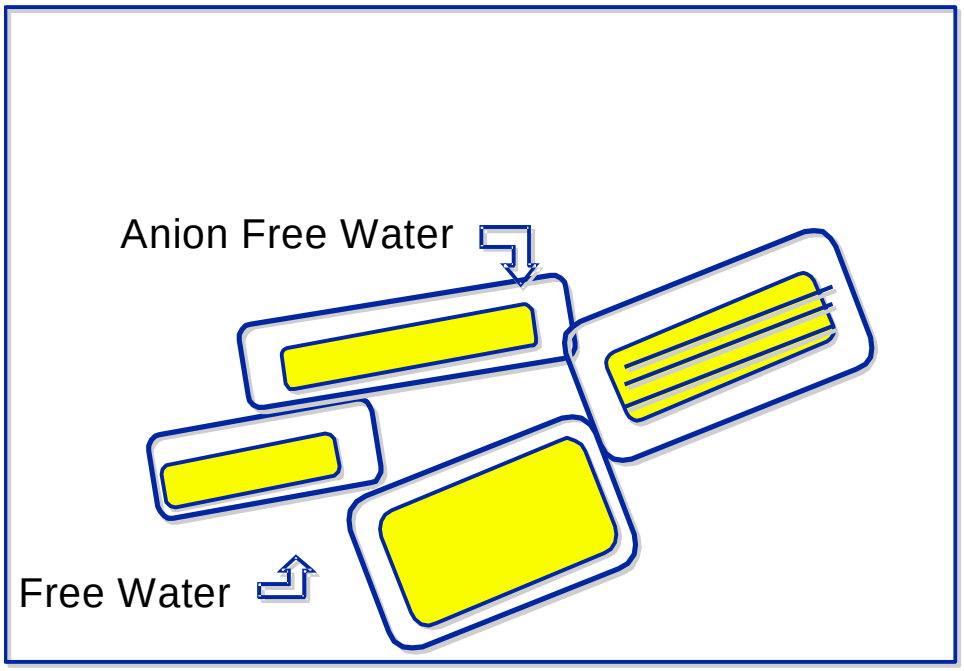

Figure 1.1: A cartoon picture of bound water in which bound water is defined by the anion free volume around rock grains. Grains (solid squares) are supported by a thin-film of bound water.

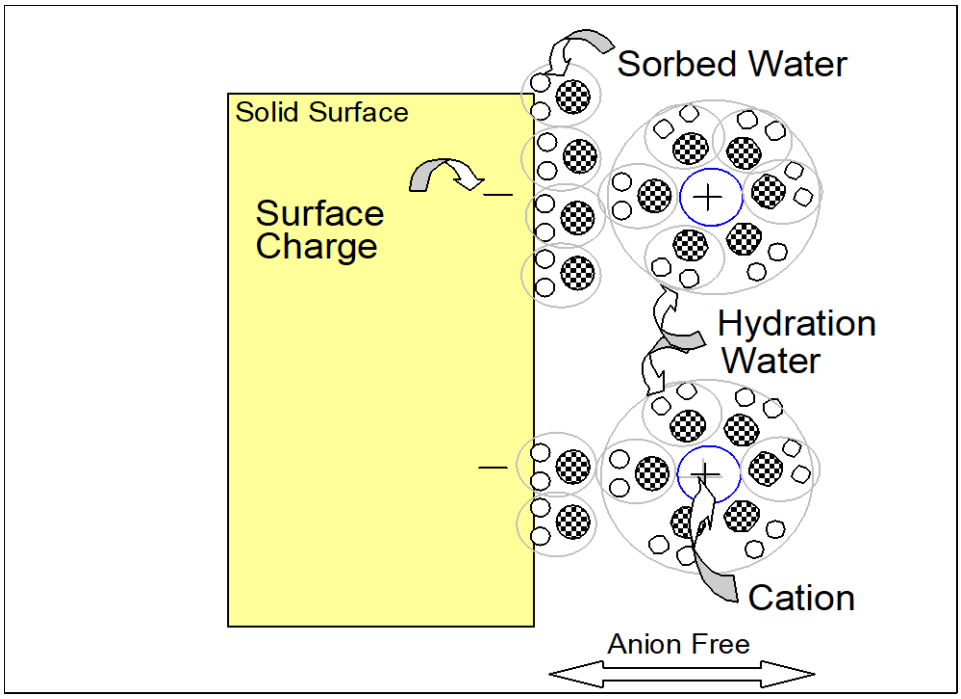

Figure 1.2: A schematic of bound water (modified from Clavier et al., 1984). The small open circles are hydrogen atoms of the water molecule. The larger (checker) circles are oxygen atoms and the two large circles are sodium cations. The sorbed layer is H-bonded to the solid surface.

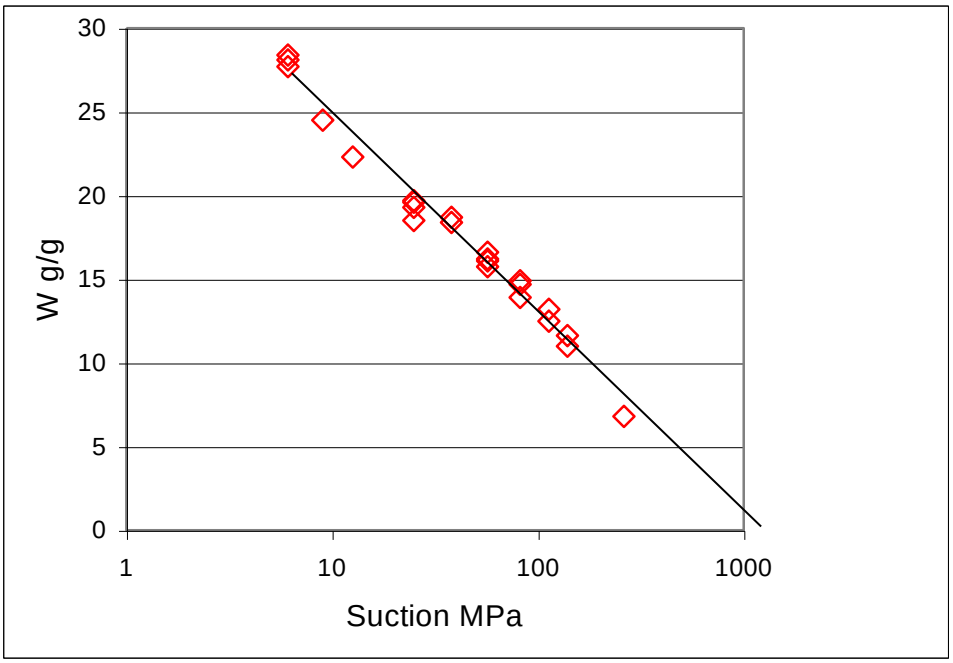

Figure 1.3: Water content data for a clay sample measured at 10 different relative humidity values, i.e., at ten different suctions. Data are from Delage et al. (1998).

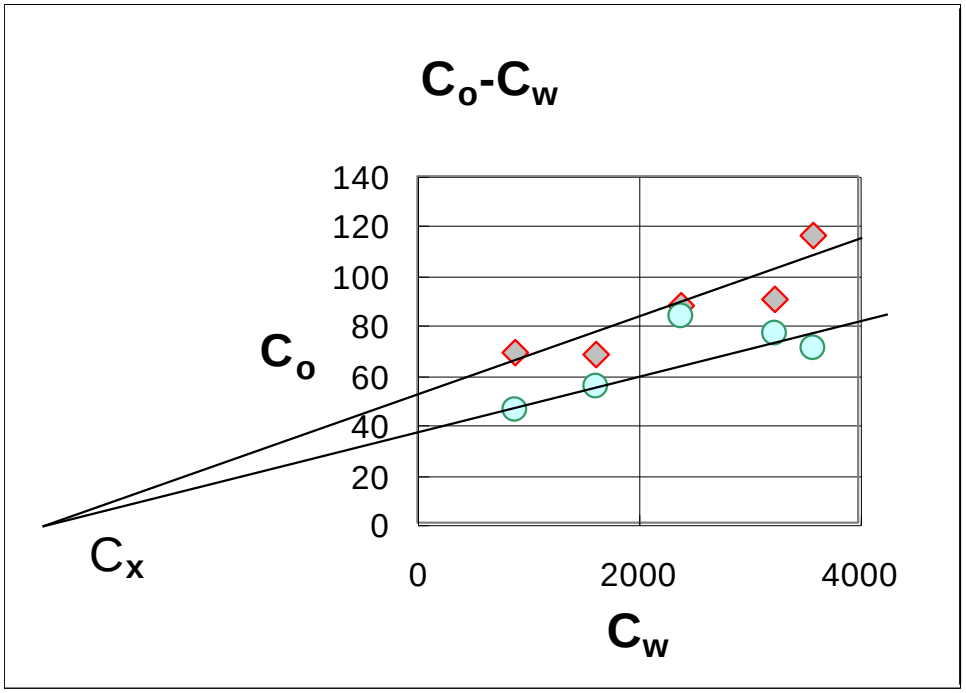

Figure 1.4: Bulk rock conductivity (C_o) versus pore water conductivity (C_w) for two mudstone samples (from Katsube et al., 1996). The intercept on the ordinate is bound water conductivity. The intercept on the abscissa (C_x) is a function of CEC.

Dielectric Constant (ε) is an inverse measure of the electrostatic force between electric charges, e.g., the electrostatic attraction between the ions of a crystal of sodium chloride placed in water (ε=80) is only 1/80 as strong as that in air (ε=1) (Pauling, 1953). The dielectric constant of free water is about 80 at 20 °C and varies with temperature in accordance with Curie's law (Brady, 1979) and salinity (Wang and Anderko, 2001). The dielectric constant of bound water, in contrast, is about 4 (Robinson et al., 2002), and is temperature independent (Booth, 1951; Hill et al., 1969). General thermodynamics principles dictate that cations move from regions of low dielectric constant to regions of high dielectric constant (from references cited in Zhmud et al., 1997). It is important not to confuse dynamic-derived dielectric values with static values. The two can be very different: e.g., Carrier and Soga (1999) showed that the static and dynamic value for 0.1 molar saltwater is 80 and $5x10^4$, respectively, as measured with a capacitance probe at a frequency of 1000 hertz. As a reference, Carrier and Soga (1999) suggested that the large reported values for relative permittivity (i.e., ε) are an artefact of polarization effects. It is generally believed that time-domain reflectometry (TDR) accurately measures static dielectric constant in soils and clays (Robinson et al., 2002).

Electric Field (E) is a potential field generated by surface charge (σ). From Coulomb's equation, $E=\sigma/(\varepsilon\varepsilon_o)$ where ε_o is the permittivity of free space (Israelachvili, 1991). Israelachvili (1991) computed a typical value for E in clays of 4.2×10^8 volts/m. Lockhart and Kim (1992) made direct measurement of E on protein surfaces using the Stark effect and found values similar to that reported for clays. Du et al. (1994) suggested that a silica surface could produce an electric field of up to 10^9 volts/m. The electrostatic energy density (P) in Pascals generated by an electric field is expressed by the standard textbook equation $P=E^2 \varepsilon\varepsilon_o/2$ (Coelho, 1979). For typical clays, P is about 500 MPa (80,000 psi) (van Olphen, 1963).

Molecular Simulation is a relatively new technology for studying surface chemistry at the atomic level. Simulation results will be cited from the literature that relate to the density and structure of bound water, e.g., Skipper, Chang and Sposito (1995). Of the different types, Monte Carlo (MC) simulators are the most simple. Force and trajectory of all particles in the MC simulation cell are moved randomly millions of times until the chemical energy stays constant. Molecular dynamic (MD) type simulators are more complex, better account for the trajectories of each particle, and are

less problematic. Bleam (1993) compared models for a phyllosilicate model and found that simulator results depend on boundary conditions and that determination of water density is problematic. According to Warne et al. (2000), most simulators keep the clay structure rigid, or allow unrealistic movements of Al and Si atoms at the clay surface. Hensen et al. (2001) reported that modified methods, called biased models, better handle the water density problem.

Surface Forces Apparatus (SFA) is a laboratory method for directly measuring forces at molecular scale (Fröberg et al. 1999). One method developed by Israelachvili et al. (1990) measures force in fluid confined between two crossed mica cylinders. Another method measures force between silica sheets (Horn et al., 1998). The results confirm a bound water structure consistent with simulation and neutron diffraction results. The SFA methods do not come without uncertainties. Schulz and Warr (2000) suggested that SFA data have to be used with discretion because mica has an anomalously high surface charge. As an important observation, the surface charge of mica approaches that of mudstones at what will be defined here as the gating depth.

Effective Stress (σ') is a term that depends on the context. In the context of laboratory tests, effective stress is confining pressure (usually isotropic) minus pore pressure. In the context of pore pressure prediction, effective stress is lithostatic stress minus pore pressure, unless it is defined explicitly as mean effective stress, in which case it is the average of the three principal stresses minus pore pressure.

1.05 Data

The literature is rich in mudstone data pertinent to this research. Patchett (1975) published 137 measurements of CEC and specific surface area (SSA) on mudstone samples at a wide range of depths in several different geological settings and included borehole-derived acoustic slowness (inverse velocity), formation temperature, and borehole-derived electrical resistivity for each sample. Katsube et al. (1996) published laboratory-derived resistivity and porosity information on two shale samples where effective stress was varied from 2 to 50 MPa. They also presented C_o-C_w plots on two companion samples. Waxman and Smits (1968) listed raw data on C_o-C_w, porosity and permeability for a large shaly sand data set from Shell. Goode et al. (1995) published a similar set. Henry (1997) tabulated data on shales from the deep water JOIDES project.

Thompson et al. (1977) tabulated (in an obscure report) permeability and water content on three shale samples taken below seafloor at locations with different water depths. To the knowledge of this author it is the most pristine data set available since the samples never dried and since all permeability measurements were with seawater. Much of the raw data cited here are presented on an attached CD. In addition, a large data set from BP was available and contained borehole data on about 500 wells in 30 basins worldwide (compiled by the author when working as principal pore analyst at BP). And mudstone data were also available from the **Geo**science **P**roject into **O**ver**P**ressure (GeoPoP). No interpretations from the BP or GeoPoP data, however, are included in this thesis. Both are confidential and were used strictly as a practice set to test concepts developed here.

1.06 Synopsis

This thesis is intentionally concise. Chapter 1 is this introduction. Chapter 2 describes pertinent mudstone properties and introduces a petrophysical method for determining cation exchange capacity from borehole data. Chapter 3 lists what is known about bound water and focuses on those properties that are different from those of ordinary water. Chapter 4 is a comprehensive discussion of methods for determining bound water volume and represents (to the author's knowledge) the first comparison of many of the methods. Chapter 5 outlines comments that lead to a new gating depth concept. Chapter 6 focuses on the application to pore pressure prediction in which a new gradient standard is introduced and where the Eaton equation is derived explicitly for the first time. This chapter also describes software developed for testing and putting into practice the procedures set out here. Chapter 7 contains a discussion of core issues in this thesis. This chapter also lists the main conclusions and sets out recommendations, e.g., simple hygroscopic methods for determining bound water volume.

Chapter 2: Mudstone Properties

The following is a summary of mudstone properties that are relevant to this research. Some of the properties such as velocity and conductivity are important to pore pressure prediction and others, such as porosity and cation exchange capacity, are important to bound water calculations. Each section lists typical values and sets out a description of procedures for measuring the property.

2.01 Pore Size

The average pore radius is typically less than 10 nm in tight mudstone (Katsube, 1993); e.g., the range reported in the Scotian area of Canada is 3 to 14 nm, with pore size decreasing with depth (Best and Katsube, 1995). As a frame of reference, the size of a hydrated sodium ion is 0.78 nm (Lambe and Whitman, 1979).

Common methods for deriving pore size are mercury intrusion porosimeters such as the Micromeritics Autopore 9200 (Katsube and Issler, 1993) or the Quantachrome Autoscan 60 (Schlömer and Krooss, 1997). Most porosimeters are limited to an operational pressure of 400 MPa which limits pore size resolution to about 3 nm. It should be noted that the derived pore size is the radius of the connecting pores (pore throats) - i.e., mercury porosimeters tend to underestimate true pore size (Tiab and Donaldson, 1976).

Sample preparation requires that the samples be heated to 105° C to remove bound water. If sample preparation has not removed bound water, mercury penetration is limited to pore volume defined by effective porosity. It must be noted that mercury intrusion is a destructive process and results in irreversible damage to the sample. Otherwise, it would be greatly illuminating to measure mercury intrusion volumes on the same sample before and after drying at 105° C.

Another method for deriving pore size is the differential scanning calorimeter (DSC) method based on freezing point suppression, in which the magnitude of suppression is an inverse function of pore radius in accordance with Kelvin's law (Antoniou, 1964; Letellier, 1998; Courivaud et al., 2000). To test this method, data have been collected here from Ishikiriyama and Todoki (1995b) and Schmidt et al. (1995) and statistically evaluated using Minitab software. The resultant equation follows:

$$R\ (nm) = 0.627 + 28/\Delta T \qquad N=10,\ R^2=0.98 \qquad [2.01]$$

where R is pore radius and ΔT is freezing point suppression in degrees Celsius. Letellier (1998) cites a similar relationship.

As an example, Figure 2.1 shows a representative DSC trace for a Na-vermiculite sample from Bergman et al. (2000) that has a freezing-point suppression of 40 °C. This translates to a pore radius of 1.33 nm from Equation 2.01. The upper detection limit for DSC method is about 30 nm, based on an uncertainty in the measurement.

In theory, the intercept in the equation (i.e., 0.627) is the thickness of bound water as discussed by Ishikiriyama and Todoki (1995a). The volume (of bound water) that a thickness of 0.67 nm represents is of interest. From simple geometry, 0.627 nm represents a bound water volume of 72 percent of the total pore volume for a pore size of 1.33 nm, assuming a cylindrical pore (the same assumption as used with mercury intrusion pore size calculations). This value (i.e., 72 percent) compares to 76 percent computed from the area under the endothermic peak on the DSC data as reported by Bergman and Swenson (2000).

It is recommended here that calorimetric analysis become a more common practice for analysis of mudstones: currently there has been limited application. Other experimental methods for determining pore size, not discussed, are nuclear magnetic resonance (Schmidt et al., 1995), positron annihilation lifetime spectroscopy (Liu and Yao, 2001), and nitrogen adsorption (Dollimore and Heal, 1964).

2.02 Acoustic Velocity (Inverse Slowness)

Interval velocity (V) varies from 1500 to 5000 m/s for sandstones and mudstones as a linear function of porosity (Eberhart-Phillips et al., 1989). Johnston (1987) reported a 6 to 10 percent increase in velocity in mudstones for 55 MPa (8000 psi) change in effective stress, but all the change was accounted for by a concomitant 10 percent decrease in porosity. Holt et al. (1997) reported laboratory results on soft high porosity mudstones that showed almost no dependence on effective stress. A notion that emerges is that velocity in mudstones is affected most by pore volume and the compliant nature of the bound water layer that separates grains, and that any apparent sensitivity to effective stress in laboratory samples is the result of a change in porosity as effective stress varies.

Velocity information can be borehole, seismic or laboratory derived. Borehole-derived acoustic data are generally accurate and represent a baseline for vertical velocity.

Laboratory-derived velocity data are less accurate and are affected by coupling and coring induced artefacts. According to Vernik (1998), 40 MPa effective stress is required to close coring induced cracks and to generate good acoustic coupling between a transducer and a sample.

Seismic-derived interval velocity data are affected by the complexity of the geology. Kan and Swan (2001) suggest an accuracy of about 10 percent for conventional processing. Ray-tracing or pre-stack processed data are better (Peng, 2001; Littleton et al. 2002; de Franco, 2001). Accuracy is also a function of the illumination angle, which decreases with depth. A common quality-control guideline is to accept interval velocity data to a depth equal to one cable length (offset from source to receiver).

A problem with velocity data is anisotropy. Acoustic velocity parallel to the sedimentary bedding plane is faster than that normal to bedding (Vernik and Liu, 1997). In practice, seismic-derived velocities are corrected for anisotropy before application to pore pressure prediction. Based on the experience of D.A Herron at BP (personal communication), the P3 software developed for this thesis takes seismic-derived interval velocity as vertical at the seafloor (i.e., normal to bedding and no correction) and adjusts it linearly with depth to a maximum correction of 0.94 at a depth of 1000 m below seafloor and deeper. This is consistent with the understanding that seismic-derived interval velocity is a measure of horizontal velocity (Alkhalifah and Tsvankin, 1995).

2.03 Electrical Conductivity (Inverse Resistivity)

Conductivity, C, in tight mudstones varies between 30 and 3000 mS/m as a function of the second power of porosity (Waxman and Smits, 1968; Clavier et al., 1984). Conductivities also vary with variation in CEC, temperature, water saturation, and effective stress (Johnston, 1987; Katsube et al., 1996; Gomaa et al., 2001).

Borehole-derived conductivity data are extremely accurate but, if questionable, can be checked with the method set out by Traugott (1982). Laboratory data are reasonably accurate if recorded with a four-electrode system (Glover et al., 1994) and if electrode polarization effects are monitored.

A major component of electrical conductivity in mudstones is conductivity of the bound water layer. Katsube et al., (1996) measured surface-conduction on two tight mudstone samples using C_o-C_w procedures. They also measured bulk conductivity, and porosity, in steps, while increasing effective stress from 3 to 50 MPa. Those are plotted in Figure 2.2 to show that, with increasing effective stress, conductivity converges to the

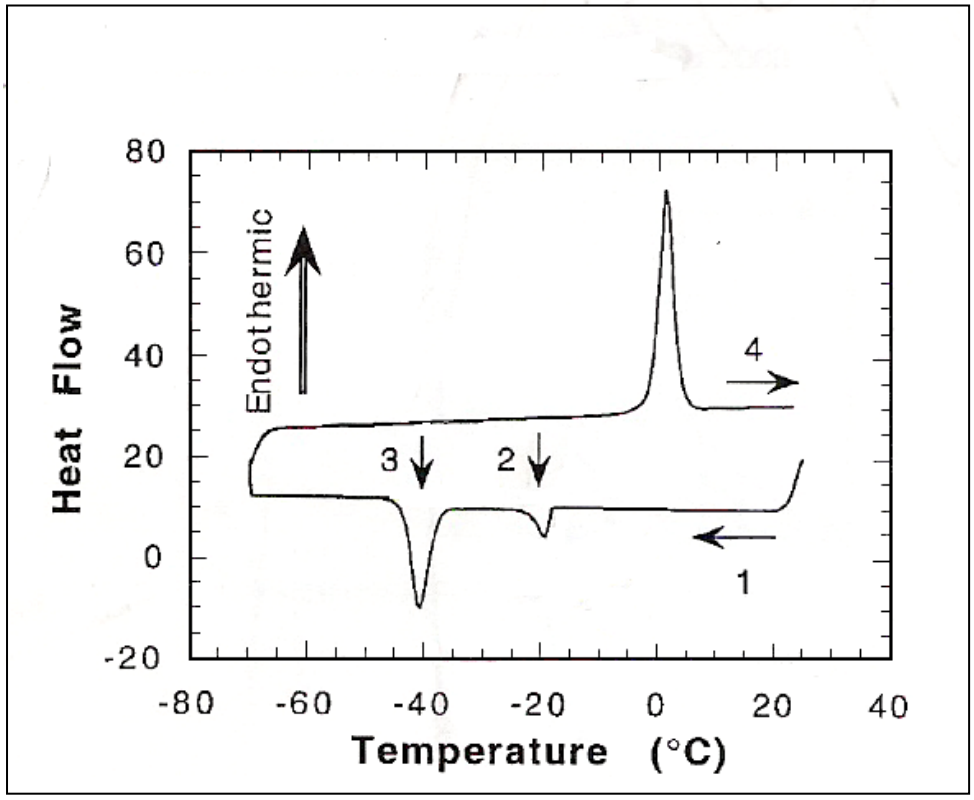

Figure 2.1: A typical DSC plot on Na-vermiculite from Bergman et al. (2000). The peak at (2) is a surface effect that disappears when the sample is dried with a paper towel. The peak at 3 represents freezing of non-bound water.

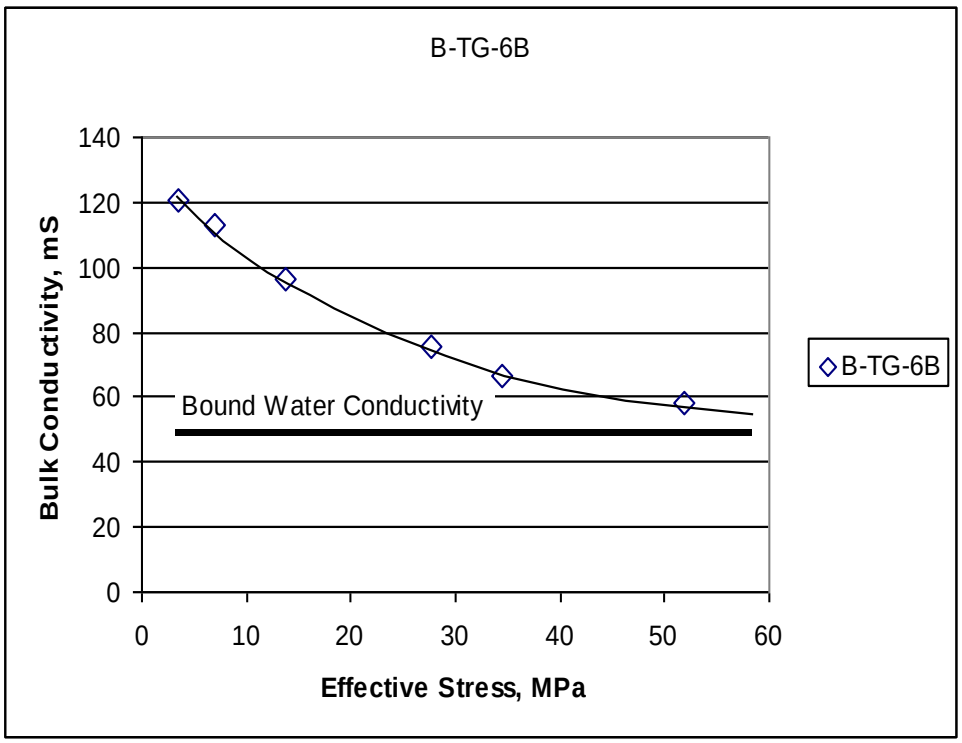

Figure 2.2: Conductivity versus effective stress for a mudstone sample (Katsube et al., 1996). Bound water conductivity is from C_o-C_w data from the same reference.

bound water value. This observation is evidence that borehole resistivity sensors are responding predominately to bound water volume when effective stress is large, i.e., if depth is greater than a few kilometres, and fluid pressure is near hydrostatic. It will be proposed later that there is a strong link between conductivity and effective stress.

As a point of interest, Katsube et al. (1996) subtracted surface conductivity from measured values and presented the results as true formation resistivity. This practice has not been helpful to the understanding of the bound water component of conductivity.

2.04 Bulk Density

Bulk density varies from 1.9 to 2.7 g/cc as a linear function of porosity, grain density and fluid density in mudstones. Bulk density data are obtained in boreholes with a gamma-gamma device that measures electron density (Tittman, 1965). Bulk density is computed assuming the ratio of atomic number (Z) to atomic weight (A) is 0.5. This is problematic for measurements in salt that has a Z/A ratio less than 0.5, e.g., density logs record a value of 2.07 g/cc in bedded salt compared to a true value of 2.16 g/cc. It may also be a problem for the condensed zone in the bound water layer that contains a concentrated layer of sodium cations.

Determination of porosity using density logs requires knowledge of grain density. According to Hansen (1996) grain density is 2.742 g/cc for North Sea shales based on a collection of laboratory measurements. This compares to a value of 2.706 g/cc for eleven samples from Yang and Aplin (1998). In this thesis a global value of 2.72 g/cc is used for mudstone.

For the variation in grain density observed by Yang and Aplin (1998), i.e., 2.53 to 2.82 g/cc, the error generated by assuming a constant value of 2.72 g/cc is small when applied to the calculation of bound water. As demonstrated by Henry (1997), the large variation reported in grain density reflects to a great extent the uncertainty in the laboratory methods. Henry (1997) builds a case for the use of a constant global value and shows that the resulting error is small (about 5 percent error).

2.05 Total Porosity

Total porosity ranges from 1 to 40 percent in tight mudstones and varies as a function of the consolidation stresses. Porosity is often assumed to decrease exponentially with depth. A better approximation may be a sigmoid shaped Fermi function introduced by Thompson et al. (1977).

Equations for relating fractional porosity (Φ) to interval velocity, bulk density, and water content are listed next. Equation 2.02 relates Φ to seismic or borehole derived interval velocity (V) where V_{ma} in the equation is matrix velocity and 2.19 is an empirical exponent developed for areas in Canada (Issler, 1992):

$$\Phi = 1 - (V/V_{ma})^{1/2.19.} \quad [2.02]$$

Stump and Flemings (2002) independently verified the 2.19 exponent for mudstones in the Gulf of Mexico. Hansen (1996) derived an exponent of 2.17 for the Norwegian shelf. Regardless of the common usage, there are issues with this equation that will be discussed in Chapter 7.

Equation 2.03 is a standard textbook equation (Dewan 1983) that relates Φ to borehole-derived bulk density, ρ, grain density, ρ_{grain}, and fluid density, ρ_{fluid}. The equation is based on a linear mixing law given in Equation 2.04.

$$\Phi = (\rho-\rho_{ma})/(\rho_{fluid}-\rho_{grain}) \quad [2.03]$$

$$\rho=\Phi\rho_{fluid}+(1-\Phi)\rho_{grain}. \quad [2.04]$$

An issue with application of this relationship is bulk density of the bound water, which will be discussed. The next equation is another standard equation that relates Φ to water content (Lambe and Whitman, 1979).

$$\Phi = W\cdot\rho_{grain}/(1+W\rho_{grain}) \quad [2.05]$$

Water content, W, is determined gravimetrically by $(M_{wet}-M_{dry})/M_{dry}$ where M_{wet} is mass of the sample saturated with water and M_{dry} is mass after heating to 105°C. This procedure is called immersion porosimetry.

Other laboratory methods for determining porosity are helium porosimetry, mercury intrusion, nuclear magnetic resonance (Martinez and Davis, 2000), and gas diffusion (Schlömer and Krooss, 1997). The gas diffusion approach seems particularly attractive.

Katsube et al. (1992) and Issler and Katsube (1994) provide an excellent discussion of porosity values calculated in tight mudstones by helium porosimetry,

mercury porosimetry, and gravimetric immersion porosimetry. What stands out in the Katsube et al. (1992) report is how effectively mercury and helium penetrate nanosize pores. It is assumed that the samples were heated to remove bound water before mercury intrusion, and helium injection.

2.06 Effective Porosity

Effective porosity is total porosity minus bound water volume (Juhasz, 1979; Truman et al., 1989). Effective porosity can be calculated if bound water is known or measured directly using mercury intrusion or gravimetric methods. Truman et al. (1989) reported effective porosity on seven shale samples from a depth of 1650 metres in Jim Wells County in Texas. The average effective porosity was 9 percent from gravimetric methods and 8.1 percent from air/brine injection (one sample). This compared to a total porosity of 18.8 percent.

Schlömer and Krooss (1997) recorded mercury porosimeter data on eight tight samples from Germany and offshore Norway. The average effective porosity from mercury intrusion was 0.73 percent for claystone samples N5, N6 and N9 cited in that reference. The average total porosity derived from diffusion experiments was 3.2 percent for the same samples. As verification, both methods measured the same value on sample N3 that had pores large enough not to contain bound water. It is assumed that the Schlömer and Krooss (1997) samples were dried at room conditions and thus contained (hygroscopically adsorbed) bound water.

2.07 Cation Exchange Capacity

Bulk CEC ranges from 0.01 to 1.50 meq/g in mudstones as shown in Figure 2.3. Two wet chemistry methods are commonly used for CEC determinations, i.e., ammonium exchange, and barium exchange methods (Hill et al., 1979). Alternate wet methods are cobalt hexamine trichloride exchange (Bigorre et al., 2000) and methylene blue methods (Bujdak et al., 1998; Bujdak and Komadel, 1997). There has also been limited application of ammonia electrode methods (Busenbery and Clemency, 1973). To provide accurate results, Kahr and Madsen (1995) have shown that the popular methylene blue process requires that the sample be sodium saturated and at neutral pH.

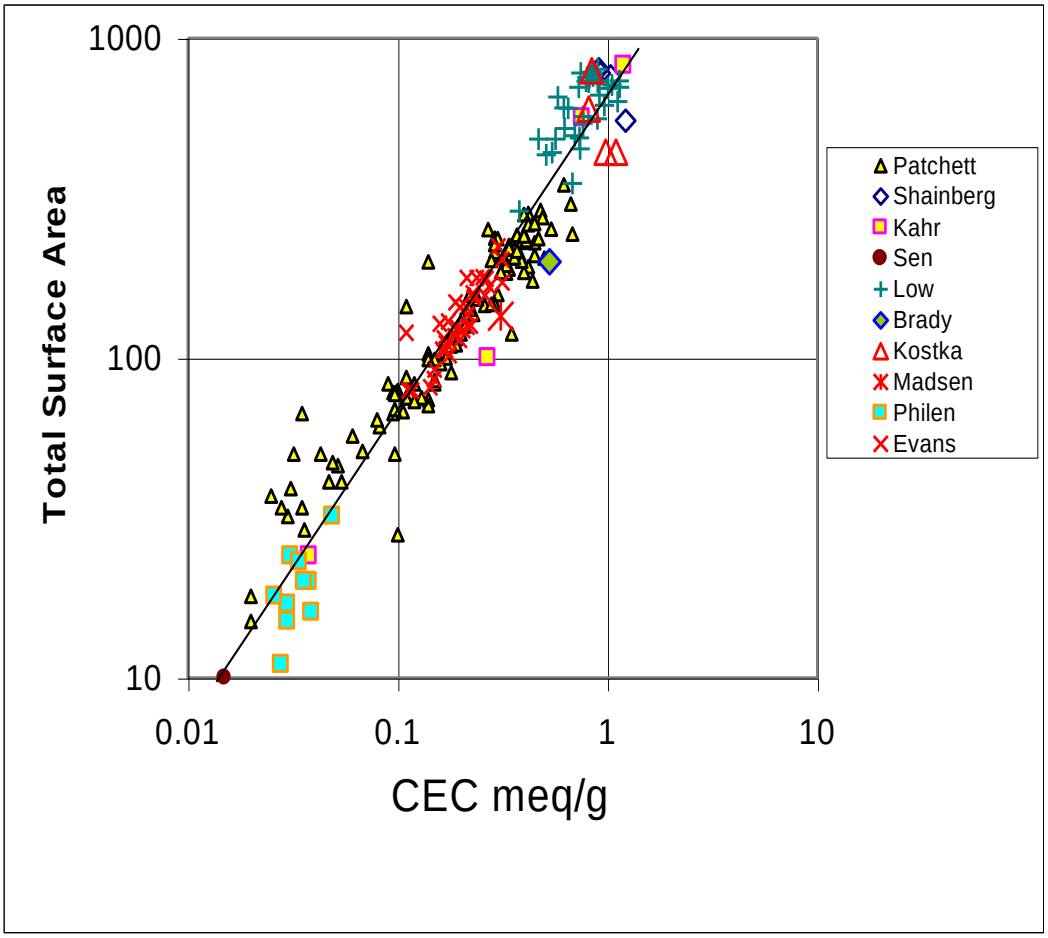

Figure 2.3: A collection of cation exchange capacity and surface area data for mudstones, soils, and clay showing a strong linear relationship (slope of line is unity). Data are from Patchett (1975), Shainberg et al. (1987), Kahr and Madsen (1995), Sen and Goode (1992), Low (1980), Brady (1992), Kostka et al. (1999), Madsen and Müller-Vonmoos (1983), Philen et al. (1971), and Evans (1981).

Bush and Jenkins (1977), Newman (1983) and Bigorre et al. (2000) correlated CEC to water content (W) derived by suction methods at a constant relative humidity. The data from Bigorre et al. (2000) are for 50 soil samples from eastern France. Water content was determined at 46 percent relative humidity. The equations below give the published regressions. Equation 2.06 is for the clay size component only and Equation 2.07 for the bulk samples, from Bigorre et al. (2000). The data from Newman (1983) are for 58 sub-soils of widely different origin from the United Kingdom show as Equation 2.08. Water content was determined at 47 percent humidity. The strong agreement between Bigorre and Newman is interesting, particularly given that Bigorre did not reference the work of Newman.

$$CEC = (W_{46}-0.0107)/0.200 \quad \text{from Bigorre, clay fraction,} \quad R^2=0.940 \qquad [2.06]$$

$$CEC = (W_{46}-0.0170)/0.167 \quad \text{from Bigorre, bulk soils,} \quad R^2=0.787 \qquad [2.07]$$

$$CEC = (W_{47}-0.0050)/0.167 \quad \text{from Newman, soils,} \quad R^2=0.932 \qquad [2.08]$$

Water content was not reported for the data from Patchett (1975) but there was a good correlation between CEC and specific surface area, SSA, as demonstrated by this regression of data from the 132 samples (see Figure 2.3 for a plot of that data).

$$CEC\ (meq/g) = 0.001695 \cdot SSA \qquad N= 132\ ,\ R^2=0.85 \qquad [2.09]$$

Patchett (1975), Demircan et al. (2000), Goode et al. (1995) and Lauer-Leredde (1998) have proposed determining CEC from borehole data. The last two references used gamma ray data while the first two references used acoustic and resistivity information. Interestingly, Johnson and Linke (1978) found no correlation between CEC and neutron vs. density cross-plotted values. The proposed Patchett (1975) equation is

$$CEC\ (meq/g) = A_1(DT-42)^{A2}(R_{100})^{A3}(D)^{A4} \qquad [2.10]$$

where DT is slowness, R_{100} is resistivity corrected to 100 °F, and D is depth. No regression constants were published, but raw data were published including borehole derived acoustic, temperature and resistivity data for a depth range of 500 to 4700

metrers. (This author had worked with Patchett at the Amoco Research Centre and is impressed with the remarkable quality of this particular data set.)

To derive the regression constants, raw data from Patchett (1975) were analysed using multi-linear functions in MiniTab. The result is

$$CEC\ (meq/g) = 34.67 \cdot ((DT-190)/3.281)^{-0.311} (R)^{-0.753} (1.8T+32)^{-0.683} \qquad [2.11]$$

where T is formation temperature in Celsius, R is resistivity in ohm-metres, and DT is interval travel time in microseconds per metre. By trial and error, it was found that a matrix travel time of 190 microseconds/metre gave the best regression. It was also found that adding depth to the equation did not improve the regression coefficient.

The regression coefficient (R^2) is 0.7 for Equation 2.11. That goodness of fit is slightly better than Patchett (1975) reported for Equation 2.10 and is remarkably good given that it is a statistical fit of wireline-derived log data and drill-pipe-derived core data. This relationship will be used extensively as part of this thesis and the Patchett data set is included on the attached CD.

2.08 Total Surface area

Specific surface area (SSA) varies from 10 to 800 m^2/g in tight mudstones (see Figure 2.3). The common method to determine SSA is the ethylene glycol monoethyl ether (EGME) method. The method involves mixing EGME with a sample of known weight; placing it in a vacuum (to remove all but one monolayer) and reweighing it to determine the remaining EGME weight. A complete procedure from Cerato and Lutenegger (2002) is given in the appendix. The computed surface area is total area including that of all nanopores. An older method uses glycerol (Madsen and Müller-Vonmoos, 1985). Chiou and Rutherford (1997) discuss the effect of layer charge on EGME methods.

The adjective *specific* in SSA implies area per unit mass. Padmanabhan and Mermut (1995) suggest that surface area is better expressed as area per unit pore volume.

Katsube et al. (2000) determined surface area from mercury porosimetry. As stated in the reference, the values are excessive by a factor of about 2 for shales. On the other hand, mercury does not penetrate pores smaller than 3 nm resulting in an understatement of surface area.

Other methods to derive surface area include suction (Bigorre et al., 2000), differential scanning calorimetry (DSC) (Ishikiriyama and Todoki (1995b) and nuclear magnetic resonance, NMR, (Overloop and Van Gerven, 1993). The suction method is the most direct. According to Newman (1983), water content (W) measured at a suction of 100 MPa (i.e., measured on a sample dried at a relative humidity of about 45 percent) equates to one monomolecular layer of adsorbed water. This is in agreement with laboratory data (Bergman et al., 2000), e.g., Hu et al., (1995) imaged the condensation on thin films using atomic force apparatus and found full layer coverage at a relative humidity of 45 percent. The published relationships from Bigorre et al. (2000), Newman (1983) and Robinson et al. (2002) are listed below.

SSA (m^2/g) = 2500 (W_{46}-0.0104)	Bigorre	R^2=0.96	[2.12]
SSA (m^2/g) = 3636 (W_{46}-0.0104)	Newman	R^2=0.96	[2.13]
SSA (m^2/g) = 3575 W	Robinson	R^2=0.94	[2.14]

Surface area determinations are not without uncertainties. Newman (1983) challenged that ethylene glycol adsorption may be larger than one monomolecular layer and suggested that the method may actually overestimate surface area by as much as a factor of 1.7. It is unclear if the same comment applies to EGME.

2.09 External Surface Area

External surface area (SSA_e) varies from 5 to 100 percent of total surface area depending on interlayer volume (and volume of nanopores) and correlates strongly with particle size (Madsen and Müller-Vonmoos, 1983). For example, external and total surface area values for smectite are 50 and 800 m^2/g respectively (van Olphen and Fripial, 1979). Figure 2.4 is a comparison of external and internal surface area for soils from Lutenegger et al. (2003).

External surface area is usually measured with nitrogen adsorption with application of BET theory (Brunauer, Emmet and Teller, 1938). Nitrogen does not penetrate the interlayers in clays and, depending on how the sample is prepared, does not measure bound water surface area. BET methods, unlike EGME, are non-destructive

processes. A variant of the BET method was reported by Singh et al. (2001) and captured below in Equation 2.15 where S is the Caurie slope (Caurie, 1981)

$$SSA\ (m^2/g) = 54.45/S \qquad [2.15]$$

The SSA data in the literature are sometimes not useful because total and external measurements are not differentiated. For example, eleven samples from Yang and Aplin (1998) had an average surface area of 21 m^2/g with a range of 7 to 50. This information becomes more useful when it is understood that it is liquid nitrogen derived on freeze-dried samples, i.e., it does not include surface area occupied by bound water. Bound water does not freeze (and is not removed by freeze drying?). It is recommended that both SSA_e and SSA are important and that the comparison of the two provides information about the pore system. For example, it would have been enormously illuminating to have measured water content (W) gravimetrically on the GeoPoP samples after running nitrogen tests, with the intent to compute SSA from Equation 2.13. To emphasize the importance of both numbers, consider that Laird (1999) reports that change in W with change in surface charge occurs only on the external surface. This will be an issue when discussing the surface charge induced gating effect.

2.10 Permeability

Permeability in mudstones varies over five orders of magnitude from 0.1 to 10,000 nD depending on porosity and effective stress. Figure 2.5 shows representative data from Thompson et al. (1977) and Katsube (2000). The lowest value reported in the literature is 0.2 nD (0.197×10^{-21} m^2) at an effective stress of 50 MPa (Katsube et al., 1996). The value reported above is at the limit of sensitivity for most laboratory equipment.

There are three methods for directly measuring permeability in tight mudstones in the laboratory. These are steady-state methods (Schlömer and Krooss, 1997; Thompson et al., 1977), pulse-transit methods (Katsube et al., 1991; Kwon et al., 2001) and oscillation techniques (Faulkner and Rutter, 2000). Each method comes with uncertainties. The large pressure gradients required to establish detectable flow in a steady-state method are a problem and can affect results. Sample storage effects are a problem for the pulse method and cause under-estimation of permeability (Neuzil, 1986). Storage corrections are complex and rarely applied (Hsieh et al., 1981).

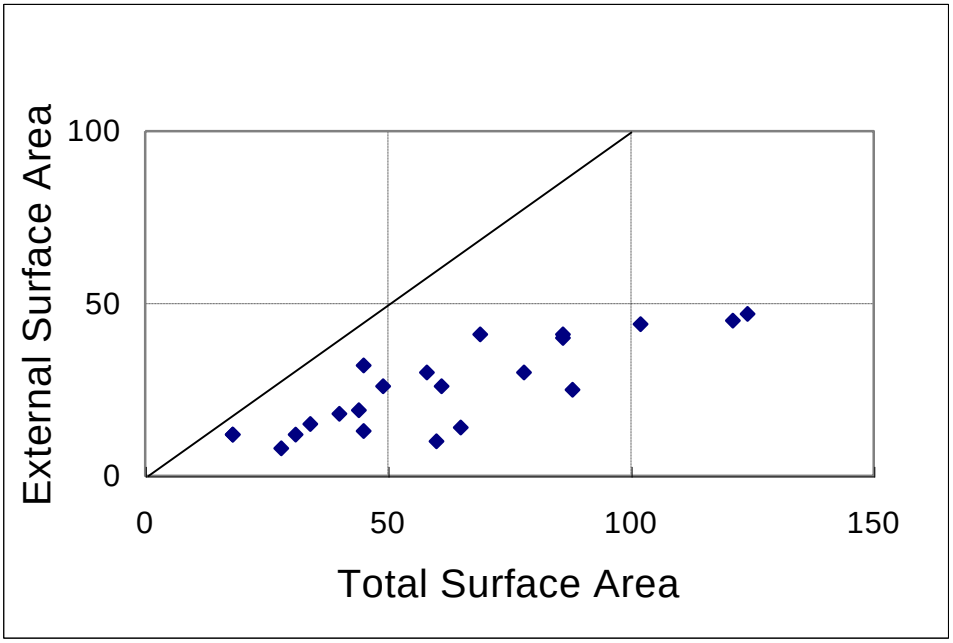

Figure 2.4: Internal surface versus total surface area for clays and soils. Data are from Lutenegger et al., 2003.

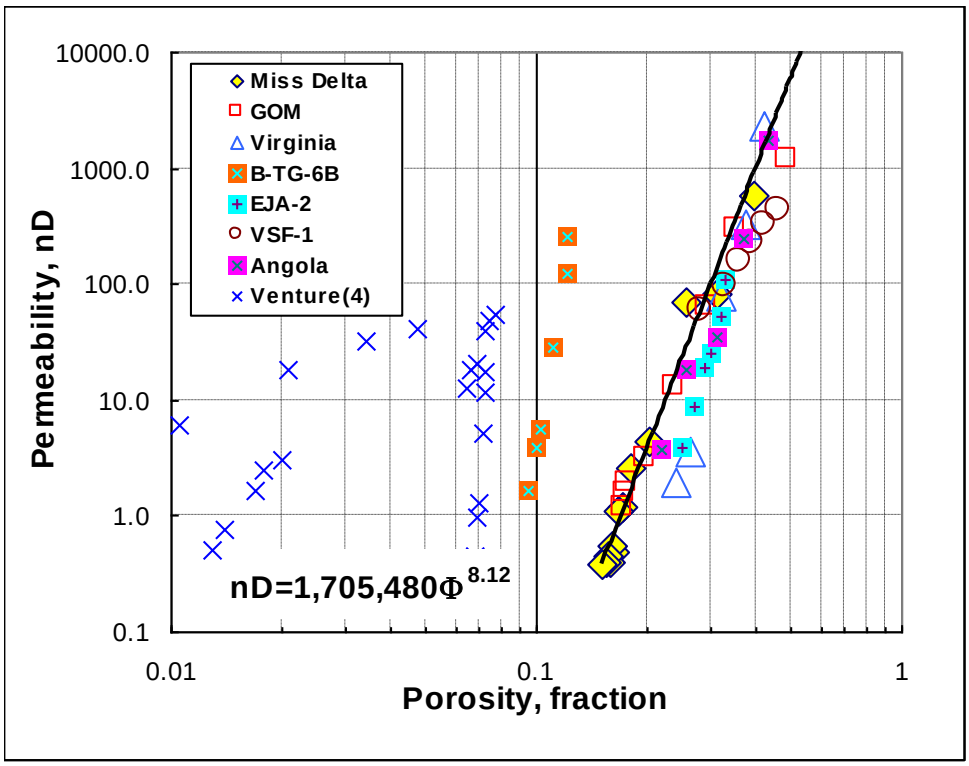

Figure 2.5: Permeability versus porosity for mudstones. Miss-Delta, GOM, Virginia, and VSF-1 are seafloor samples. B-TG-6B and EJA-2 are sub-surface samples from the Beaufort-Mackenzie Basin. The top three samples are from Thompson et al. (1977). The Angola sample is from Lee (1980). The others are from Katsube et al. (2000).

An explanation of storage is best described by an experiment on a shale core from central Utah (United States). In laboratory flow measurements at the University of Texas, Chenevert and Sharma (1993) measured volume injected at the inlet port and withdrawals from the outlet ports. After 100 hours, 0.7 cm^3 of water had been injected into the inlet of apparatus containing a mudstone sample but only 0.27 cm^3 had been measured from the outlet. The difference (0.7-0.27=0.43 cm^3) is the storage volume. Storage is an artefact of clay swelling, core compressibility, and expansion of the flow lines in the equipment. For this mudstone sample, it took a reported 170 hours to reach steady-state conditions.

The oscillation method is self-correcting for storage effects. In this method, a sinusoidal pressure pulse with a period of about 100 seconds and amplitude of about 2 MPa is applied to the upstream side of a confined sample in a flow cell. Permeability and storage is a function of phase shift and change in amplitude between the upstream and downstream sides (Faulkner and Rutter, 2000).

Experience suggests that permeability measurements require critical quality-control evaluation. A measure of data quality for pulse methods (used for GeoPoP samples) is an examination of the linearity of the raw pressure plots (see Figure 2, Kwon et al., 2001). Chenevert and Sharma (1993) used the Trimmer method (Trimmer, 1980) to determine which part of the raw pressure curve to use in the permeability calculation. To verify data quality, Chenevert and Sharma (1993) ran both steady-state and pulse-transit on two shale samples. One sample showed nearly identical values for both methods for the range 0.3 to 1 nD. The other sample showed permeability almost one order of magnitude higher than steady-state results, for permeabilites less than 1 nD.

Data from Katsube (2000) and Chenevert and Sharma (1993) show that permeability in mudstones varies over three orders of magnitude as effective stress is varied from 3 to 50 MPa. But according to Revil and Cathles (1999) and Sigal (2002b) this large variation of permeability with effective stress is due to reduction in porosity during compaction. That is, the porosity term captures all the stress effect: permeability can be estimated without knowledge of effective stress if total porosity is known.

Permeability tends to vary as approximately the 8^{th} power of porosity in mudstones. This observation comes from basin model results from Smith (1973), England et al. (1987), and Wangen (2000). To test the relationship, a regression was run on two selected samples as illustrated in Figure 2.5. These two samples were selected

because they represented uncompacted sea floor samples. But this relationship is not without question. Connolly and Podladchikov (2000) argued that the 8^{th} power value is an artefact of a transient function effect. As another counterpoint, much of the data in Figure 2.5 do not describe an 8^{th} power relationship. But those data (B-TG-6B and Venture samples from Katsube et al., 2000) are core samples from a depth below 3500 metres where unloading effects during core recovery are an issue. The sea floor sample VSF-1 and the shallow core sample from the Beaufort-Mackenzie Basin match those for Mississippi Delta and GOM. This provides interesting verification since the first two samples are pulse-decay measurements from Katsube et al. (2000) and the latter two are steady-state measurements from Thompson et al. (1997).

The data set from Thompson et al. (1977) in Figure 2.5 is particularly interesting and may represent some of the most pristine data available. The three samples were collected from sea bottom in water depths from shallow water to 2379 metres deep. The samples were not dried or otherwise altered, and permeability tests were run with seawater. One sample is Virginia sediment with 52 percent illite and 36 percent kaolinite. The other two samples are Mississippi Delta and Gulf of Mexico sediments with 61 and 67 percent smectite, respectively. For reference, the permeability data from Thompson et al. (1977) were converted from units of cm/s (to nD) using the conversion 1.005×10^{12}.

Two methods to calculate permeability (when direct measurements are not available) are the Swanson capillary-pressure method and the Sen log-derived method. Swanson (1981) defined an apex parameter on mercury capillary pressure curves for sandstones and related it to permeability. It is proposed that the Swanson method applies to mudstones if the bound water has not been removed before mercury injection. The Swanson equation is as follows:

$$K\ (nD) = 3.5 \times 10^{4}\ (\Phi \cdot S_A / P_A)^{2.005} \qquad [2.16]$$

where Φ is fractional porosity, and S_A and P_A are, respectively, percent mercury saturation (pore volume) and mercury injection pressure at the apex position. To test the application of the Swanson method, it was applied here to data from GeoPoP and data from Schlömer and Krooss (1997). The Swanson method did not work on the GeoPoP data collection or other collections where bound water has been removed. It overestimates permeability by 1 to 2 orders of magnitude.

Sen and his collaborators (1990) empirically related permeability to porosity and CEC for a shaly sand data set, where CEC was derived from direct laboratory measurement. The Sen data set is reproduced in the attached CD and his relationship is presented below (Equation 2.17). Goode and Sen (1988) and De Lima and Niwas (2000) presented similar data.

$$k\,(nD) = 1 \times 10^{8.65}\,(\Phi^{m}/Q_v)^{2.11} \qquad \text{from Sen} \qquad R^2=0.88 \qquad [2.17]$$

The exponent m is the Archie formation factor exponent. The parameter Q_v is CEC expressed with reference to pore volume using the standard conversion Equation 2.18 (Juhasz, 1979) where Φ is fractional porosity and ρ_{grain} is matrix density assumed to be 2.72 g/cc for mudstones.

$$Q_v\,(meq/cc) = CEC\;\rho_{grain}\,(1-\Phi)/\Phi \qquad [2.18]$$

The Sen relationship is included as an experimental component of the P3 software developed as part of this research. In P3, porosity and CEC are derived from acoustic and resistivity data. It is the opinion of this author that a newer petrophysical relationship developed by Yang et al. (2002) is probably better than that developed by Sen et al. (1990). But the value of the Sen equation is that it establishes a relationship between bound water and permeability (it will be shown later that the fraction of bound water is proportional to Q_v).

Application of the Swanson or Sen method assumes that water transport operates as a hydraulic continuum down to the nanosize scale. That is, permeability relationships developed for tight sandstones can be extrapolated to the mudstone pore size range. This assumption appears to be verified by atomic force data, on salt water on a highly charged surface, that shows normal mobility to within 1 nm of the surface where 1 nm is about the thickness of the bound water layer (Horn et al., 1998). As a counterpoint, Li (2001) suggests that electro-viscous effects cause non-Darcy flow in confined pores. Rough et al. (2002), Travis et al. (1997), Rao and Mathew (1995), and Miller and Low (1963) give similar arguments. But all these assumptions are based on esoteric theory or based on experiments with non-polar fluids in thin films on charged electric surfaces. For non-polar fluids the electric field associated with charged surfaces produces a liquid-to-solid transition that is not observed in aqueous fluids (Klein and Kumacheva, 1998a, 1998b).

Chapter 3: Bound Water Properties

The properties of bound fluids have been of interest for a long time: e.g., Henniker (1949) cites 149 references. But bound water is still not fully understood. Brovchenko et al. (2001) and Miranda et al. (1998) debated an ice like structure, based on new molecular simulations and scanning force microscopy data. Many references indicate that bound water properties are markedly different than ordinary water (Israelachvili and Pashley, 1983; Chan and Horn, 1985; Skipper et al., 1995; Horn et al., 1998; Miranda et al., 1998; Sutmann, 1998; Brovchenko et al., 2000; Woelki and Kohler, 2000; Bhattacharyya and Bagchi, 2000; and Israelachvili and Gourdon, 2001). Listed below are the properties of bound water that are important to pore pressure prediction.

3.01 Molecular Structure

Bound water has a layered structure as pictured in Figure 3.1. This picture is based on numerous investigations using X-ray scattering (Toney et al., 1994), atomic force measurements (Israelachvili et al., 1990), atomistic molecular simulations (Senapati and Chandra, 2000), and high beam neutron diffraction (Skipper et al., 1994, 1995). All the investigations confirm the periodic, exponentially decaying, oscillations in the oxygen density population shown in the figure (Cheng et al., 2001); Israelachvili and Pashley, 1983). The first layer (illustrated more clearly in Figure 1.1) is H-bonded to the surface and densely packed as a result of an electrostriction effect (Danielewicz-Ferchmin and Ferchmin, 1996). The structure is not unlike a liquid crystal based on MD simulations, according to Brodsy et al. (1991). While most of the information on bound water has been derived on interlayer water in clays, Bergman and Swenson (2000) suggest that the structural picture is similar in small pores.

3.02 Thermal Properties

Bound water does not freeze (Antoniou, 1964; Stapf and Kimmich, 1995; Morishige and Kawano, 1999). Bergman and Swenson (2000), for example, show that 76 percent of water in a clay sample did not freeze at temperatures of –70 °C. In addition bound water has an increased coefficient of thermal expansion (Murad and Cushman, 2000), and Liltorp et al. (2001) claim that bound water has a higher enthalpy and higher entropy than bulk water.

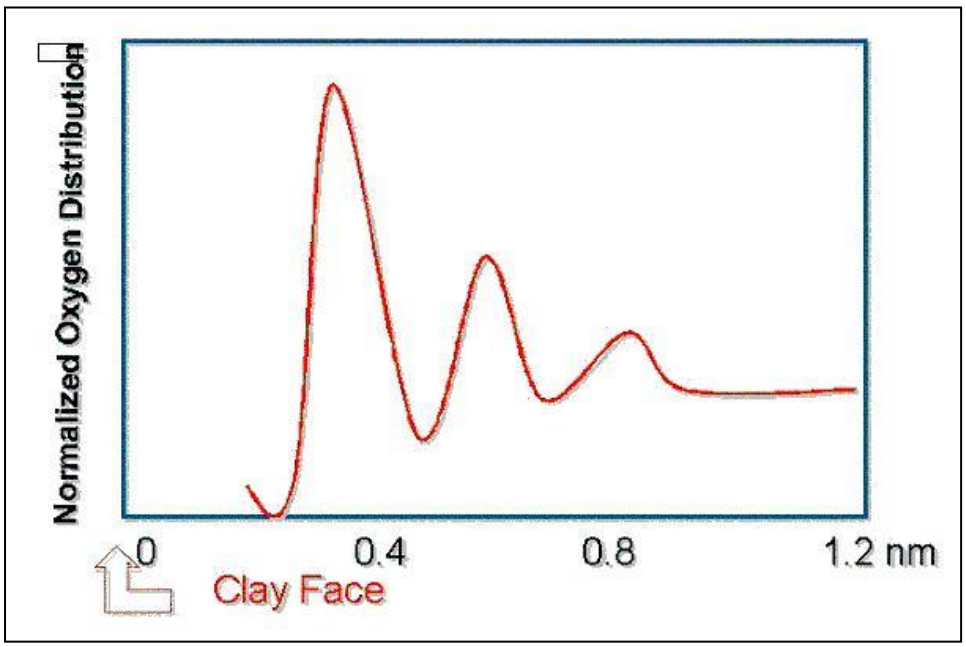

Figure 3.1: Bound water structure. The large oxygen density peak at 0.35 nm from clay surface is a 1-dimensional layer of water molecules H-bonded to the surface. At distances greater than 1 nm oxygen density is that of ordinary water.

3.03 Dielectric Properties (Permittivity)

The dielectric constant (ε) of bound water is an order of magnitude lower than that of ordinary water and does not vary with temperature (Hill et al. 1969). Teschke et al. (2001) determined a value of 4 on mica. Typical reported values for mudstone are 3 to 8 from empirical data (Jones and Or, 2002) and experimental data (de Souza et al., 2001). For comparison, the dielectric constant of bulk water at ambient conditions is 80 and, in contrast to that of bound water, decreases with increasing temperature in accordance with the Curie law (Booth, 1951). This large contrast in permittivity between bulk pore water and surface-bound water is confirmed by experimental observations. For example, neutron diffraction experiments on clays (Skipper, Smalley and others, 1995) show an apparent expulsion of cations from the near surface at the interface between clay matrix and interlayer water. This observation is in agreement with theory that cations are expelled from regions of low dielectric constant (low permittivity) to regions of high permittivity (Basu and Sharma, 1994; Basu and Sharma, 1997).

3.04 Mobility

Based mostly on anecdotal information, bound water is thought to be completely immobile. For example, Byerlee (1990) and Miller and Low (1963), believed there is a threshold state below which no fluid moves, and Clavier et al. (1984) believe that a perfect shale with 100 percent bound water has zero permeability. Zhu and Granick (2001) referred to bound water as caged.

Supporting data for this notion is somewhat limited. Bellissent-Funel el al., (1995) and Liu and Yao (2001) indicate that lateral mobility of bound water is reduced by a factor of 15, based on NMR spin data. Bhattacharyya and Bagchi (2000) used laser spectroscopy to indicate restricted flow in bound water. Chan and Horn (1985) demonstrated that two molecular layers are immobile on charged surfaces, but for non-polar liquids. Muller-Plathe (1998), Heinbuch and Fischer (1989), and Greathouse et al. (2000) used MD simulations to indicate lack of mobility. Kagunya (1996) employed neutron scattering to determine that the diffusion coefficient is spatially restricted. Hill et al. (1979) demonstrated that calculated permeability in shaly sands is reduced by four orders of magnitude when extrapolated to 100 percent bound water. And, according to Titiloye and Skipper (2001), close attachment to the surface charge sites immobilizes at least the hydrated sodium cations in bound water.

As a counter point, Shelley et al. (1997) suggested bound water does have mobility parallel to, but not normal to the surface. And Fripiat et al. (1965) suggest that bound water in the interlayers in clay is mobile while that in pore space is not. This last observation is interesting because deeply buried compacted shales tend to have relatively little interlayer water.

3.05 Thickness

Hatschek in 1912 (cited in Henniker, 1949) calculated the thickness of the bound water layer to be 0.87 nm. This value agrees well with 0.8 nm obtained experimentally for the thickness of nonfreezable water using NMR methods (Overloop and Van Gerven, 1993; Letellier, 1998). It also agrees with observations that most counterions lie less than 1 nm from the surface (Israelachvili, 1991). It is in disagreement with other published values. Brovchenko et al. (2000) derived a thickness of 0.7 nm using Gibbs ensemble simulation methods, but no counterion concentration was included in the model. In theory the thickness of the bound water varies as a function of temperature, effective stress, dielectric constant, and chemical activity of the associated free water in accordance with the Debye-Huckel osmotic model (Renard and Ortoleva, 1997). Hill Shirley and Klein (1979) showed experimentally that the thickness decreases as salinity of the associated water increases. Clavier et al. (1984) used C_o-C_w data from Waxman and Smits (1968) to suggest that the bound water volume decreases 30 percent when temperature is increased from 25 °C to 200 °C for isobaric conditions. But this issue is contentious and more discussion follows later. Marcial et al. (2002) stated that the thickness should be temperature dependent.

There are other methods to determine thickness. Using the arguments from Schmidt et al. (1995), the intercept of Equation 2.1 is the thickness of the unfrozen water. Singh et al. (2001) relate water activity to thickness of bound water on white leghorn spent chicken. Thickness is 0.65 nm assuming that a relative humidity value of 47 percent represent bound water conditions. Prost et al. (1998) used a similar activity function to determine thickness.

It is a common practice to calculate bound water thickness with application of the volumetric equation $W_b/(SSA\ \rho_w)$ where thickness is in metres, SSA is specific surface (m^2/g) and ρ_w is bound water density at 10^6 g/m^3 (Lambe and Whitman, 1979). Katsube et al. (2000) used this method to determine bound water thickness on eleven mudstone samples from the Mackenzie Delta and derived values from 0.1 nm to 64 nm. The

problem here is twofold: first, bound water density may not be unity; second, pore space is not planar as assumed by the equation. Ishikiriyama and Todoki (1995b) assumed spherical and cylindrical pore shape and computed a thickness smaller by a factor of 2.

Given that the size of a fully hydrated Na^+ counterion is 0.78 nm (Lambe and Whitman, 1979), and that the diameter of a water molecule is 0.24 nm (David et al., 2001), the thickness the bound water is about 1 nm, assuming that bound water is make up two discrete layers as pictured in Figure 1.2 (i.e., a hydrated cation layer and a water layer).

According to Renard and Ortoleva (1997), the thickness of the bound water layer varies approximately as the inverse of effective stress

$$\Delta \text{ (nm)} = 800 / \sigma'^{(1.008+0.41\cdot\sigma)} \qquad [3.01]$$

where Δ is the thickness of bound water, σ' is effective stress in MPa, and σ is surface charge in C/m^2. For an effective stress of 50 MPa and surface charge of 0.2 C/m^2, thickness is equal to 0.91 nm. The relationship was based on a complete Debye-Hückel osmotic model for parallel clay plates and includes the double-layer diffuse zone, not included as part of the bound water volume in this thesis. For normal values for surface charge (to be discussed in Chapter 5), the exponent is approximately unity.

3.06 Density

There is no agreement in the literature on bound water density. Tscaper in 1934 (cited in Grim, 1953) put the density of bound water at about 1.7 g/cc. De Siqueira et al. (1999) computed 1.22 g/cc for shales. Hawkins and Elgelstaff (1980), using neutron diffraction, found the density of bound water no more than 5 percent higher than bulk water. Bagchi et al. (1997) suggested 1.29 g/cc. Iiyama et al. (2000) and Anderson and Low (1957) derived values in the 0.8 to 0.9 g/cc range. Ishikiriyama and Todoki (1995b) determined values less than 1 g/cc using pycnometer data. Svergun et al. (1998) presented some of the best data for high surface charge protein at about 1.2 g/cc. Mackenzie (1958) pointed out that it is possible that some water molecules could interpenetrate clay surfaces and appear to have infinite density in calculations from pycnometer data.

To independently examine bound-water density, a private BP data set was examined using a method similar to that reported in the literature. Magara (1986) cited

an example by Youn, who cross-plotted neutron and density-derived porosity for mudstones and derived a value of 1.4 g/cc for fluid density by extrapolating the plot to a porosity value of 100 percent porosity. As an adaptation of that method, acoustic-derived data have been plotted here for depths below 3500 metres for a test well from South America. The derived value is 1.75 g/cc as shown in Figure 3.2. To date this value cannot be verified on other wells in other geological regions. As another source, laboratory data from Overloop and Van Gerven (1993) were examined. Those data showed a value of 1.48 g/cc for samples with small pores, and 1.16 g/cc for large pores.

Discussion to follow in Chapter 5 (on dielectric saturation) will add clarity to the density issue. The picture set out there is that bound water density at shallow depth of burial is normal (i.e., about 1.0 g/cc) and at deep burial depths (below what will be defined as a gating depth), is about 1.2 times more dense than normal. This is based in part on Giese and Oss (2002) who demonstrate that swelling clays have normal or less than normal water density, but non-swelling clays tend to have water density greater than normal. This new concept helps reconcile historic data, e.g., the 0.8 to 0.9 g/cc data reported by Anderson and Low (1957) are for swelling clays from outcrops in Wyoming.

3.07 Load Bearing Capability

According to Ball (2001) and Rutter (1983) bound water on clay and silica surfaces can support a compressive load, i.e., bound water can support lithostatic stress in the subsurface. Klein and Kumacheva (1998a, 1998b) used direct atomic force apparatus to show confinement-induced liquid-to-solid phase transitions in certain fluids. References cited therein suggest that under progressive confinement the solid-like phase takes place abruptly at a well-defined film thickness. Raviv and Klein (2001, 2002) show similar conclusions. Renard and Ortoleva (1997) and Sherwood (1994) discussed the load supporting effect as an osmotic pressure phenomenon, i.e., as charge related repulsion between surfaces. Paunov et al. (2002) demonstrated that the load bearing capability of the bound water increases with dielectric saturation. Odelius et al. (1997) discussed the solid-like structure of water, detected in scanning polarization force microscopy on hydrated muscovite.

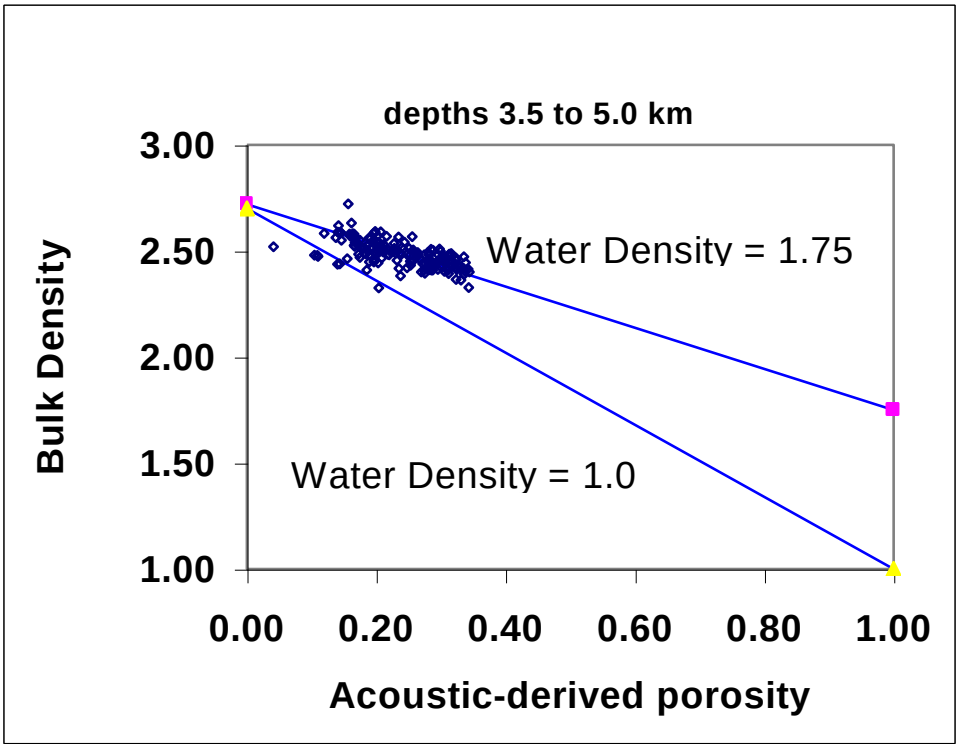

Figure 3.2: Bulk density versus acoustic-derived porosity for a Trinidad well for depths below 3500 m. Water density is determined by projecting the linear trend to 100 percent porosity, i.e., 100 percent water.

3.08 Electrical Conductivity (inverse Resistivity)

Bound water has anomalously large conductivity (Street, 1961) as shown by C_o-C_w measurements noted in Chapter 1 and 2. Bound water conductivity, i.e., surface conductivity is a function of CEC and formation temperature (Waxman and Thomas, 1974; Gravestock, 1991). It is not (at least not strongly) a function of the salinity of the associated water (Giese and Oss, 2002).

The electronic transport mechanism is not well understood. Kaviratna et al. (1996) argued for cation transport and Poinsignon (1997) and Fripiat et al. (1965) argued for proton transport. Skipper et al. (2000) added to the debate by reporting a proton producing H_30 population on clay surfaces (using neutron diffraction). Another question is the conductivity behaviour of the two individual layers in bound water. Fukue et al. (1999) suggested that the near surface H-bonded layer is non-conducting - a notion supported by data from Kaviratna et al. (1996). Bergman et al. (2000) reported that the bulk conductivity of clay allowed to collect water one layer at a time shows the same value for the first layer as for the first two layers combined, implying that only one of the two is contributing.

As an interesting note, there is no agreement on which water layer collects first during water adsorption, i.e., the near (H-bonded) layer or the far (cation hydration) layer. As a last note, the parameter most affecting bulk conductivity in tight mudstones may be the thickness of the bound water film, which is a function of effective stress (Renard and Ortoleva, 1997) and thus a function of pore pressure.

Chapter 4: Measurement of Bound Water

The following is a comprehensive list of methods for measuring bound water, as reported by the food, electrical, agricultural, waste disposal, chemistry and medical industries (methods rarely cross-referenced or compared in the literature). A few non-quantitative techniques are not included, e.g., infrared (Herrera-Gomez et al., 2001) and chemical potential methods (Guarnieri and Mezei, 1996). Several new methods developed here are included.

4.01 Anion Exclusion Method

This method takes advantage of the unique attribute that, when crushed dry rock is mixed in a salt-water solution, the salinity of the solution increases in accordance with the anion exclusion properties of bound water. Hill et al. (1979) give the details for the calculation of bound water content (W_b) from anion exclusion data. Figure 4.1 is anion exclusion derived data for shaly sandstones from Shell Development laboratory (Hill et al., 1979) and for mudstones from the Deep Ocean Drilling team (Henry, 1997). The resulting relationship between CEC and bound water content (W_b) will be used extensively in this thesis:

$$W_b\,(g/g) = 0.27\ CEC \qquad (R^2=0.81) \qquad [4.01]$$

The coefficient in the equation, defined below as V_Q, is the unit weight of bound water per exchangeable cation:

$$V_Q\,(g/meq) = 0.27 \qquad \text{Anion exclusion derived.} \qquad [4.02]$$

A discussion will follow in Chapter 7 on the variation of V_Q with temperature, pressure and salinity of the free water. Hill et al. (1979) reported that V_Q varied as a function of salinity in accordance with osmotic theory. According to Watanabe and Mizoguchi (2002), the amount of unfrozen water in soils is a function of salinity of the free water, which supports a salinity dependence of V_Q.

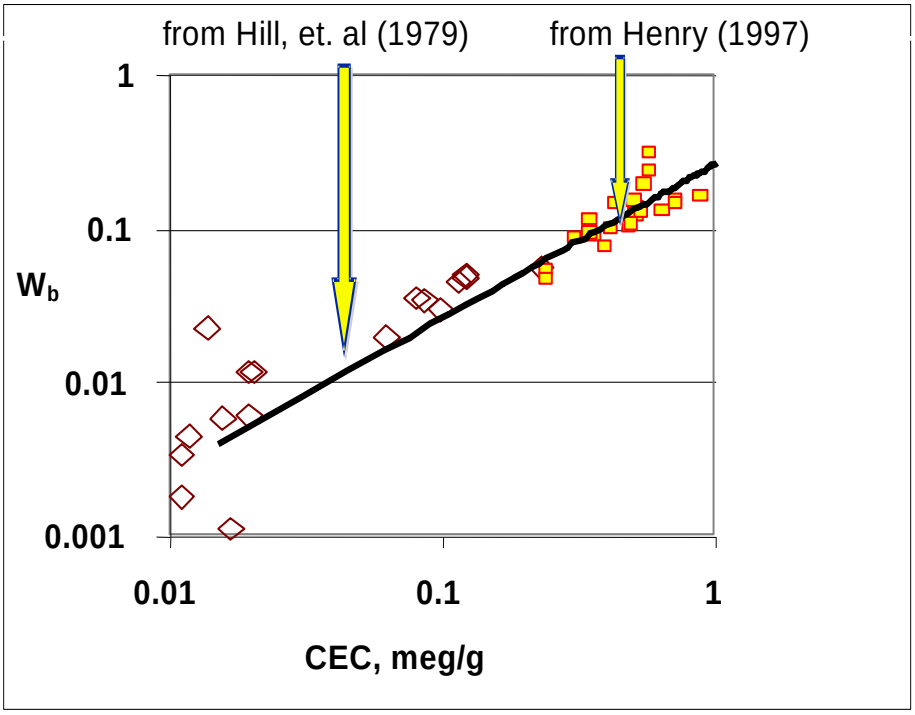

Figure 4.1: A log-log plot of cation exchange capacity versus bound water as derived from anion exclusion methods for shaly sandstones (diamonds) and mudstones (squares). The black line is a linear regression line warranted by the linear relation given by theory (Hill et al., 1979), i.e., the black line has a 45-degree slope on a log-log plot. This figure is the first known comparison of the two important data sets.

4.02 Suction Method

This method assumes that the amount of water that dry rock adsorbs from moist air (hygroscopic suction) is related to bound water (W_b). Robinson et al. (2002) proposed that W_b equals W_{50} where W_{50} is the weight of water in a sample dried at a relative humidity of 50 percent. One can argue that the structure of bound water has at least two layers and that W_b should more correctly equal 2 times W_{50}. This argument is based on Bergman et al. (2000) and Hu et al. (1995), who experimentally found only one layer of water coverage at a relative humidity of 45 percent. But things become more complex when it is understood that the outer (thicker) hydrated cation layer, which may be adsorbed first (Hensen et al., 2001), is thicker than the inner H-bonded layer - i.e., a simple multiplier of 2 is not justified. More discussion and references on this issue are cited later.

To develop a modification for the Robinson relation, CEC is taken equal to (W_{45}-0.005)/0.167 from Equation 2.08 in Chapter 2. Substituting this into Equation 4.01 gives the following improved relation:

$$W_b \text{ (g/g)} = 1.62 \, (W_{45} - 0.005) \qquad [4.03]$$

This modification to the Robinson method is an important contribution: i.e., Equation 4.03 provides a serviceable relationship for the determination of bound water in mudstones. It can be run in any facility with an oven and mass balance. Basically after a sample is equilibrated in a closed container at 45 to 50 percent humidity (or dried in storage at room conditions) mass (M) is measured with a balance. The sample is heated to 105° C. The mass (M_{dry}) now is measured again. Water content (W_{45}) is ($M-M_{dry}$)/M_{dry}. W_b is computed using equation 4.03. As noted previously, establishing a controlled relative humidity is accomplished by placing the sample in close proximity to a salt solution in a closed container. Newman (1983) used a saturated $LiNO_3$ solution. In the field or at a well site, water content (W_{45}) can be measured with an inexpensive Ohaus moisture balance (Bourgoyne et al., 1991). As a point of information, the Ohaus balance uses an infrared halogen heat lamp to dry samples.

4.03 Compaction Method

It is proposed here that water content (W) determined from a drained compressive test at 100 MPa is equal to W_b. The suction pressure of bound water is 100 MPa at a relative humidity of 45 percent at ambient conditions as given by the equation

$$\text{Suction (MPa)} = 137.837 \ln(RH) \qquad \text{(at 20 °C)} \qquad [4.04]$$

where ln(RH) is the natural logarithm of relativity humidity (RH) expressed as a fraction (based on Kelvin's law from Delage et al. 1998).

From the theory of reciprocity, if full bound water coverage exists at a RH of 45 percent as noted above, a compressive force of 100 MPa would squeeze out all but the bound water. As verification, compaction data from Chilingar and Knight (1960) show a water content of 0.27 g/g for a montmorillonite sample compressed to 100 MPa, a value for W which is in agreement with Equation 4.01 if CEC for montmorillonite is 1 meq/g. Moreover, it agrees with the theoretical value that the water content for one monolayer coverage in montmorillonite is 0.23 g/g (Newman, 1983).

Marcial et al. (2002) published comparisons between suction and compaction for a synthetic mudstone. That data support the notion of reciprocity. The compaction method is not new. Dirksen and Dasberg (1993) experimented on soils with (wilting) measurements between pressure plates at 1.5 MPa. Wu et al. (1997) experimented on sludge with compression tests at 7 MPa. Both experiments gave bound water values an order of magnitude too high. The reason for failure is that the compression levels were too low.

4.04 Differential Scanning Calorimetry (DSC) Method

In this method, bound water (W_b) is equated to the amount of water that does not freeze when a sample is super-cooled, as measured with a calorimeter (Ishikiriyama and Todoki, 1995a, 1995b; Liu and Yao, 2001). The experimental process is relatively complex. The samples are immersed in distilled, deionized water and slow dried at room temperature while the mass is monitored. Drying is stopped when a desired water content is obtained. The samples are hermetically sealed in a crucible. The process is repeated several times until a wide range of water contents are available on each sample. The DSC-derived endothermic peak of the freezable pore water (on each sample) while cooling to –50° C is correlated to the volume of non-bound water in the

sample. By material balance the bound water fraction is calculated. Equation 4.05 is a least squares fit to the results of five samples from Ishikiriyama and Todoki (1995a).

$$W_b\ (g/g) = 0.000482\ SSA \qquad N=5,\ R^2=0.932 \qquad [4.05]$$

From Equation 2.09 (in Chapter 2) SSA equals CEC/0.001695. Substituting into Equation 4.05 yields Equation 4.06.

$$W_b\ (g/g) = 0.28\ CEC \qquad \text{from DSC Method} \qquad [4.06]$$

$$V_Q\ (g/meq) = 0.28 \qquad \text{from DSC method} \qquad [4.07]$$

The constant 0.28 in the equation, again defined as the weight of bound water per exchangeable cation, is in remarkable agreement with the 0.27 value found by anion exclusion methods (Equation 4.02).

4.05 Dilation Method

Dilation is a measure of how much a saturated sample expands when frozen. Since bound water does not freeze, a volumetric comparison of total dilation to expected dilation for 100 percent frozen water, is a measure of bound water volume. This method is used to measure bound water on sludge from sanitation plants (Wu et al., 1997). A simple procedure and the associated equation are described in that reference.

4.06 Dielectric Method

Dielectric methods exploit the one order of magnitude difference between the dielectric constant of free water and bound water. Henry et al. (2002) used dielectric spectroscopy in the microwave domain in the agriculture industry to determine the bound water content of corn seed. Overloop and Van Gerven (1993) also made use of the method. Dielectric measurements will be described later as a method to infer a change in bound water volume, i.e., to infer dehydration with increasing temperature.

4.07 Freeze-Dried Method

It is proposed here that the water content of a freeze-dried mudstone sample is equal to W_b. According to Whitworth and Gu (2001), freeze drying (lyophilization) removes all but the bound water in clays. No reference has been found for previous

application of this method for the determination of bound water content. No test was made here because the concept was developed after the experimental stage of this research had ended. To understand some complications, note that common freeze-drying methods incorporate a two stage drying process. The primary phase is normal sublimation of crystallized water after a sample is frozen and the vapour pressure has been reduced. Bound water does not sublime because it does not freeze. The secondary phase is the application of heat, which removes bound water. Islam et al. (1997) suggested that a partial loss of bound water may occur after freeze drying, but it is not clear if the discussed process combined both drying steps, i.e., if the sample was heated after freeze drying.

4.08 Centrifugal Method

Because bound water cannot be extracted by normal centrifugal force (Johari, 2000), the water content after centrifuge equals W_b. Yen and Lee (2001) compared centrifuge-derived bound water content to dilatation methods on sludge waste. Since centrifugal methods are sometimes been used in petrophysical studies to determine capillary pressure, it should have direct application to W_b determinations. In this search no references were found on application to mudstones.

4.09 NMR Method

This is a variant of the freezing method where NMR is used to measure the unfrozen volume. Lele et al. (1997) and Stapf and Kimmich (1995) used ^1H static line width line to measure bound water on gels and showed a two order difference in line width between free and bound water. Alternately, Overloop and Van Gerven (1993) used a time-domain method and demonstrated that the magnetic decay time for ice and unfrozen water are different by a factor of 3 or 4. Results from Overloop and Van Gerven (1993), for porous glass samples with 6 to 24 nm diameter pores, appear to overestimate W_b, e.g., regression of the data gives W_b=0.00078 SSA, compared to W_b=0.000482 SSA from Equation 4.05. The reason for the disagreement is unknown.

Another problem with NMR techniques is the (NMR) indication that there is no unfrozen water at temperatures below minus 40 °C (Watanabe and Mizoguchi, 2002). This seems inconsistent with the argument that bound water does not freeze at any temperature. But Watanabe and Mizoguchi (2002) appear to have been unaware of the Overloop and Van Gerven (1993) discussion that the suppression of NMR signal at

super-cool temperatures is not a function of water crystallization (freezing) but an artefact of reduced molecular spin. Bergman et al. (2002) discussed the same effect and confirm the unfrozen nature of bound water at all temperatures.

4.10 Petrophysical Methods

If effective porosity is total pore volume minus bound-water volume as defined in Chapter 2, the fraction of bound water, BW, is given by the petrophysical relationship

$$\text{BW (fraction of total pore space)} = 1 - \Phi_e/\Phi \qquad [4.08]$$

where total porosity (Φ) is determined by conventional methods (listed in Chapter 2), and effective porosity (Φ_e) is derived by one of the methods given below.

As an important example, Truman et al. (1989) measured effective porosity on five mudstone samples on a core from a depth of 1600 metres from a well in Jim Wells County in Texas. The average value was 0.09. The measurement specifications followed that of Bush and Jenkins (1977) with the samples dried at 60 ºC at 40 percent relative humidity to retain bound water. Truman et al. (1989) also measured total porosity on the same samples with the samples dried at 105 ºC in a convection oven to remove all water including bound water. The average value for total porosity was 0.188. The authors demonstrated that 18.8 percent porosity is consistent with that derived from density logs and is in agreement with the porosity in adjacent sandstones.

From Equation 4.08, these values for total and effective porosity translate to a bound-water fraction (BW) of 0.52, i.e., 52 percent of the total pore space is bound water. One can argue (as will be discussed in Chapter 7) that the 60-degree temperature would remove as much as half of the bound water, and that the BW value reported above is a minimum value. As a better procedure (based on current literature), Robinson et al. (2002) derived effective porosity from soil samples with the samples dried to 25 ºC at a relative humidity of about 50 percent.

To verify results, Truman et al. (1989) also measured effective porosity on one of the mudstone samples using an air-brine capillary-pressure method proposed by Hill et al. (1979). The measured value was 0.081. This translates to a value for BW of 0.57. As an adaptation of the complex air-brine method, it is proposed here that effective porosity can be derived from mercury capillary pressure data for samples that have not been dried at high temperature. To test the proposal, data were taken from Schlömer and

Krooss (1997) for samples that, apparently, dried at room temperature (based on the small about of mercury injected at 400 MPa). The result was an average value of 0.72 for the bound water fraction.

4.11 Borehole-Derived Methods

It is common practice to express bound water as a fraction of total pore volume as given below (Hill et al., 1979; Clavier et al., 1984):

$$BW = W_b(\rho_{grain}/\rho_{fluid})(1-\Phi)/\Phi \quad [4.09]$$

In the equation, the term, $(\rho_{grain}/\rho_{fluid})(1-\Phi)/\Phi$, is a transform that converts gram per gram of dry rock to fraction of pore volume and ρ_{fluid} is the density of the bound water. Note from Equation 2.04 (Chapter 2) that the volume of one gram of dry rock is equal to $(\rho_{grain})(1-\Phi)$, assuming the pore fluid has a density of about zero for dry rock.

If $W_b=V_QCEC$ (Equation 4.01) is substituted into the above equation, the result is the following:

$$BW = V_QCEC\ (\rho_{grain}/\rho_{fluid})(1-\Phi)/\Phi \quad [4.10]$$

And if V_Q is 0.27 as derived in Chapter 3 and the grain density of mudstone is 2.72 g/cc (as discussed in Chapter 2), the equation reduces to:

$$BW = 0.734\ CEC\ (1-\Phi)/\Phi \quad [4.11]$$

This relationship will be used in the next chapter to compute BW at down-hole conditions in mudstones with CEC derived from resistivity and acoustic data as described in Chapter 2 in Equation 2.11.

The approximation in Equation 4.11 assumes that the density of the bound water is 1 g/cc. As a note of caution, in one example where the relationship was compared to another petrophysical method, the agreement was disturbingly poor (Truman et al., 1989). If bound water density were increased to 2 g/cc (or V_Q reduced 0.15), the agreement would be good. Discussion follows in the next chapter that makes a case for a density of bound water greater than 1 g/cc.

Chapter 5: Surface Charge and Overpressures

This chapter introduces a link between surface charge and the entrapment of overpressures. The organization of the chapter is as follows. The first section defines surface charge and shows typical values for mudstones and clays (taken from the literature). The next two sections describe the way a small increase in surface charge can cause dielectric saturation. The following sections introduce the gating-depth and retention-depth concepts. The last section is an example from Venture field in Canada.. The reader should understand explicitly that while the gating depth is a powerful new idea, developed here, it has not yet been fully verified with experimental data.

5.01 Surface Charge

As stated previously, there is one counter-ion per charge site at the bound-water/ solid interface. Thus surface charge (σ) is equal to cation exchange capacity (CEC) divided by specific surface area (SSA) as cited by Newman (1987). Common practice is to express σ in terms of coulombs per square metre (C/m^2) as given below in Equation 5.01. To understand the constant in the equation, one should remember that 1000 meq equals 1 mole and that the charge of one mole of electrons is a faraday, i.e., 96,493.1 C as determined from X-ray or Millikan oil drop experiments (Pauling, 1953).

$$\sigma \ (C/m^2) = 96.5 \ CEC/SSA \qquad [5.01]$$

The surface charge in soils and mudstones is fairly invariant. This condition is demonstrated by a strong statistical correlation between CEC and SSA: e.g., Bigorre et al. (2000) reported CEC=0.00223 SSA for 32 soils from France with a regression coefficient (R^2) of 0.96. Substituting this into Equation 5.01 gives an average surface charge equal to 0.215 C/m^2. Using the same procedure, σ is 0.19 C/m^2 for the mudstone, silica, and clay data in Figure 5.1, which does not include the data of Bigorre et al. (2000). For comparison, Newman (1983) computed a surface charge of 0.16 to 0.25 C/m^2 for 62 soil samples from the United Kingdom using the same procedure.

Surface charge is usually determined as function of CEC and SSA as given in Equation 5.01. A troubling thought is a perception that the wet chemistry methods

normally used to measure CEC and SSA may not be totally independent. Alternate methods to determine surface charge, however, are complex (Mermut and Lagaly, 2001). An exception is for pure clay in which surface charge can be calculated based on the chemical formula (Newman, 1987).

As a reference, the surface charge of clays varies from 0.11 to 0.20 C/m^2 for montmorillonite to about 0.34 C/m^2 for mica (Shainberg et al., 1987; Osman and Suter, 2000; Rojas et al., 2002). Illite has a charge of 0.25 C/m^2 (Kahr and Madsen, 1995). And, importantly, beidellite has a charge of 0.27 C/m^2 (Gier and Johns, 2000; Teppen et al., 1997). The surface charge of silica cement is 0.35 C/m^2 or higher depending on temperature (Brady, 1992).

5.02 Increase in Surface Charge with Burial Depth

References are cited in this section to make an argument that surface charge tends to increase with increasing burial depth, and temperature, for the first few thousand metres. One example is an increase in surface charge with an increase in the percent of aluminosilicates (Meziani et al., 2001). Rask et al. (1997) and Gier and Johns (2000) discussed the transition from montmorillonite to beidellite and the associated increase in charge associated with the aluminization process. Data from Sato et al. (1996) show a 30 percent increase in charge with depth from 1500 to 3000 metres, due to beidellitization.

Figure 5.2 is a plot of surface charge versus depth computed from Equation 5.01 for the data set from Patchett (1975). The increase in surface charge from 500 to 2000 metres is consistent with the alteration of (low charge) montmorillonite to (high charge) beidellite as reported by Sato et al. (1996). There is no independent confirmation for the alteration interpretation for the data in Figure 5.2. Montmorillonite and beidellite are both smectites, and generally both are lumped together and reported as smectite, because of the difficulty in discriminating between the two minerals.

An increase in the percent silica in a mudstone is another diagenetic process that will increase surface charge. Silica cement is expected to increase with depth because of silica dissolution and precipitation (Renard and Ortoleva, 1997). Brady (1992) showed an increase in surface charge from 0.25 to 0.35 C/m^2 for a temperature change of 25 to 60 °C for silica. Presumably it continues to increase with increasing temperature. Clearly the silica effect will be smaller in the deepwater region where temperature gradients are lower. For non-silica rich mudstones, Heller-Kallai (2001) demonstrated no change in CEC or surface charge for temperatures to 220 °C.

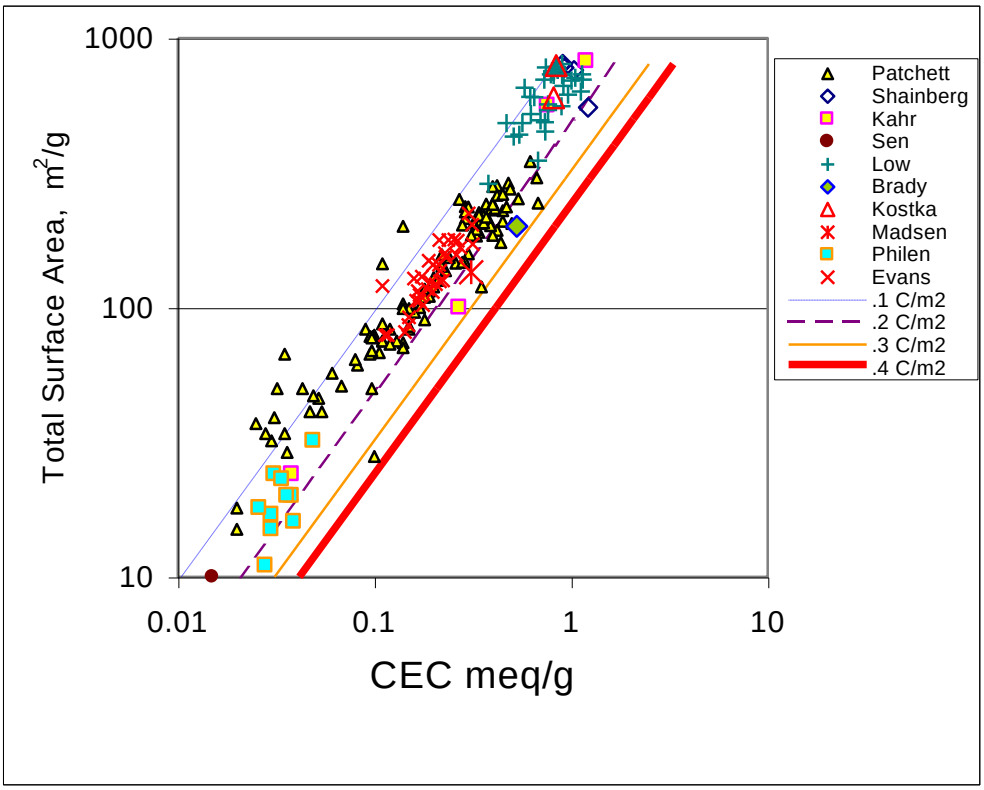

Figure 5.1: The same data as cited in Figure 2.3 with surface charge delineated by a family of straight lines from 0.1 C/m^2 on the left to 0.4 C/m^2 on the right.

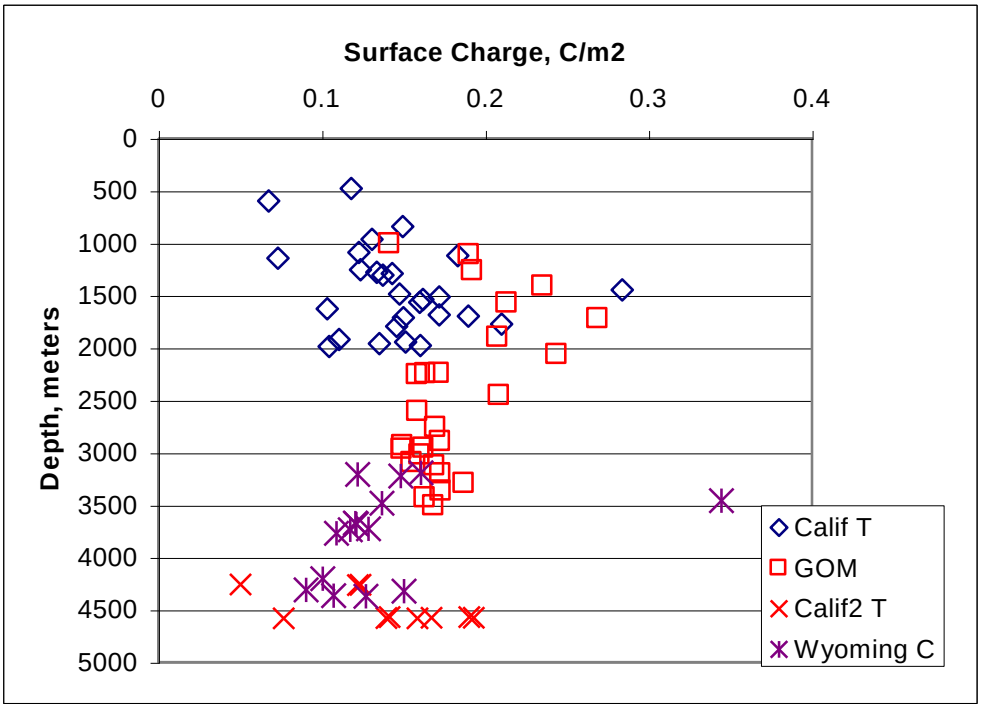

Figure 5.2: Surface charge versus depth for mudstones for four areas in the United States. Data are from Patchett (1975). Converted to surface charge using Equation 5.01.

Reduction of ferric to ferrous iron with depth can also increase surface charge. Champion et al., (1967) reported pressure induced reduction of ferric to ferrous iron at extremely high stress conditions but much higher than experienced in normal petroleum conditions. More details on iron reduction are given below. Figure 5.3 is a summary plot that captures the effect of iron reduction, and temperature effects on surface charge.

5.03 Dielectric Saturation

To illustrate the importance of small changes in surface charge with depth, consider Figure 5.4 from Danielewicz-Ferchmin and Ferchmin (1996). A small increase in surface charge can trigger condensation of the bound water with a concomitant increase in water density. This condition is caused by dielectric saturation. The effect is analogous to electrostriction effects on hydrated ions, e.g., the density of hydrated water on a divalent calcium ion is 1.35 g/cc (Danielewicz-Ferchmin and Ferchmin, 1998).

Numerous investigators have reported a decrease in dielectric constant (ε) with an increase in electric field (E), above an intensity of 10^7 V/m (Basu and Sharma, 1994; Woelki and Kohler, 2000; Danielewicz-Ferchmin and Ferchmin, 2002). At high electric field strength, bound-water molecules develop a specific orientation that causes a decrease in the dielectric effect. The effect is circular. A decrease in permittivity increases the electric field in accordance with Coulomb's law. The regenerating feedback triggers an avalanche effect called dielectric saturation (Watanabe et al., 1991; Lebedev et al., 2000; Carnie and Stell, 1982). As shown in Figure 5.4, dielectric saturation occurs at a surface charge of 0.25 to 0.3 C/m^2.

Given that the electrostatic energy density (P) generated by an electric field is $E^2\varepsilon\varepsilon_o/2$, N/m^2 (Coelho, 1979; Green and Lu, 1997), permittivity of free space (ε_0) is 8.8542×10^{-12}, $C^2/(Nm^2)$, and electric field (E) at a solid surface is $\sigma/(\varepsilon\varepsilon_o)$ (Danielewicz-Ferchmin and Ferchmin, 1996; Israelachvili, 1991), the electrostriction pressure is:

$$P\ (MPa) = 5.647 \times 10^4\ \sigma^2/\varepsilon. \qquad [5.02]$$

For example, if surface charge (σ) is 0.3 C/m^2 and dielectric constant (ε) is 5 (dimensionless), the electrostriction pressure is 1016 MPa. To summarize, the electrostriction effect is the increase in bound-water density due to the pressure generated by a strong inhomogeneous electric field (Yeh and Berkowitz, 2000).

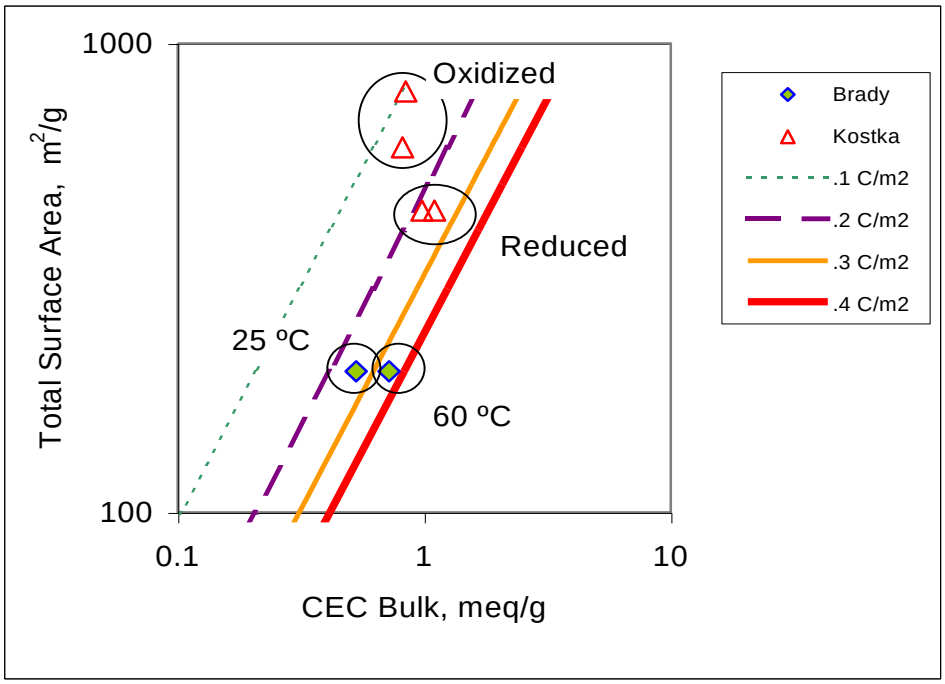

Figure 5.3 – Effect of iron reduction and temperature effects on surface charge. Brady (1992) measured CEC and SSA on one SiO_2 sample at two temperatures (diamonds). Surface charge at 60 ºC increased to about 0.35 C/m^2. Kostka et al. (1999) measured CEC and SSA on two smectite samples (triangles) before and after reduction of iron. Surface charge increased sharply.

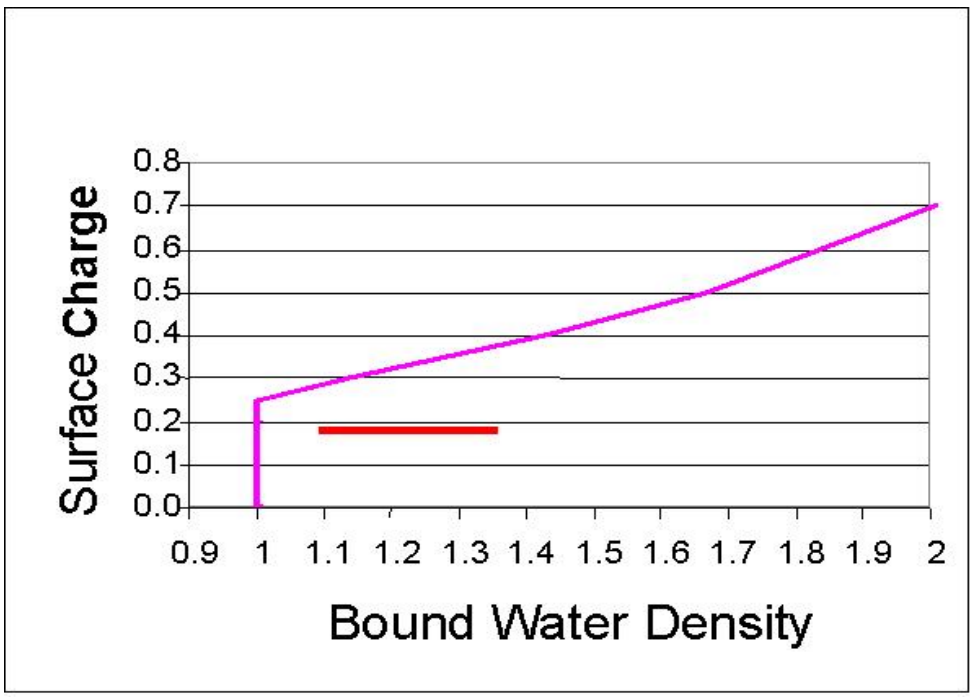

Figure 5.4: The dielectric saturation effect (from Danielewicz-Ferchmin and Ferchmin, 1996). The red horizontal is the average surface charge for soils. Surface charge is expressed in C/m^2 and bound water density is expressed in g/cc.

5.04 Gating Depth Concept

It is proposed here that one trapping mechanism for overpressures is a condensation of the bound water layer caused by dielectric saturation. It will be shown later that this is consistent with a sharp increase in the bound water fraction. Important in the gating depth concept is notion that there is a sharp increase in bound water density at the gating depth. This effect can have a large effect on bulk density interpretations.

More importantly, it can be argued that below the gating depth a fluid expansion will occur as dense bound water is expelled with a concomitant increase in overpressures. The idea is not entirely new. Magara (1986) proposed a dense-water expulsion mechanism for overpressure generation. The problem here is that the issue of dehydration (of the bound water) is a complex issue, e.g., De Siquera et al. (1997) suggested that a higher water density retards enthalpy-driven dehydration.

It is proposed that condensation of bound water can produce a no-flow boundary that can trap hard overpressures in the subsurface. The concept is based on observations from biological systems in which fluid flow is gated on and off by a small change in surface charge in nanosize capillaries in bio-systems (Green and Lu, 1995, 1997; Lu and Green, 1999). As support for the concept, Manning (1996) described a condensed counter-ion layer at a critical charge density. Xia and Berkowitz (1994) suggested that the structure of bound fluids on charged surfaces jumps to a solid state when surface charge increases to about 0.3 C/m^2. Hartnig et al. (1998) showed an increased immobilization at fluid-solid interface as an interaction to surface charge. Tao et al. (1989) calculated that when the electric field exceeds a critical value, the osmotic pressure becomes negative triggering solidification of bound water.

A large unknown is the effect of formation temperature on the gating depth. Data in Figure 5.5 demonstrate the diversity in temperature gradients. More discussion on temperature effects will follow later.

The concept of a critical depth that controls overpressures is not new. Figure 5.6 (a classic GOM data set) is a plot is for 63 fields across a wide region where the top of overpressures coincides with a depth of about 3000 metres (from Jones, 1967; Lane and MacPherson, 1996). Mello et al. (1994) proposed that the critical depth occurs at 14 percent porosity. Fertl and Timko (1970) suggested a cemented caprock factor. Others have proposed a smectite to illite factor (Lahann et al., 2001) at an isotherm of 105 °C. Neuzil (2000) discussed an osmotic component.

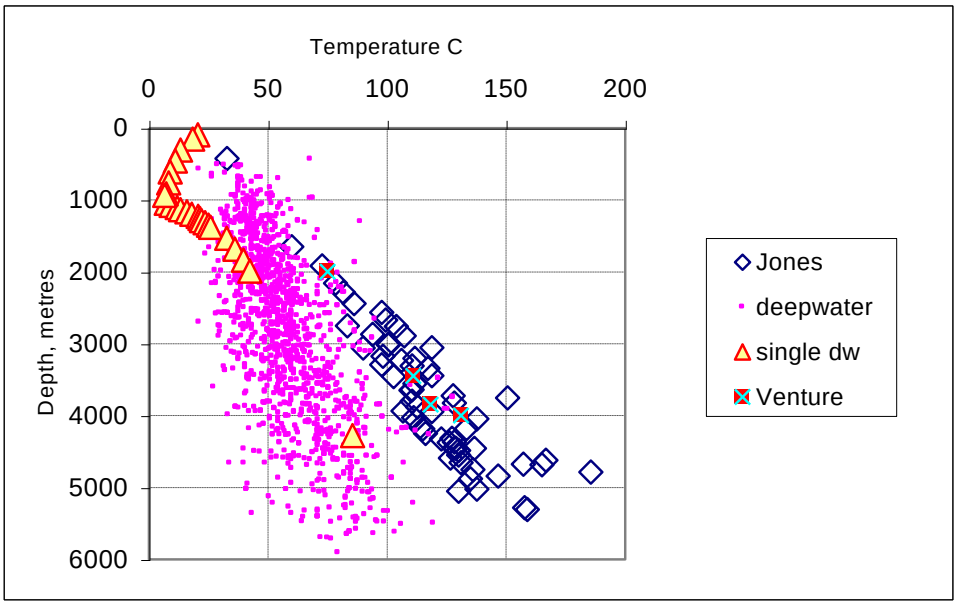

Figure 5.5: Formation temperature for 62 wells from the GOM shelf (diamonds), 1000 wells from the GOM deepwater area (dots), and one well from Venture field in Canada (boxed crosses). Included is a deepwater well (triangles) showing the reduced temperature at the sea floor at 1050 metres. The data for the shelf are from Jones (1967). The other data are from an unknown source. Depth is referenced to sea level.

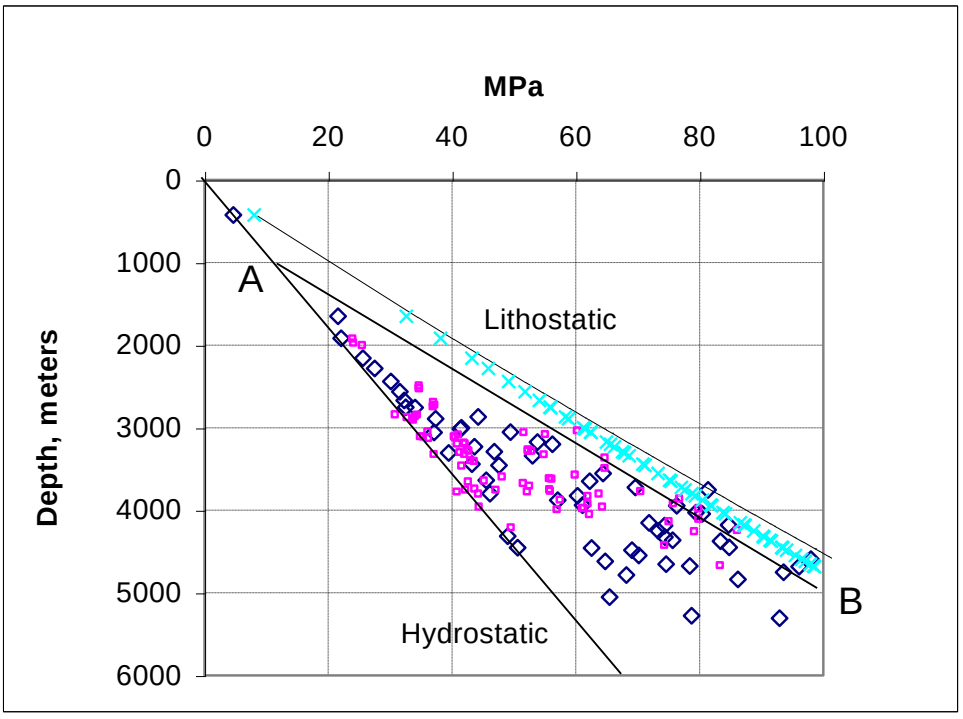

Figure 5.6: Pressure data from the shelf area in the Gulf of Mexico. Data are from Jones, 1967 (diamonds) and Lane and Macpherson, 1976 (squares). The crosses (cyan colour) mark a line equal to an effective stress of one-tenth of normal stress. Line A-B indicates the expected pressure profile for a retention depth at 1000 m.

5.05 Retention Depth Concept

The retention depth concept is not to be confused with the gating depth concept. Ham (1966a, 1966b) proposed a depth-of-sealing below which mudstones can trap overpressures if inter-bedded sandstones reservoirs do not drain pore pressure to normal hydrostatic pressure. Swarbrick et al. (2002) advanced the retention depth concept to general application.

The picture that emerges from this research is that bound water fraction in mudstones increases with depth, as compaction expels free water. Permeability drops rapidly and sediments become slow to drain. At a burial depth when the rate of water loss is not sufficient to establish pressure equilibrium, overpressures occur. This is the retention depth (RD), i.e., the depth of sealing as defined by Ham (1966a, 1966b). To think of retention depth a different way, sediments below RD are undrained. Below this depth pore fluids support part of the lithostatic load. Another part of the picture is that undrained compaction retards dehydration of bound water that occurs at higher temperature states (Colten-Bradley, 1987). Since bound water is immobile, mudstones remain undercompacted below RD. Depending on sedimentation rate, RD is typically 1000 to 2000 metres below sea floor (based on the authors experience). An anomaly is deepwater regions where overpressures often occur at very shallow depths.

The largest mitigating factor to overpressure generation below the retention depth (RD) is lateral pressure transfer. Interbedded sandstones below RD, with lateral continuity, drain pressures to normal hydrostatic (Bredehoeft et al., 1988). If sedimentation rate is not sufficient to generate overpressures, or if lateral pressure transfer dissipates overpressures, compaction continues with depth and at some critical condition a gating depth can occur.

5.06 Effects of Iron Reduction on Surface Charge

The reduction of ferric iron to ferrous iron and the resultant increase in surface charge affects both gating and retention depths. Khaled and Stucki (1991) reported that the oxidation state of iron is an important control of surface charge Kostka et al. (1999) reported that CEC increased and SSA decreased with the reduction of iron for two mudstone samples. As shown in Figure 5.3, this change results in a sharply higher surface charge. The process is reversible.

Stucki and Roth (1977) reported similar results with CEC increasing from 1.15 to 1.42 meq/g with reduction of iron in mudstones. The effect again was reversible. Drits

and Manceau (2000), Gates et al. (1993), Heller-Kallai (2001) and Kocherginsky and Stucki (2000) provided more information on ferric to ferrous effects. It is proposed here that iron reduction is another factor affecting mudstone permeability and the formation of pressure seals, e.g., ferrous iron reported in samples in the overpressured Tertiary section in the North Sea (Carstens, 1978) may have had an influence on the occurrence of shallow overpressures in that area. In summary, iron reduction is a major factor in charge evolution. To illustrate, note in Figure 5.3 that iron reduction drives surface charge near the 0.3 C/m^2 charge threshold.

5.07 Effect of pH on Surface Charge

Another parameter that may affect retention and gating depths is pH of the bound water. According to Evans (1981) CEC is 1.6 to 2.4 times larger at a pH of 8 than at a pH of 4 for silica samples. Assuming constant surface area, surface charge increases by the same percentage as CEC. As contradictory information, Avena and De Pauli (1998) showed that pH effects are large on illite with zero (no effect) on montmorillonite. Sposito (1998) added more information to the pH discussion but no clarity. Shubin et al. (1993) discussed the dissociation effect of pH on the surface charge on latex. There is, unfortunately, little (uncontaminated) data to show how pH varies in subsurface fluids.

5.08 Discussion of the Gating Depth Concept

To support the gating depth concept several hundred overpressured wells were examined from a worldwide data set provided by BP. It was found that the wells could be grouped into two categories based on interval velocity, bulk density, and pore pressure prediction response, somewhat similar to that found by Bowers (2001). Well A and Well B in Figures 5.7 and 5.8 are representative examples of the two groups.

It is reasonable to interpret that the Well A group represents a retention-depth case. As illustrated in Figure 5.9, velocity-derived pressure gradients are in agreement with a retention depth (equivalent depth) model. In addition, density log data clearly show the expected under-compaction profile for a retention model.

It is also reasonable to interpret that the Well B group represents a gating-depth case. Figure 5.9 shows that velocity-derived pore pressure gradient is sharply higher than expected, indicating a secondary cause of overpressure such as expulsion and expansion of bound water. Bulk density data show normal compaction to total depth, indicating a late stage pressure entrapment, again consistent with a gating effect model.

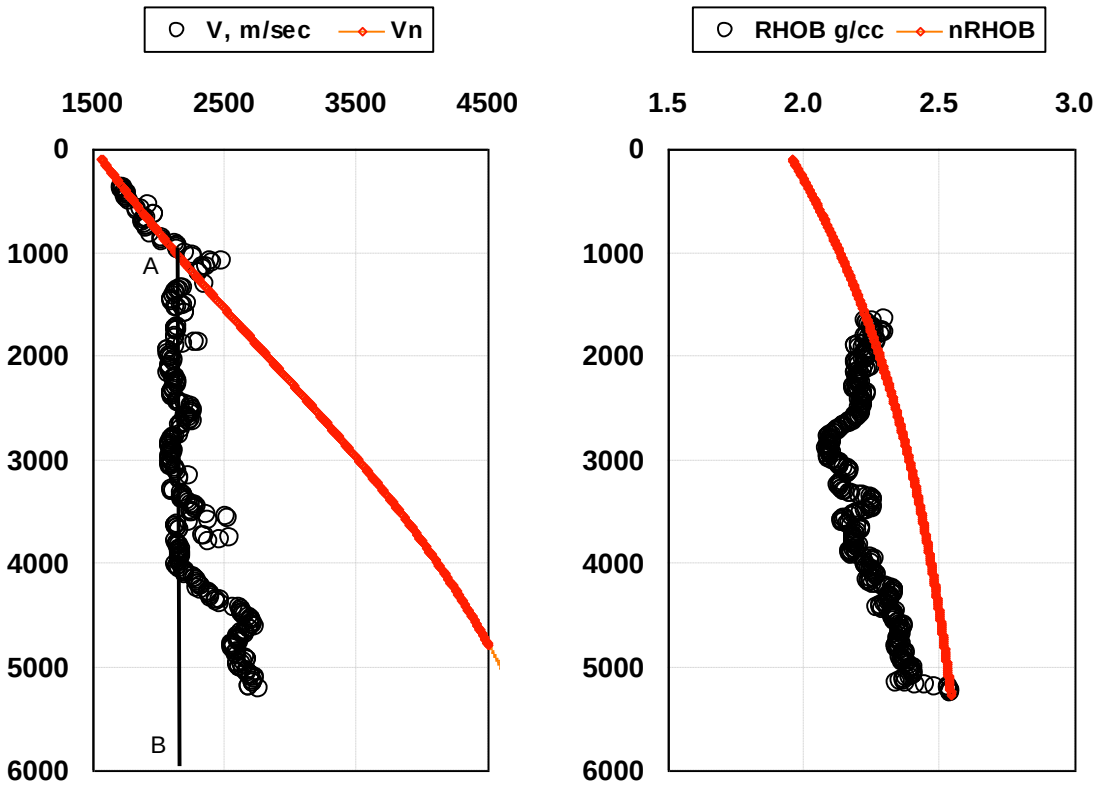

Figure 5.7: Well A example. V is mudstone velocity. RhoB is bulk density. V_n and nRhoB are normal compaction lines. Data indicate a retention depth at 1000 metres.

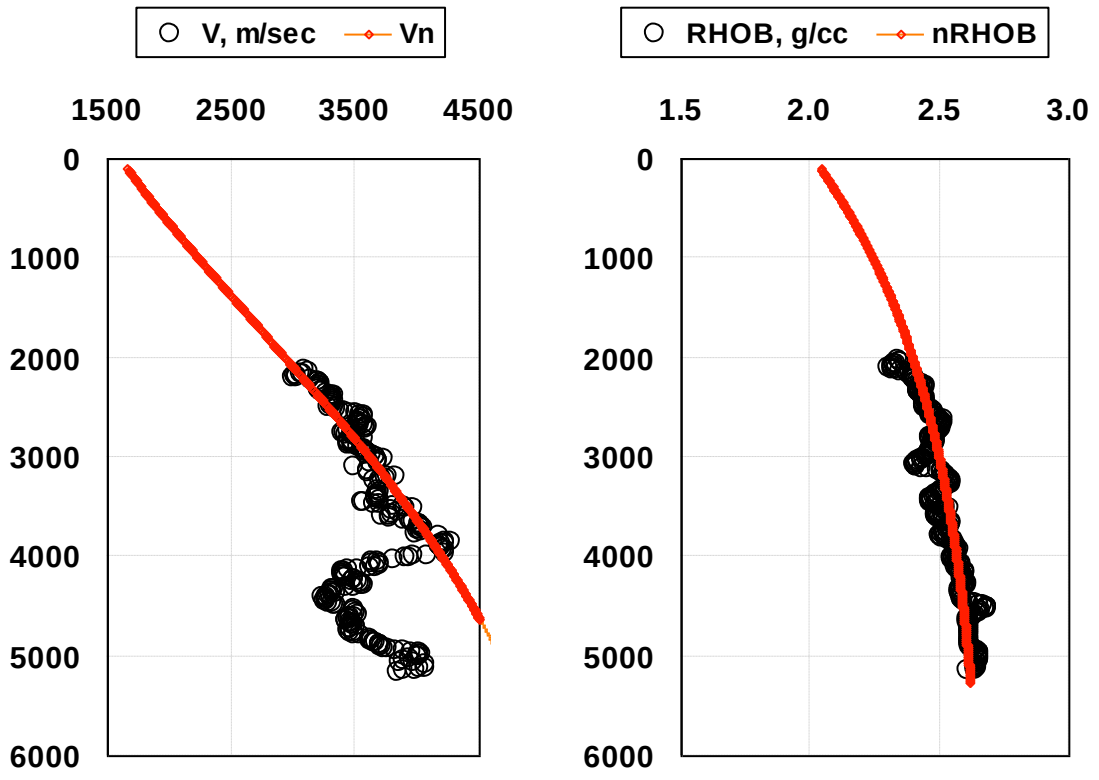

Figure 5.8: Well B example. Velocity and bulk density data indicate a gating depth at a depth of 4000 metres. V_n and nRhoB are normal compaction trends.

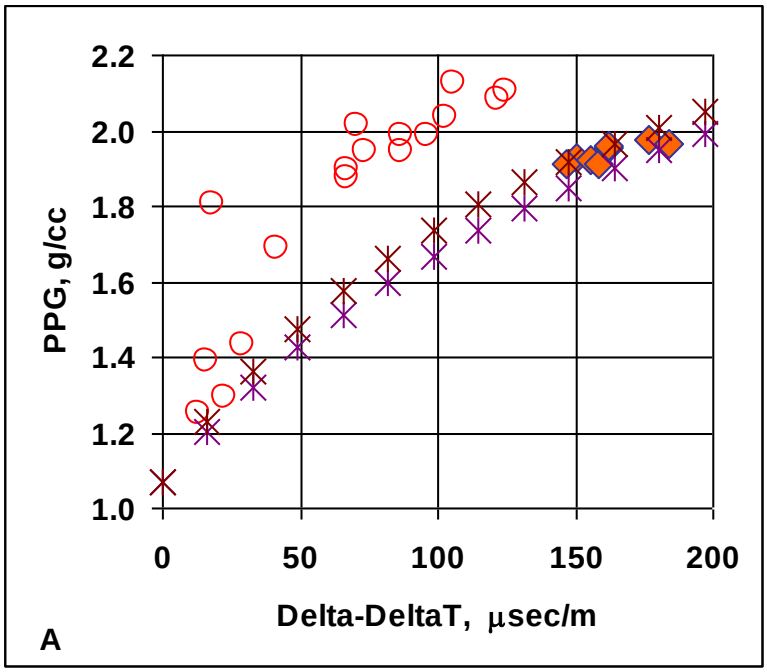

Figure 5.9: Delta-DeltaT ($10^6/V$-$10^6/V_n$) versus pore pressure gradient (PPG) from Hottman and Johnson (1965). Diamonds are data from Well A. Crosses represent the expected relationship for Well A, assuming constant effective stress along line A-B in Figure 5.7 in accordance with an equivalent depth model. The top set of crosses assumes a mean-stress model and bottom set assumes a (standard) vertical-stress model. More details will be given later on the method for determining the predicted values.

To add geologic context, most of the Well A examples are in Tertiary sediments in geologic areas with high sedimentation rates, favourable to retention depth effects. For example, the well illustrated in Figure 5.7 is in Vermillion Bay in the GOM where sedimentation rates are well in excess of 500 metres per million years (A. Pepper, personal communication). In contrast, most of the Well B examples are either in geologic areas with low sedimentation rates OR in areas with a permeable (sandy) lithology that inhibits over-pressuring above a depth of about 3000 metres. Well B in Figure 5.8 is a Jurassic example from Venture gas field, offshore Nova Scotia where sedimentation rate averaged only 17 metres per million years over the last 95 million years (Mudford and Best, 1989). Most of the Well B examples come from the GOM shelf, offshore Nova Scotia, the Caspian Sea, and the deep Jurassic trend in the North Sea. All of GOM examples in Figure 5.9 are normally pressured above about 3000 metres (see Figure 5.6).

The Venture area is of particular interest because the geologic conditions are favourable for a gating effect. Sedimentation rates are low, i.e., no fast sedimentation development of under-compaction to retard the expulsion of non-bound water (bound water fraction increases with depth without restriction). Pore size is in the nanometre range at depth in the mudstones (Katsube and Williamson, 1994), i.e., the nanometre thickness of bound-water becomes a large fraction of total pore volume. Formation temperature is relatively high (Figure 5.5) and silica cement concentrations are high (Katsube and Williamson, 1994) – factors that could contribute to an increase in surface charge with depth as set out above. And, reported amounts of pyrite (Katsube and Williamson, 1994) are indicative of an environment favourable for iron reduction.

To use Venture area data to verify a gating effect, BW was computed for Well B as illustrated in Figure 5.10. The plot shows an increase in BW with depth to almost 100 percent at the top of overpressures, consistent with a gating effect. The plot also shows a gross overestimation of BW below the top of overpressures, for the BW data derived from bulk density porosity data, consistent with an increase in bound water density. The plot is strikingly similar to that computed for the Patchett data illustrated in Figure 5.11. The increase in BW with depth in Figure 5.10 and 5.11 is in agreement with the resistivity interpretation (from Venture field) in Figure 2.2 that indicates an increase in BW to near 100 percent at an effective stress equivalent to a depth of about 4000 metres.

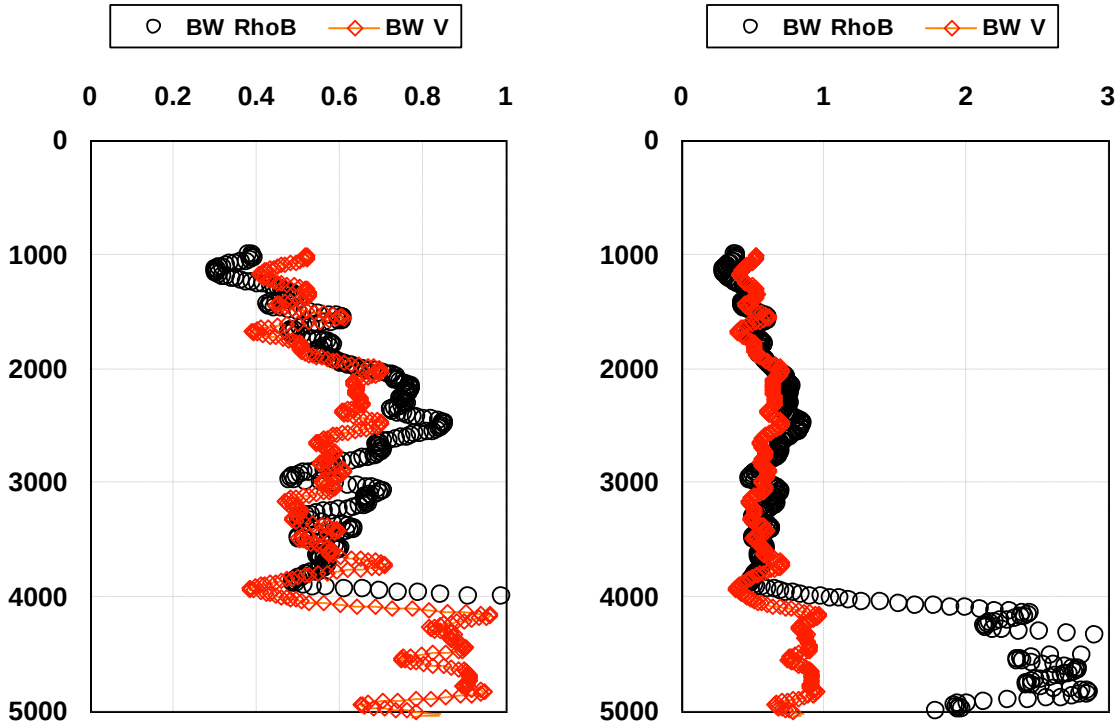

Figure 5.10: Depth versus bound water fraction for Well B. CEC computed from Equation 2.11. BW computed as a function of porosity from Equation 4.11. For the V case, porosity was computed from Equation 2.02 and for the RhoB case from Equation 2.05, assuming a water density of 1.0 g/cc. Top of overpressures is at about 4000 metres.

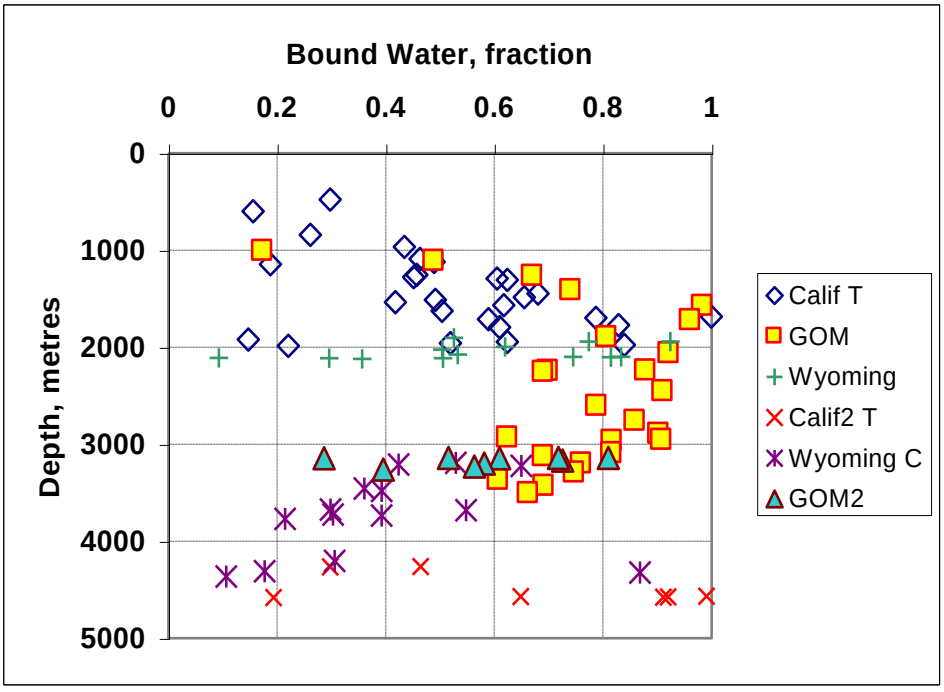

.

Figure 5.11: Bound water fraction derived from Equation 4.11 for laboratory measured CEC data from Patchett (1975). Porosity was velocity-derived using wellbore data reported by Patchett (1975).

Chapter 6: Application to Pore Pressure Prediction

Up to this point, this thesis has been concerned with understanding how to measure bound water in mudstones and how bound water reduces permeability, and cause the entrapment of overpressures. This chapter introduces the development of a software package called P3 that helps put the concepts to practice. Much of what follows is drawn from participant feedback in pore pressure prediction courses taught by the author. That is, drilling engineers, geologists, and geophysicists have been part of the referee process for methods set out below and have been directly responsible for the development of the P3 software. A new term (PPG_o) is here introduced to express the pore pressure gradient in offshore deepwater conditions.

6.01 Fundamentals of Pore Pressure Prediction

To understand the basics of pressure prediction methods, consider four normal compaction parameters V_n, R_n, P_n and σ_n where V_n is normal interval velocity, R_n is normal resistivity, P_n is normal pore pressure, and σ_n is normal vertical effective stress. A value for P_n is generally known from regional catalogue data and V_n is known from seismic or sonic data or from global velocity-versus-depth trends. The global acoustic trend in P3 is an adaptation of Heasler and Kharitonova (1996) as was shown in Figure 5.7. As an option, Alberty and McLean (2003) proposed a smectite/illite trend line.

Next consider the dimensionless abnormality factors V/V_n, R/R_n, P/P_n and σ'/σ'_n where velocity (V), resistivity (R), pore pressure (P) and effective stress (σ') are reduced to a relative number by dividing by the corresponding normal value. As an example, if P/P_n is 1.5, pore pressure is 1.5 times higher than normal.

Now suppose that relative stress (σ'/σ'_n) is set equal to relative velocity (V/V_n) raised to a power as given by the following equation.

$$\sigma'/\sigma'_n = (V/V_n)^x \qquad [6.01]$$

This is the Eaton pressure prediction formula (Eaton, 1976) in which the empirical exponent (x) varies between 2.8 and 5.5 as demonstrated in Figure 6.1. This dimensionless relationship is attractive because the parameters can be expressed in any (consistent) set of units.

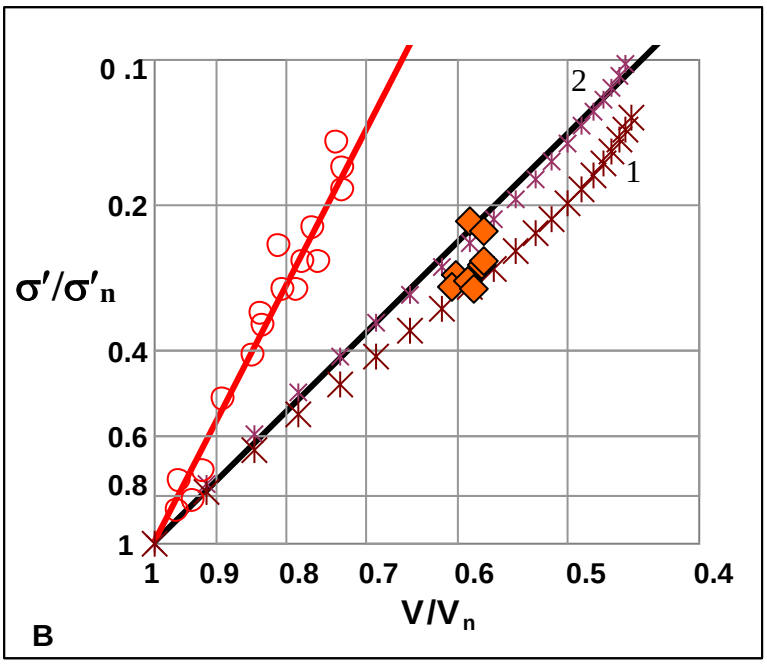

Figure 6.1: A log-log plot of σ'/σ'_n versus V/V_n with data from Well A (diamonds) and from Hottman and Johnson, 1965 (circles). The red line is an Eaton exponent of 5.5 and the black line is an exponent of 2.8. The crosses represent the expected relationship for a retention depth (equivalent depth) model, assuming (1) a vertical stress model and (2) a mean stress model. To generate the expected values (crosses) effective stress was calculated, at increments, from a retention depth at 1000m to a depth of 8000m, i.e., along line A-B in Well A in Figure 5.7. In accordance with a retention depth model (Ham, 1966a), σ'/σ'_n was set equal to σ'_e/σ'_n where σ'_e is the normal-compaction effective stress at the retention depth. For Case 1 (bottom set of crosses), effective stress was taken equal to $D(OBG_o\text{-}NPG_o)$ where D is depth below sea floor, OBG_o is normal lithostatic gradient referenced to sea floor, and NPG_o is normal pore pressure gradient, referenced to sea floor. For Case 2 (top set of crosses), effective stress was taken as $D(OBG_o\text{-}NPG_o)(1+2k)/3$ where k is a horizontal to vertical stress ratio as defined in the text. For this exercise, NPG_o was set equal to 1.074 g/cc (0.465 psi/ft) based on local knowledge of formation water density, and OBG_o was set to $(16.3+(D/952)^{0.6})/8.335$ g/cc based on local knowledge of average bulk rock density (Traugott, 1997). The stress ratio (k), to represent a high side case, was assumed to increase with depth as characterized by the empirical equation $0.039\ (D/0.305)^{0.33}$ (Traugott, 1997). The velocity function (V_n), for normal compaction, was taken as $10^6/(180+(639-180)\exp(-D/1965))$ with parameters adjusted to agree with actual velocity data above the retention depth (from Heasler and Kharitonova, 1996). For verification, a second set of values was computed (but not shown) where D was held constant at 3500 metres and the retention depth varied in increments from 1000 to 3500 metres. The results were nearly identical to that presented above. As a point of interest, the Hottman and Johnson data in the plot (re-published by Lane and Macpherson, 1976, to three place precision) represents a full range of gradients from 1.24 to 2.24 g/cc (0.54 to 0.97 psi/ft). That is, a value of 0.1 for σ'/σ'_n is a reasonable lower limit as displayed.

As a resistivity variant of the equation, one can set σ'/σ'_n equal to $(R/R_n)^{1.2}$ where now the exponent (for resistivity) can be defined explicitly as having a global value of 1.2 from published data (e.g., Lane and Macpherson, 1976). And last, $(V/V_n)^x$ can be set equal to $(R/R_n)^{1.2}$ as a method to determine x when both resistivity and velocity data are available. This last relationship, taken from an idea set out by Kerimov et al. (1996), is implemented in P3 as an experimental option.

As a troublesome point, it has been noted that Equation 6.01 seems incorrect at the end point, i.e., V cannot (physically) go to zero when σ' goes to zero (G.L. Bowers, personal communication). This issue will be addressed later but the importance here is that the equation, like other empirical relationships, is accurate over a useful range.

As another point, consider how Equation 6.01 may change if expressed as mean effective stress, as proposed by Harrold et al. (1999) and Moore and Tobin (1997). One may recall that mean-effective stress in terms of the three principal stresses is just $(\sigma'_1+\sigma'_2+\sigma'_3)/3$. This reduces to $\sigma'_1(1+2k)/3$ with k defined as σ'_3/σ'_1 and σ'_2 set equal to σ'_3 (assuming transversely isotropic conditions). If k is not pressure dependent, relative vertical stress, σ'/σ'_n, equals relative mean stress, $(\sigma'(1+2k)/3)/(\sigma'_n(1+2k)/3)$, i.e., the (1+2k)/3 terms cancel. That is, the Eaton model is effectively a mean stress relationship.

6.02 Pressure Gradients – a New Standard

Pore pressure (P) is commonly given as a gradient as (P/D)(CF) where D is vertical depth measured from derrick floor and CF is a conversion factor that converts to equivalent mud density, e.g., specific gravity (SG), kg/m^2, or lbs/gal. A part of CF is the gravitational constant that converts force to mass. For common oil field units (i.e., psi, feet and lbs/gal) CF is 19.25. In common terminology equivalent mud density is symbolized as PPG (pore pressure gradient).

PPG is a serviceable way to express overpressures if water depth (D_W) is zero and if the height of the drilling rig (H) is small, i.e., H<<D. For this case PPG is essentially an abnormality coefficient: e.g., if the PPG is 1.5 SG (13 lbs/gal), pore pressure is about 1.5 times higher than normal hydrostatic (actually 1.44 times higher if normal hydrostatic is, say, 1.04 SG). The use of abnormality coefficients has been a common way to express overpressures in Russia (Belonin and Slavin, 1998).

But PPG is not a helpful way to describe overpressure gradients in deepwater environments. For example, if the abnormality factor is 1.5, it translates to an

equivalent mud density of 13 lbs/gal if D_W is zero. But if D_W equals D/2 it can be easily shown that it translates to a PPG of only 10.8 lbs/gal, where 10.8 is simply the weighted average of seawater density (8.6) and formation abnormality (13). Expressing overpressure in absolute terms (e.g., MPa) is one solution. But pressure is a measurement whereas pressure gradient is a physical property.

A better solution is to express overpressures in terms of interval gradient (PPG_o) in which the interval is defined as the depth below seafloor (D_{BSF}). Mathematically, $PPG_o=(P-P_o)/(D_{BSF})$ where P_o is measured pressure at the seafloor. The relationship between PPG and PPG_o is expressed by the following two equations (from Traugott and Swarbrick, 2002)

$$PPG = (D_{BSF} \times PPG_o + D_W \times G_{sw}) / D \quad [6.02]$$

$$PPG_o = (PPG \times D - D_W \times G_{sw}) / D_{BSF} \quad [6.03]$$

where G_{sw} is the density of the seawater expressed in the same units as PPG. Note that the equations are dimensionless as long as consistent units are used, i.e., it does not matter if D and D_{BSF} are in feet or metres. The physical meaning of PPG and PPG_o is equivalent mud density. PPG is the density of a single mud column extending from the derrick floor to depth D, the hydrostatic pressure of which is exactly equal to formation pore pressure. PPG_o is the density of a dual-density system that produces the same hydrostatic pressure at the formation. As an explanation, a dual-density system is the way the top leg of every deepwater well is drilled, i.e., the interval drilled before installing a riser to the surface. The mud system has two parts - seawater from sea level to seafloor and mud from the sea floor to D. Thus, PPG in Equation 6.02 is simply the weighted average of the two parts.

Expressing pressure gradients as PPG_o is a new standard that evolved as part of this research (Traugott and Swarbrick, 2002). It simplifies greatly velocity-derived pressure predictions as illustrated in Figure 5.9. The procedure is to enter interval the velocity difference. This gives PPG_o. Next PPG is computed from Equation 6.02. A special attribute of this procedure is, that since D in Equation 6.02 is a function of the height of the derrick floor, PPG calculations can be easily adjusted if rig specifications are changed. An alternate practice presented by Kan and Swan (2001) that relates

velocity difference directly to PPG (instead of PPG_o) requires a complex adjustment of parameters for each water depth condition.

A parallel to Equation 6.02 is development of matching equations for overburden (lithostatic) gradients (OBG) and normal pressure gradient (NPG), as illustrated below where OBG_o is the average bulk sediment density and NPG_o is the average formation water density, expressed in the same set of units as PPG.

$$OBG = (DBSF \times OBG_o + D_W \times G_{sw}) / D \quad [6.04]$$

$$OBG_o = (OBG \times D - D_W \times G_{sw}) / D_{BSF} \quad [6.05]$$

$$NPG_o = (NPG \times D - D_W \times G_{sw}) / D_{BSF} \quad [6.06]$$

6.03 Effective Stress

It is important to note that effective stress (σ') can be expressed either in terms of OBG or OBG_o as shown below.

$$\sigma' = (OBG - PPG) \times D \quad [6.07]$$

$$\sigma' = (OBG_o - PPG_o) \times D_{BSF} \quad [6.08]$$

As a fundamental principle, note from Equation 6.08 that seawater depth does not affect effective stress, and thus does not affect compaction, velocity, porosity, or amount of overpressure. To state the principle more strongly, interval velocity at 1000 metres below sea floor is the same regardless if water depth is 1 metre or 1000 metres, given that other parameters (e.g., lithology) are constant. This explains why the core data collected a few feet below sea floor by Thompson et al. (1977) recorded about the same porosity regardless of water depth.

Bound water effects could cause uncertainty in the above effective stress equations. For example, Murad and Cushman (1996), Lade and De Boer (1997), and Bennethum et al. (1997) suggested that the standard Terzaghi effective stress law should be modified in mudstones to account for the hydration stress of the bound water. The effect may be non-linear (Teew, 1971). As a counterpoint, Kwon et al. (2001) gave convincing evidence that the above effective stress equations are correct for tight

mudstones. It could be debated that a variance in the effective stress laws from that expressed by Equation 6.07 and 6.08 is more problematic in explicit pressure prediction methods like that developed by Harold et al. (1999). That is, errors are partly cancelled in the Eaton ratio implementation where the ratio is the division of effective stress at one state divided by the effective stress at a second state.

6.04 Model-Derived Pore Pressure

Basin modelling based on permeability and sedimentation rate is an important pore pressure prediction method (Katsube and Williamson, 1994; England et al., 1987). Smith (1973), for example, used modelling to show that the sharpness of the transition zone below thick hydro-pressured sandstones sections is a function of the exponent in the permeability/porosity relation. A simple 1d basin model is included in P3 as a guide. Complex basin modelling, as used in the industry, requires a determination of mudstone permeability. For experimentation, P3 includes the Sen model form Chapter 2.

6.05 Acoustic-Derived Pore Pressure

To understand acoustic methods consider this derivation of the Eaton equation based on Baldwin and Butler (1985) and Issler (1992). From Baldwin and Butler (1985) $\sigma'=C'\ (1-\Phi)^{\beta}$ where C' equals a compaction parameter and β is equal to 9.348 for average mudstone (Holbrook, 1999). From Issler (1992), $(1-\Phi)=(V/V_{ma})^{(1/2.19)}$ where Φ is porosity. Combining the two yields the following equation.

$$\sigma' = C'\ (V/V_{ma})^{4.29} \qquad [6.09]$$

If one writes the same relation for normal stress (i.e., in terms of σ'_n and V_n), it leads to a second equation as shown below.

$$\sigma'_n = C'\ (V_n/V_{ma})^{4.29} \qquad [6.10]$$

Now if one divides Equation 6.09 by Equation 6.10, the parameters C' and V_{ma} cancel and the result is the Eaton equation as listed above (Equation 6.01), where x is 4.29 which is about an average of that in Figure 6.1. In practice a value of 3 or 5.5 is taken for x depending on conditions as illustrated in Figure 6.1.

This derivation should not be taken as endorsement for the Baldwin and Butler (1985) compaction model. It is only used here as a way to determine the Eaton exponent and to illustrate that the form of the Eaton equation is logical. One might debate that a soil mechanics compaction model is better (Harrold et al., 1999) or that an exponential model is best (Shi and Wang, 1986). As a consideration, Shi and Wang pointed out that the soil mechanics model goes negative at deep depths.

If the Eaton equation (Equation 6.01) is written in standard form as a function of pressure gradients, as shown below, an important difference becomes apparent from the published equation (Eaton, 1976). There are two separate overburden terms with which to deal. One is OBG and another is nOBG, where nOBG is the overburden gradient if compaction had been normal. This modification is an improvement to the Eaton relationship (but an incrementally small improvement).

The two equations below give identical results if NPG correctly accounts for the rig elevation.. The preference in P3 is to use Equation 6.12 and to convert to PPG using Equation 6.02, once water depth and rig elevation are known.

$$PPG = OBG - (nOBG\text{-}NPG)\,(V/V_n)^3 \qquad [6.11]$$

$$PPG_o = OBG_o - (nOBG_o\text{-}NPG_o)\,(V/V_n)^3 \qquad [6.12]$$

To address the end-point issue, i.e., the noted objection that, in the Eaton equation, velocity converges to zero at zero effective stress, consider the following examination of the empirical relationships between stress ratio and velocity ratio in Figure 6.1. Clearly the relationship is linear and well behaved to a velocity ratio (V/V_n) of 0.45. For an Eaton exponent of 2.8 this corresponds to a stress ratio (σ'/σ'_n) of about 0.1, which is a reasonable minimum value for compaction-generated overpressures as demonstrated in Figure 5.6. Only two data points in Figure 5.6 have an effective stress ratio less than 0.1 and these two data points are likely the result of a gating depth effect and would have an exponent of 5.5. For an exponent of 5.5 the Eaton equation is linear for the full data range as was illustrated in Figure 6.1. Therefore, the perceived end point problem appears to be a non-issue.

6.06 Shale Discrimination

The Eaton velocity relation (and most prediction methods) works only for mudstones and shales, i.e., shale/non-shale discrimination has to be a major part of the exercise. And shale discrimination is difficult with seismic data but easier with borehole data where gamma ray data are available for shale/non-shale identification. Presgraf (written by this author and now commercialised by Landmark) uses, with success a CEC discrimination where CEC is computed from a Waxman/Smits model assuming a bound water fraction of 100 percent (Waxman and Smits, 1968). The problem with the Presgraf implementation is twofold. Bound water is not 100 percent in mudstones, and CEC (expressed as a weight percent) decreases with depth as bulk density increases, such that a large scanning window is required to cover all depth ranges. P3 uses a better implementation where (1) CEC is computed more accurately from a Patchett model as discussed here, and (2) CEC is expressed as Q_v, i.e., as a percent pore volume (see Equation 2.18) where BW is proportional to Q_v. As seen in Figure 6.2, BW is less variable with depth. As a point of interest for Presgraf users, since it is known from this work that bound water is not 100 percent in mudstones, CEC values computed in Presgraf are too high (about twice too high if the true bound water averages 50 percent). This was previously suspected based on limited comparison to measured data.

6.07 P3 Software

Software called P3 has been developed as a part of this research. P3 is focused toward 1d pressure prediction in regions of deep water. P3 works well for drilling groups doing well planning and for geophysical groups doing calibration of 2d and 3d prediction tools, e.g., Presgraf. P3 is new. It is not a derivative of Presgraf. The discussion that follows is a summary of the software. The reader can view the user guide on the attached CD for more details.

P3 is a Visual Basic application that uses the engines in Excel for data storage, manipulation, and plotting. To the non-Excel user, complex Excel features are opaque, e.g., Figure 6.2 is the simple front panel in P3 where the Excel menu bar is not visible. The experienced user still has excess to all Excel features such as scaling plots.

A main component of P3 is a spreadsheet called the ***Stack***. Data and pressure predictions are stored in two partitions in the ***Stack***. One partition (the master) stores data referenced to depth below sea floor including formation test pressures (FT_o), interval velocity (V), leak off test data (LOT_o), mud density (MW_o), overburden

gradients (OBG_o), and predicted pore pressure (PPG_o). The second partition in the ***Stack*** stores a copy of pertinent data referenced to derrick floor. Values in this partition change dynamically when the user changes water depth or rig height. The ***Stack*** allows the user to project predictions and/or well data to any water depth or rig height.

The main features in P3 are borehole-derived BW and CEC and BW-derived shale discrimination (as a supplement to the gamma ray) using Equations 2.11 and 4.10. Features also include user-defined tools for developing and testing new models for Φ, CEC, BW, and PPG_o.

To understand basic P3 operations, consider the following workflow for a well in Venture field in Canada. Data are taken from Mudford and Best (1989) and selected because formation pressure data are available. This is a normal workflow to calibrate the well data, with extrapolation to a deepwater prospect on trend -i.e., to a well with unknown pressure gradients. Another application of the normal workflow would be as a calibration step before applying the relationships to seismic data in regions where pore pressure is unknown.

The first procedure in the workflow is data entry. All imported pressure-related data (e.g., formation pressure or mud density) are automatically converted to a seafloor reference using Equation 6.03 before adding to the ***Stack***. This allows data from several wells from several different water depths and rig heights to be stacked together.

Next is a diagnostic step. P3 automatically displays a diagnostic plot like that in Figure 6.4 when the predict pressure option is selected. A menu for selection of pressure prediction methods is also displayed. In Figure 6.3, one can observe an (overpressure?) anomaly at a depth of about 4600 metres on the acoustic data, but not on the density data.

A logical next procedure (among several options) is selection of an acoustic model prediction option, with overlay of measured data. This step, in this example, leads to a gross underprediction of pore pressure as seen in Figure 6.4. A logical next step would be to change the Eaton exponent to a value of 5.5 to match pressure data (Figure 6.5). To verify the atypical shift in exponent, a best practice would be to display BW and CEC, as displayed in Figure 6.2. The spike in BW at 4500 metres and the departure of density-derived BW values, to excess of 1.0, is indicative of a gating depth condition.

The last step in the workflow is unique. When the pressure interpretation (at the calibration well) is considered correct, projection to a location is needed at the next drill site to a location where water depth and rig height are different. This is no problem in P3: a new water depth and rig height is simply associated with the ***Stack*** and P3 adjusts

all gradients to the new conditions. For example, not shown is a projection of Venture data to prospect A (actually a real case) with a water depth of 1000 metres. All of the predictions and all of the Venture formation tests (and leak off test data if they had been available) are extrapolated to prospect A.

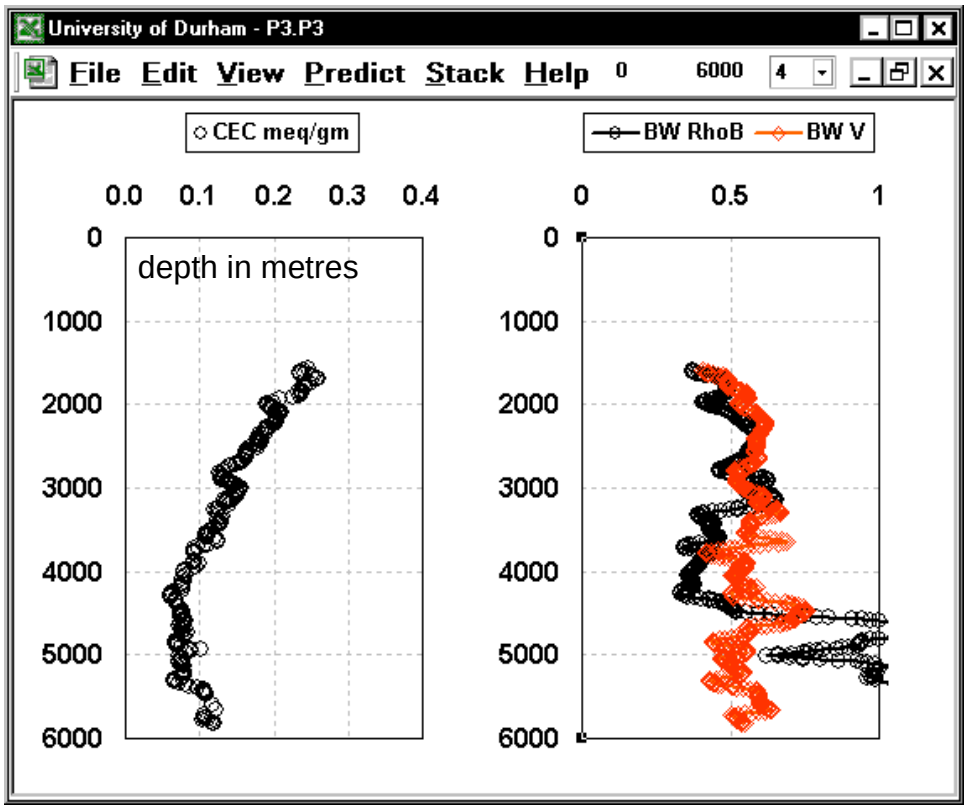

Figure 6.2: CEC from Equation 2.11 for a well in Venture field in Canada. Bound water (BW) from Equation 4.11 for porosity density derived (black) and velocity derived (red).

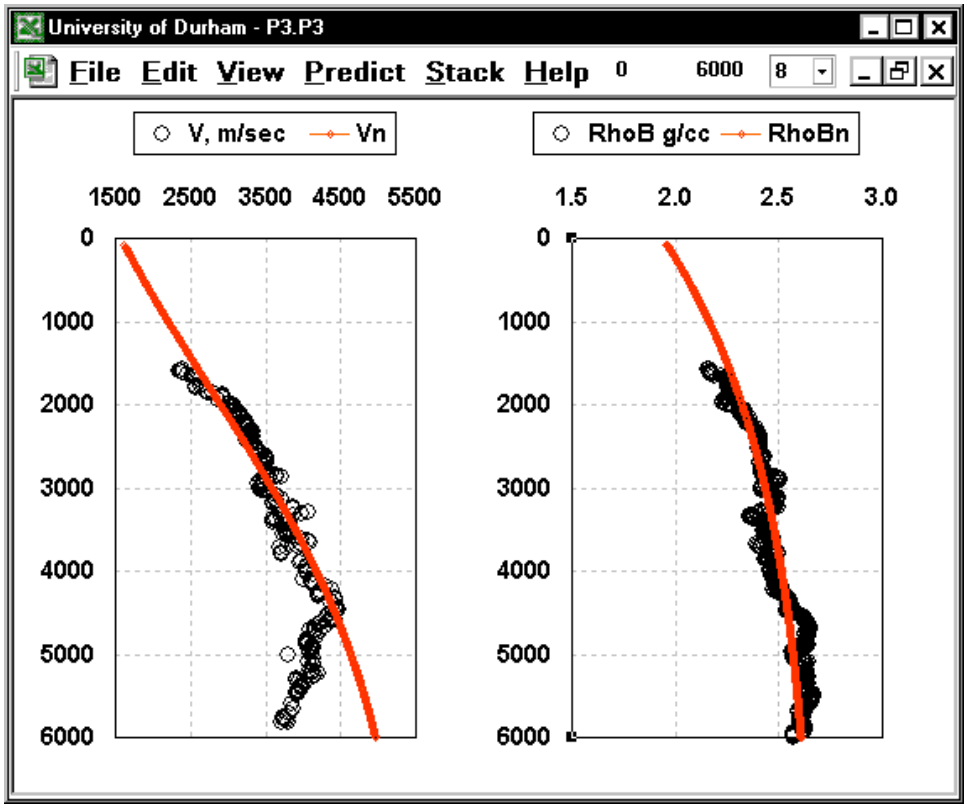

Figure 6.3: Same well as Figure 6.2. Shows raw data and normal compaction lines from model with options that allow for interactive adjustments of normal (red) trend lines.

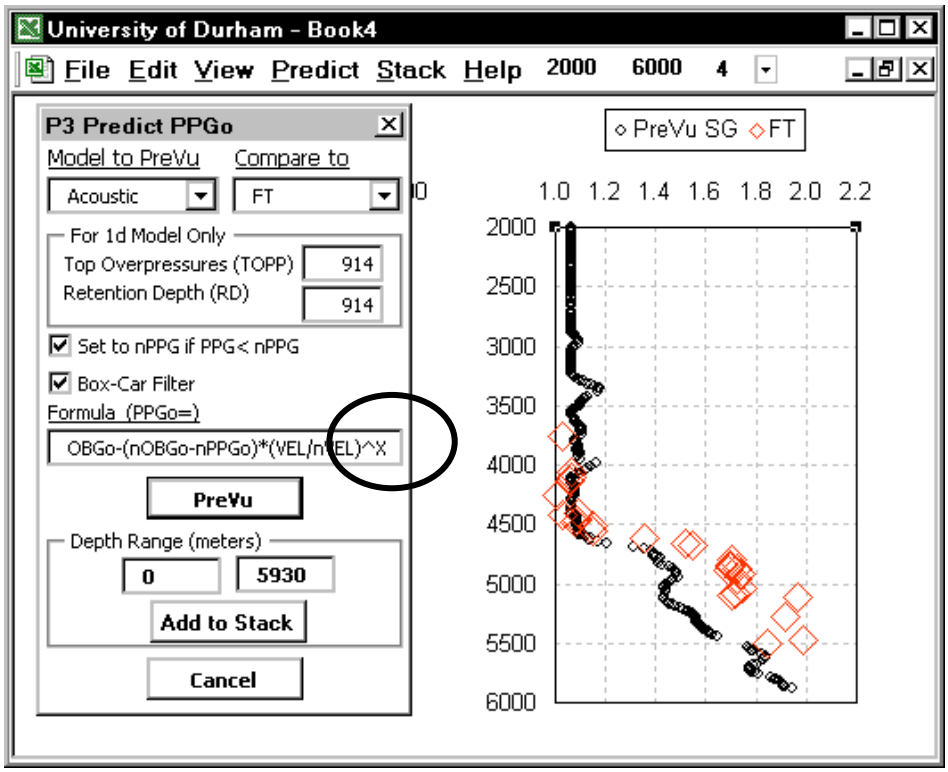

Figure 6.4: Results for a preview (PreVU) of acoustic-derived pressure gradient (SG) compared to measured formation pressure gradient (FT). The formula box is active.

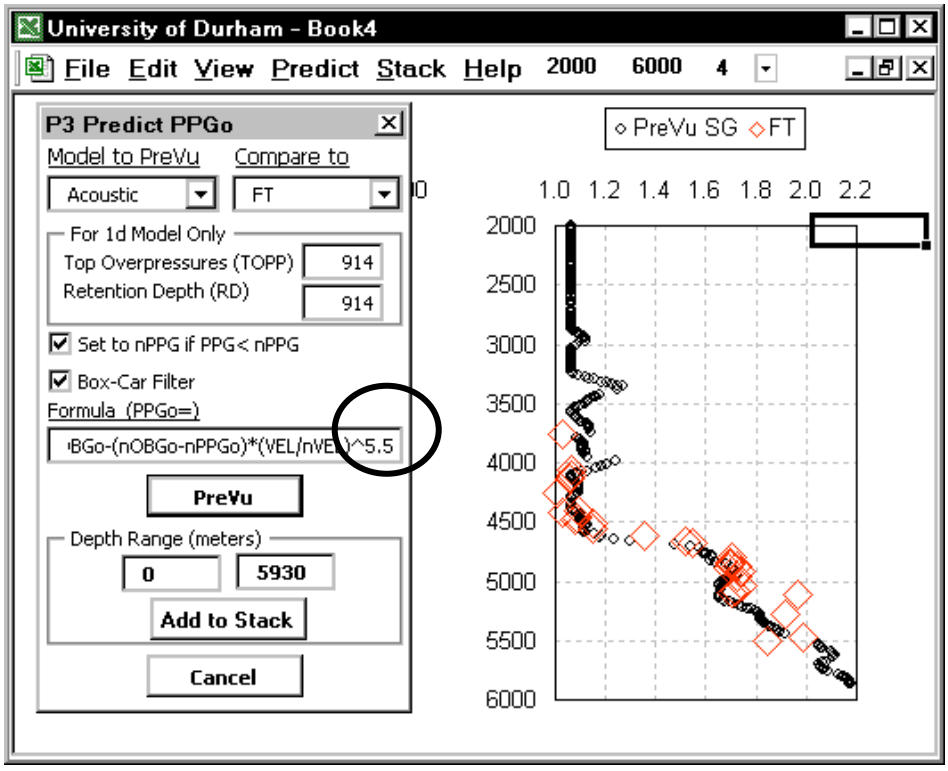

Figure 6.5: Same as Figure 6.4 but with the exponent in the formula box changed to 5.5. Notice the agreement with measured values (FT). Depth is in metres.

Chapter 7: Conclusions and Discussion

This research has established a link between overpressures and the surface-charge and bound-water properties of mudstones. It has been demonstrated that both anion exclusion and differential-scanning calorimetric data give the same value for the weight of bound water per cation-exchange capacity (i.e., V_Q is about 0.27 g/meq). In addition, this research has introduced a simple single-point suction method for determining bound water (in the laboratory) and has developed a new borehole method for measuring bound water in the subsurface. Most importantly, it is reasoned that the density of bound water increases sharply at a critical depth of burial (a gating depth) as a result of surface charge changes. In addition, as an adjunct part of this research, a software package (P3) has been created for putting the concepts to practice. A detailed discussion of the uncertainties involved with some of these conclusions is addressed below, with recommendations for future improvement.

7.01 Uncertainties in Single-Point Suction Measurements

Suction procedures are simple and have been evaluated at Durham on several chalk and shale samples. Results are shown in Table 1. Samples were humidity-dried at about 50 percent relative humidity for two months. Mass (W_{wet}) was determined with a precision balance (four place accuracy is required). The samples were heated to 105 °C to remove bound water and the mass (W_{dry}) measured. W_{50} equals $(W_{wet}-W_{dry})/W_{dry}$. Next, W_b was estimated as 1.62 W_{50} and the bound water fraction was computed by Equation 4.09. An important conclusion about single point measurements is the demonstration that W_b does not directly equal W_{50} as used by Robinson et al. (2002) and Dirksen and Dasberg (1993). There is a multiplier to apply (i.e., 1.62).

Sample	W_{wet}	W_{dry}	W_{57}	W_b	Porosity	BW	Residuals
Chalk	12.03834	11.99179	0.00388	0.00660	0.150	0.01	9.09
Chalk	13.84579	13.82107	0.00179	0.00304	0.165	0.04	2.88
Chalk	15.70309	15.52299	0.01160	0.01972	0.080	0.62	47.35
Chalk	14.12059	14.08326	0.00265	0.00451	0.055	0.21	6.57
Chalk	15.51313	15.48529	0.00180	0.00306	0.070	0.11	3.24
Shale-921	9.74382	9.43661	0.03256	0.05534	0.140	0.92	100.00
Shale-925	14.64810	14.22103	0.03003	0.05105	0.140	0.85	100.00

Table 1: A suction test of chalk and shale samples. Residuals are the percent sediment remaining after dissolving in acid, i.e., a measure of clay and silica content.

But the procedure does not come without uncertainties. Consider the absorption data from Delage et al. (1998) for soft mudstone plotted in Figure 7.1 and 7.2. Clearly there is variance in W between 45 and 55 percent relative humidity, i.e., W_b determined at 45 percent will differ from that determined at 55 percent. Newman (1993) did not consider such variance as a source of error in his classic paper. In contrast, Bigorre et al. (2000) measured suction at two points and related both to CEC.

A better practice introduced here is to measure suction at several different relative humidity values, and to use an apex method to determine W_b. This is illustrated in Figures 7.1 and 7.2. The apex can be determined one of two ways. The ratio of RH/W can be calculated to determine the peak value, as illustrated in Figure 7.2, or a line can be drawn through the origin, tangent to the sigmoid shaped curve in Figure 7.1. The point of tangency is the apex. Both methods are identical in the determination of the apex. It is assumed here that $W_b=W_{apex}$ whereas for the single point method $W_b=1.62\ W_{47}$. Note from Figure 7.1 that W_{apex} is about 1.5 times W_{47}. That fact reflects a second uncertainty in the single point method – the value for the (1.62) multiplier in the single point method.

The rationale for assuming $W_b=W_{apex}$ is as follows: Zone 1 on the plot in Figure 7.2 is bound water adsorption. (There is no hysteresis in this zone, i.e., it is the same for the drying or wetting cycle.) Zone 2 is a pore size zone caused by condensation of water in pores in accordance with Kelvin's law. Swelling and external surface effects may also be a component of Zone 2. One can reason that the slope reversal, identified by the apex, is the transition from full bound water to the start of condensation into the pores. To test the concept it was applied to an argon adsorption curve for a case where W_b was determined independently using a DSC method (Wallacher and Knorr, 2001). Both methods gave essentially the same value for W_b. The salt solutions needed for establishing the five or six relative humidity values are given in Table 2.

Salt	RH %	Comments	Reference
K_2SO_4	97		Delage et al., 1998
KCl	85	80 at 50° C	Greenspan, 1977
NaCl	76	76 at 10°C	Delage et al., 1998
NaBr	58	(-0.67 % change per degree)	As Above
$Mg(NO_3)_2$	55		As Above
$LiNO_3$	47		Newman, 1983
K_2CO_3	43	43 at 50°C	Greenspan, 1977
$MgCl_2$	33	34 at 10° C	Delage et al., 1998
LiCl	12	14 at 10° C	As Above
ZnCl	10	(-0.2 % change per degree)	As Above

Table 2: A list of relative humidity for different saturated salt solutions.

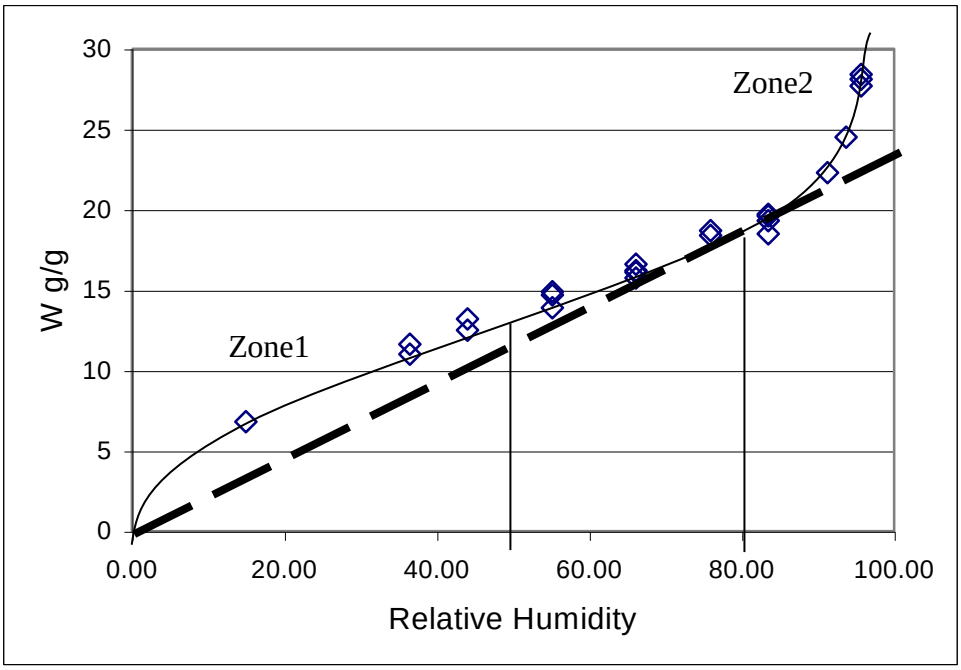

Figure 7.1: Water content versus relative humidity from Delage et al. (1998). The Apex is defined as the tangent of a line drawn to the origin.

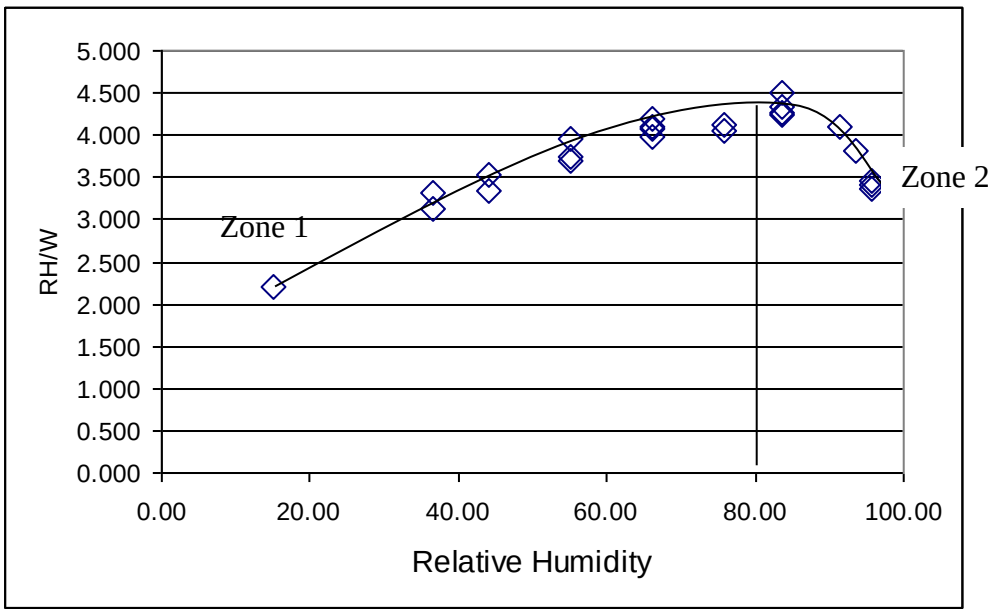

Figure 7.2: Example of the apex method on data shown in Figure 7.1.

7.02 Uncertainties in Acoustic-Derived Porosity

The Issler transform is used here and in P3 to determine porosity in mudstones as part of bound water determinations. This is common practice, e.g., see Audet (1996), Stump and Flemings (2002), and Harrold et al. (1999). But the practice is somewhat troubling because there is no effective stress term in the equation (see Equation 2.02). Also matrix velocity is held constant. Althaus (1974) and Traugott (1997) argued that matrix velocity should vary with depth, i.e., with effective stress.

Figure 7.3 shows velocity versus effective stress for a mudstone sample (similar to samples observed from a GeoPoP collection). Velocity is presented as a relative value to compare directly to sandstone data from Eberhart-Phillips et al. (1989). It would appear that mudstones are less sensitive to effective stress. This too was the conclusion by Johnston (1987). But things are less clear if most of the observed stress sensitivity is a laboratory artefact. According to Vernik (1998) data up to 40 MPa are questionable. Accepting this premise, the data in Figure 7.3 were scaled in reverse order (see Figure 7.4). Now it appears that mudstones have about the same sensitivity (to effective stress) as sandstones, above an effective stress value of 20 MPa.

To test a notion that the concern is unimportant, linear regressions were run on the Issler data set (Issler, 1992). When predicting velocity from porosity data, the regression coefficient improved sharply when depth was included as a second variable in the regression (depth was used as a proxy for effective stress which was not available). This result is reasonable since knowledge of effective stress is needed to predict velocity. But when the regression was inverted to predict porosity from velocity, adding depth did not improve the regression at all. That is, effective stress is not needed (apparently) to predict porosity from velocity data. Thus, use of the simple Issler relation is justified. Perhaps this result is not surprising since one knew from the Eaton relationship that effective stress is intrinsically captured in the velocity term.

As a counterpoint, the effective-stress term in the common EHZ relationship (Eberhart-Phillips et al. 1989) is statistically significant when correlating velocity to porosity. But the reason is simple: the porosity term in the EHZ data is a fixed porosity value at 50 MPa for each data sample. That is, porosity at each effective stress was not recorded.

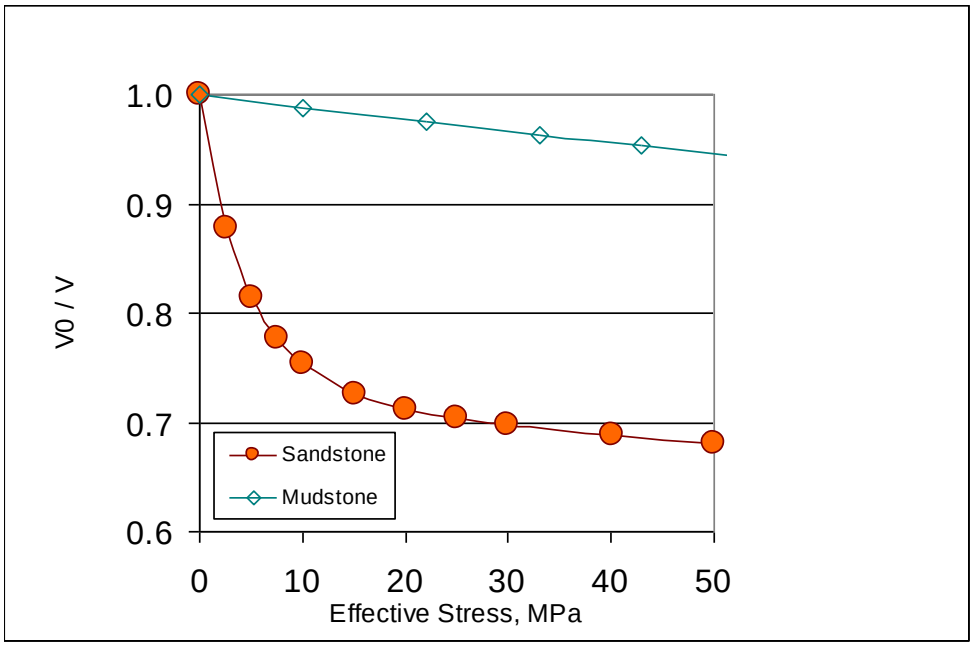

Figure 7.3: Comparison of interval velocity between mudstone (from Johnston, 1987) and average sandstone (from Eberhart-Phillips et al., 1989) normalized by dividing velocity at zero effective stress by velocity at given stress.

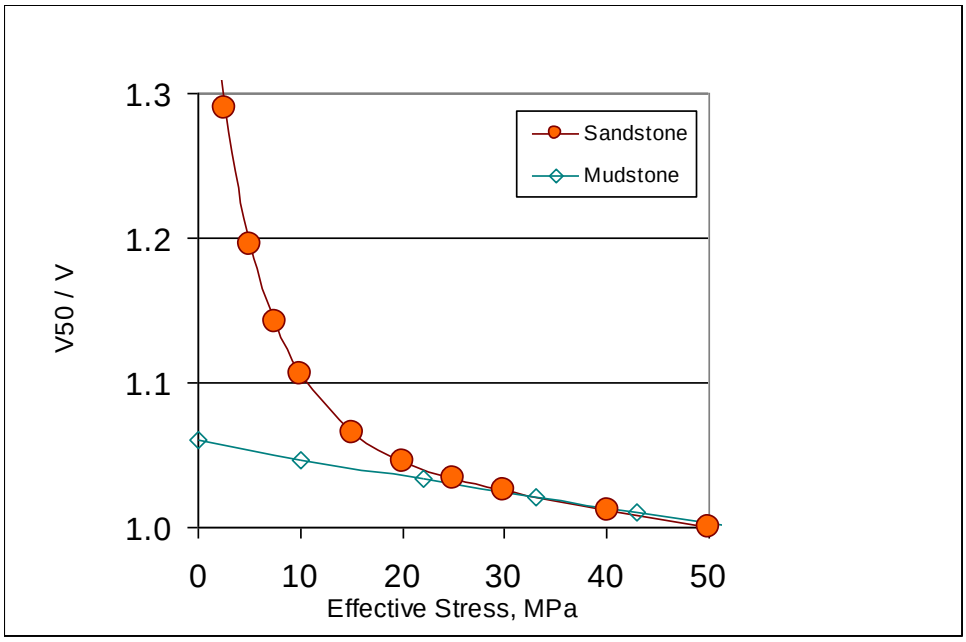

Figure 7.4: Data in Figure 7.3 plotted in reversed order i.e. normalized to velocity at an effective stress of 50 MPa. The plot suggests that sandstones and mudstones are similar if data below 20 MPa are clipped.

7.03 Uncertainties in Immersion-Derived Porosity

The recommended laboratory method for determining porosity is immersion porosimetry (using equation 2.04) but one point to consider is the saturation procedure. Katsube et al. (1992) described saturating the sample with deionised, distilled water, degassing in a vacuum chamber for 15 minutes and wiping dry with a kimwipe to remove surface moisture. Katsube et al. (2000), however, described a different procedure. The sample is saturated with deionised water in a beaker with just enough to fully cover the sample. The beaker is placed at room conditions until all the excess water evaporates leaving only a moist sample. One might wonder which is best and if saturation with seawater would provide different results, particularly in view of work by Watanabe and Mizoguchi (2002) showing salinity effects of the bound water volume.

Another issue is fluid density and salt effects. It is assumed that ions that contribute to bound water return to the soil matrix when dried (cited in Saarenketo, 1998). Blum as referenced by Henry (1997) offered a more general equation (Equation 7.01) that accounts for pore-fluid density and salt fraction (S) that is precipitated during drying. Henry (1997) used a value of 35 percent for S for mudstone analysis. To test the uncertainty of grain density, Henry (1997) showed with error analysis (Equation 7.02) that the uncertainty in Φ is less than 0.05 for an uncertainty range of 2.5 to 3 g/cc for ρ_{grain}. Note that porosity is expressed as a fraction in the equations.

$$\Phi = \frac{(M_{wet} - M_{dry})/(1-S)\rho_{fluid}}{(M_{wet} - M_{dry})/(1-S)\rho_{fluid} + [M_{dry} - (M_{wet} - M_{dry})S/(1-S)]/\rho_{grain}} \quad [7.01]$$

$$\Delta\Phi = \Phi(1-\Phi)\Delta\rho_{grain} / \rho_{grain} \quad [7.02]$$

7.04 Uncertainties in Bound Water Density

The conclusion that bound water condenses to a dense phase at the gating depth is addressed carefully in this thesis. This author is mindful of the polywater scandal of the late 1960's, in which scientists claimed to directly measure a dense water state on solid surfaces - claims that ended in ignominy with discovery of laboratory errors (Ball, 2001).

Israelachvili and Wennerstrom (1996) also cautioned against assuming that bound water is more dense than ordinary water.

Giese and Oss (2002) added greatly to the understanding of the bound water density. They show that AB water is less dense than ordinary water and LW water is denser where AB and LW refer to energy states. According to Giese and Oss (2002) less dense water is associated with swelling properties and more dense water will be non-swelling.

In this research, it is assumed that bound water is denser than ordinary water below the gating depth where high surface charge effects cause dielectric saturation and large electrostriction compression. Part of the justification has been based on the work from IBM laboratories that showed dense water on charge electrodes (Toney et al., 1994, 1995) and the research from Danielewicz-Ferchmin and Ferchmin (1996, 1998) supporting Toney's work.

But the IBM work has not gone without challenge. Halley et al. (1998), Yeh and Berkowitz (1999b) and Yeh and Berkowitz (2000) questioned the basic density interpretation. Senapati and Chandra (2000), Schweighofer et al. (1996), and Bopp et al. (1998) attempted to reproduce the results of Toney (1994, 1995) with molecular modelling, but failed to duplicate the dense water phase. In contrast, Nakamura et al. (2002) appeared to verify those experimental results. In summary, the serious challenge to a dense phase comes from molecular simulations and, as noted in Chapter 1, simulators are particularly problematic in accounting for water density.

It is important to understand that a component of bound water density is the density of the counter-ion layer that, as noted, has a molar concentration of 5 to 20. According to Wolf et al. (1985) the density of a sodium chloride solution is 1.2 for a molar concentration of 5.3 at ambient conditions.

7.05 Uncertainties with Resistivity-Derived Parameters

Application of resistivity-derived procedures for determining CEC, BW, and PPG requires a discussion of the temperature effects on electrical conductivity. The effect of temperature on resistivity is so large that Khatchikian (2001) proposed using near-wellbore variations in resistivity as a means to determine formation temperature. To add more complexity to the temperature issue, Gravestock (1991) demonstrated that the change in resistivity for a given change in temperature increases as CEC increases. This conclusion agrees with Johnston (1987) who found experimentally that the activation

energy is higher for mudstones than for clay free sandstones. Sen and Goode (1992) analysed data for shales from Vinegar and Waxman (1994) and Waxman and Thomas (1974) and linked the sensitivity effect to activity levels. Revil et al. (1997) also worked the temperature problem and presented similar results.

To circumvent the temperature issue, the regression used here to determine CEC from Patchett's (1975) data (Equation 2.11) took temperature as an independent variable, i.e., instead of explicitly correcting resistivity for temperature (a non-trivial process) the temperature dependence was handled statistically. The regression coefficient reported for Equation 2.11 is slightly better than that reported by Patchett (1975) who used an explicit temperature correction before doing regression. In general, resistivity data should be temperature corrected before use in pressure prediction models (Traugott, 1997).

7.06 Uncertainties in Temperature/Pressure effects on Bound Water

Clearly this issue requires discussion: e.g., Gurevich and Chilingarian (1997) stated (without evidence) that bound water is released in the sub-surface at a formation temperature of 60 to 80 ºC. Moreover it is commonly known that bound-water dehydration occurs at 105° C at atmospheric conditions.

In contrast, Faulkner and Rutter (2000) found that normal effective stress stabilizes bound water in the subsurface. Skipper et al. (2000) and his co-workers used time-of-flight neutron diffraction on clays to show that bound water is stable to a depth of about 3000 metres for undrained conditions for typical pore pressure and temperature gradients.

Colton-Bradley (1987) illuminated the issue by showing that isotropic, undrained compaction retards bound water dehydration but drained compaction accelerates dehydration. To say this differently, a closed overpressured compartment would retain bound water, with subsequent burial, while a normal pressured system that drains to the surface (because of differential stresses) would lose bound water. The Colton-Bradley work was based on Gibbs energy calculations. While it can be questioned (D. H. Powell, 2002, personal communication), it does appear to agree with empirical observations. The concept could be tested with a thermodielectric experiment in which the dielectric constant is measured on a mudstone sample while compacting.

According to Juhasz (1979), data from Shell Development (unpublished) show that bound water fraction does not decrease with increasing temperature - i.e., V_Q is

constant with depth. Clavier et al. (1984), however, used another set of Shell Development data to show that it does decrease with increasing temperature, by as much as 30 percent at 200 °C. They suggested that V_Q could be as low as 0.15 at 200 °C (at ambient pressure). As more evidence for a temperature effect, Lee (1980) and Cho et al. (2000) showed an increase in hydraulic conductivity in mudstones with increasing temperature commensurate with a reduction in bound water volume. (On analysis the variation can be accounted by viscosity variations with temperature.) Added to the picture is theoretical work cited by Renard and Ortoleva (1997) that indicates the thickness of the double layer (partly made up of bound water) is a function of temperature.

Based on empirical data from Bush and Jenkins (1977) for shaly sandstones and Bigorre et al. (2000) for soils and clays, the bound water fraction at 60 ºC is about half that at ambient conditions, as illustrated by these two equations.

W_{45}=0.097 CEC Shaly sandstones (at 60 ºC) [7.03]

W_{46}=0.189 CEC-0.0170 Soil and clays (at 20 ºC) [7.04]

Jones and Or (2002) showed a thermodielectric effect on saturated clay that they interpreted as a decrease in bound water with increase in temperature, i.e., dehydration of bound water. Johari (2000) cited a similar thermodielectric observation but both experiments were at ambient pressure. This is in agreement with Yan, Low and Roth (1996) who showed that H-bonding, and thus W_b, decrease with increasing temperature.

The thermoelectric experiment noted above is interesting. Jones and Or (2002) found that the dielectric constant of a saturated sand/clay sample increased when heated. This is the reverse of what is expected from Curie's law (Booth, 1951). The logical interpretation is that low dielectric bound water was converted to (high dielectric) free water. Bergman et al. (2000) used the thermodielectric experiments on clay samples at reduced temperatures and found results similar to those reported by Singh et al. (2001) on spent chicken, i.e., increased bound water at reduced temperature.

7.07 Main Conclusions and Recommendations

A comprehensive analysis of bound water data from several diverse sources has led to a new understanding of pore pressure prediction in mudstones. The picture that

emerges is that bound water percent pore volume increases with compaction as free pore water is expelled. With increasing depth, surface charge tends to increase and at some critical depth, defined as the gating depth, the bound water layer condenses and bound water density increases. Below the gating depth, expulsion of bound water can result in a volume expansion and can increase pore pressure (for future investigation).

A new recommended practice is measurement of W_b in mudstone samples. Gravimetric methods are simple and inexpensive and can be used in any laboratory with a balance and oven. Where possible, total surface area measurements should be included. A simple procedure from Cerato and Lutenegger (2002) is copied in the appendix. Other recommendations describe here are the new PPG_o standard for expressing pressure gradient, and a new way to compare resistivity and acoustic ratio data for the prediction of the Eaton exponent, and the onset of a gating depth process.

To confirm the bound water and gating depth hypothesis, more analytical work is required. Some recommendations for future work are listed below:

- Collect dielectric log data recorded as part of the petrophysical evaluation in selected oil and gas wells during the 1970's and 1980's. A decrease in dielectric constant with depth in mudstones would confirm the increase in BW with depth, predicted in the gating depth concept. Note that dielectric logging has been in disuse for several years.

- Investigate methods to measure the electric field directly at the water/solid interface. Use of the Stark effect is one method to consider. An increase in the surface charge with depth as predicted should be associated with an increase in electric field strength. Lockhart and Kim (1972) show that Stark effect tests are complex and require special apparatus.

- Collect X-ray diffraction data on mudstone samples, using the procedure set out by Sato et al. (1996), to confirm the effect of beidellite on retention and gating depths. It has been suggested here, without data, that the increase in surface charge with depth in Figure 5.2 is the result of an increase in surface charge associated with beidellitization. Note that standard X-ray data do not differentiate between montmorillonite and beidellite, i.e., both are reported as part of the smectite group.

- Develop new methods to measure bound water density. One possibility is the use of helium porosimeters to measure the pore volume in laboratory samples before and after removing bound water. Comparison of volume change to weight change, from standard gravimetric measurements, would give bound water density.

- Develop methods for measuring BW fraction on core samples to confirm log-derived methods. An increase in BW greater than 60 percent may be associated with a gating depth. An example of a simple method is given above.

- Investigate a possible link between formation temperature and the occurrence of shallow overpressures in deep water, where the seafloor temperature is about 5 ºC, as shown in Figure 5.3. A new notion is introduced here is that bound water on a mudstone particle increases 40 percent as it migrates from sea level to sea floor during sedimentation in deep water. If so, it is thought that the associated decrease in permeability will produce a shallow retention depth. This notion is based on the work of Singh et al. (2001) who reported a 40 percent increase in bound water on spent chicken as temperature was reduced from ambient to 5 ºC. Martin (1960) reported similar results on clays.

References

Abdullah, W.S., Alshibli, K.A. and Mohammed, M.S., 1999, Influence of pore water chemistry on the swelling behavior of compacted clays, *Applied Clay Science*, v. 15, p. 447-462.

Adams, N. and Young, R., 2004, Underground blowouts: What you need to know, *World Oil*, v. 225, n. 1. p.

Akbar, N., Mavko, G., Nur, A. and Dvorkin, J., 1994, Seismic signatures of reservoir transport properties and pore fluid distribution, *Geophysics*, v. 59, n. 8, p. 1222-1236.

Alberty, M.W. and McLean, M.R., 2003, Emerging Trends in Pressure Prediction, Paper OTC 15290, *Offshore Technology Conference*, Houston, Texas, U.S.A., 5-8 May 2003.

Alkhalifah, T, and Tsvankin, I., 1995, Velocity analysis for transversely isotropic media, *Geophysics*, v. 60, n. 5, p. 1550-1556.

Althaus, V.E., 1974, Calibration of the sonic log to calculate porosity in the deep abnormal pressured Tertiary of south Louisiana, *Society of Professional Well Log Analysts*, *15th Annual Logging Symposium*, June 2-5, 1974, Houston, Texas, Paper I.

Amba, S.A., Chilingar, G.V. and Beeson, C.M., 1964, Use of direct electrical current for increasing the flow rate of reservoir fluids during petroleum recovery, *Journal of Canadian Petroleum Technology*, v. 3, n. 1, p. 8-14.

Anderson, D.M. and Low, P.F., 1957, Density of water adsorbed on Wyoming Bentonite, *Nature*, v. 180. p. 1194.

Antoniou, A.A., 1964, Phase transformations of water in porous glass, *The Journal of Physical Chemistry*, v, 68, n. 10, p. 2754-2763.

Audet, D.M., 1996, Compaction and overpressuring in Pleistocene sediments on the Louisiana shelf, Gulf of Mexico, *Marine and Petroleum Geology*, v. 13, n. 5, p. 467-474.

Avena, M.J. and De Pauli, C.P., 1998, Proton adsorption and electrokinetics of an Argentinean Montmorillonite, *Journal of Colloid and Interface Science*, v. 202, p. 195-204.

Bagchi, K., Balasubramanian, S. and Klein, M.L., 1997, The effects of pressure on structural and dynamical properties of associated liquids: Molecular dynamics calculations for the extended simple point charge model of water, *Journal Chemical Physics*, v. 107, n. 22, p. 8561-8567.

Baker, L.J., 1984, The effect of the invaded zone on full wavetrain acoustic logging, *Geophysics*, v. 49, n. 6, p. 796-809.

Baldwin, B. and Butler, C.O., 1985, Compaction Curves, *The American Association of Petroleum Geologists Bulletin*, v. 69, n. 4, p. 622-626.

Ball, P., 2001, Water turns to jelly under pressure, *Nature News Service Web Site*, August 17, 2001.

Basu, S. and Sharma, M.M., 1994, Effect of dielectric saturation on disjoining pressure in thin films of aqueous electrolytes, *Journal of Colloid and Interface Science*, v. 165, p. 355-366.

Basu, S. and Sharma, M.M., 1997, An improved space-charge model for flow through charged microporous membranes, *Journal of Membrane Science*, v. 124, p. 77-91.

Barrat, J.-L., 1999, Large slip effect at a nonwetting fluid-solid interface, *Physical Review Letters*, v. 82, n. 23, p. 4671-4674.

Barrat, J.-L. and Bocquet, L, 1999, Influence of wetting properties on hydrodynamic boundary conditions at a fluid/solid interface, *Faraday Discussion*, v. 112, p. 119-128.

Bekele, E.B., Person, M.A. and Rostron, B.J., 2000, Anomalous pressure generation within the Alberta Basin: implications for oil charge to the Viking formation, *Journal of Geochemical Exploration*, v. 69-70, p. 601-605.

Bellissent-Funel, M-C., Chen, S.H. and Vanotti, J-M., 1995, Single particle dynamics of water molecules in confined spaces, *Physical Review E*, v. 51, n. 5, p. 4558-4569.

Belonin, M.D. and Slavin, V.I., 1998, Abnormally High Formation Pressures in Petroleum Regions of Russia and Other Countries of the C.I.S., *in* Law, B.E., Ulmishek, G.F, and Salvin, V.I. (editors): *Abnormal Pressures in Hydrocarbon Environments: The American Association of Petroleum Geologists Memoir 70*, p. 115-121.

Bennethum, L, Murad, M.A. and Cushman, J.H., 1997, Modified Darcy's law, Terzaghi's effective stress principle and Fick's law for swell clay soils, *Computers and Geotechnics*, v. 20, n. 3, p. 245-266.

Bergman, R. and Swenson, J., 2000, Dynamics of supercooled water in confined geometry, *Nature*, v. 403, p. 283-285.

Bergman, R., Swenson, J., Börjesson, L. and Jacobsson, P., 2000, Dielectric study of supercooled 2D water in a vermiculite clay, *Journal of Chemical Physics*, v. 113, n. 1, p 357-363.

Best, M.E. and Katsube, T.J., 1995, Shale permeability and its significance in hydrocarbon exploration, *The Leading Edge*, March 1995, p. 165-170.

Bhattacharyya, K. and Bagchi, B., 2000, Slow dynamics of constrained water in complex geometries, *Journal Physical Chemistry A*, v. 104, p. 10603-10613.

Bigorre, F, Tessier, D. and Pédro, G., 2000, Contribution des argiles et des matiéres organiques á la reténtion de l'eau dans les sols. Signification et rôle fondamental de la

capacité d'échange en cations, *C.R. Acad Sci. Paris, Sciences de la Terre et des planets/ Earth and Planetary Sciences*, v. 330, p. 245-250.

Bjorlykke, K., 1996, Lithological control on fluid flow in sedimentary basins, *in* Jamtveit, B. and Yardley, B.W.D. (editors): *Fluid flow and transport in rocks – Mechanisms and Effect*, Chapman and Hall, p. 15-34.

Bleam, W.F., 1993, Atomic theories of phyllosilicates quantum chemistry, statistical mechanics, electrostatic theory, and crystal chemistry, *Reviews of Geophysics*, v. 31, n. 1, p. 51-73.

Blum, P., 1994, Index Properties. *In ODP Shipboard laboratory Manual*, College Station, Texas, (Ocean drilling Program).

Bocker, J., Gurskii, Z. and Heinzinger, K., 1996, Structure and dynamics at the liquid Mercury – Water interface, *Journal Physical Chemistry*, v. 100, p. 14969-14977.

Bocquet, L and Barrat, J.-L., 1993, Hydrodynamic boundary conditions and correlation functions of confined fluids, *Physical Review Letters*, v. 70, n. 18, p. 2726-2729.

Boek, E.S., Coveney, P.V. and Skipper, N.T., 1995, Molecular modelling of clay hydration: a study of hysteresis loops in swelling curves of sodium montmorillonites, *Langmuir*, v. 11, p.4629-4631.

Bolt, G.H., 1956, Physico-chemical analysis of the compressibility of pure clays, *Geotechnique*, v. VI, p. 86-93.

Bolton, A.J., Maltman, A.J. and Clennell, M.B., 1998, The importance of overpressure timing and permeability evolution in fine-grained sediments undergoing shear, *Journal of Structural Geology*, v. 20, n. 8, p. 1013-1022.

Bonaccurso, E., Kappl, M. and Butt, H.-J., 2002, Hydrodynamic force measurements: Boundary slip of water on hydrophilic surfaces and electrokinetic effects, *Physical Review Letters*, v. 88. n. 7, 18 February 2002.

Borner, F.D. and Schon, J.H., 1991, A relation between the quadrature component of electrical conductivity and the specific surface area of sedimentary rocks, *The Log Analyst*, September-October, p. 612-613.

Booth, F., 1951, The dielectric constant of water and the saturation effect, *The Journal of Chemical Physics*, v. 19, n. 4, p. 391-394 and p. 1327 and p. 1615.

Bopp, P.A., Kohlmeyer, A. and Spohr, E., 1998, Computer simulations of electrochemical systems, *Electrochimica Acta*, v. 43, n. 19-20, p. 2911-2918.

Borden, D. and Giese, R.E., 2001, Baseline studies of the clay minerals society source clays: Cation exchange capacity measurement by the ammonia-electrode method, *Clays and Clay Minerals*, v. 49, n. 5, p. 444-445.

Bourgoyne, A.T., Chenevert, M.E., Millheim, K.K. and Young, F.S., 1991, Applied Drilling Engineering, *Society of Petroleum Engineers Textbook Series*, v. 2, p. 246-294.

Bowers, G.L., 2001, Determining an appropriate pore-pressure estimation strategy, Paper OTC 13042, *Offshore Technology Conference held in Houston, Texas*, 30 April-3 May 2001.

Brady, P.V., 1992, Silica surface chemistry at elevated temperatures, *Geochimica et Cosmochimica Acta*, v. 56, p. 2941-2946.

Brady, D.J., 1979, Thermodynamics of Electrolytes. Dielectric properties of water and Debye-Huckel parameters to 350º C and 1kbar. *The Journal of Physical Chemistry*, v. 83, n. 12, p. 1599-1601.

Bredehoeft, J.D., Djevanshir, R.D. and Belitz, D.R., 1988, Lateral fluid flow in a compacting sand-shale sequence: South Caspian basin, *The American Association of Petroleum Geologists Bulletin*, v. 72, n. 4, p. 416-424.

Bredehoeft, J.D. and Hanshaw, B.B., 1968, On the maintenance of anomalous fluid pressures, *Geological Society of America Bulletin*, v. 79, Issue 9, p. 1097-1106.

Bridgeman, C.H. and Skipper, N.T., 1995, A Monte Carlo study of water at an uncharged clay surface, *Journal Physics: Condensed. Matter*, v. 9, p. 4081-4087.

Brodsy, A.M., Watanabe, M., and Reinhardt, W.P., 1991, Anisotropic structures in water double layers, *Electrochimica Acta*, v. 36, Issues 11-12, p. 1689-1694.

Brovchenko, I., Paschek, D., and Geiger A., 2000, Gibbs ensemble simulation of water in spherical cavities, *Journal of Chemical Physics*, v. 113, n. 12, p. 5026-5036.

Brovchenko, I.V., Geiger, A. and Paschek, D., 2001, Simulation of confined water in equilibrium with a bulk reservoir, *Fluid Phase Equilibria*, 183-184, p. 331-339.

Brunauer, S, Emmet, P.H. and Teller, E., 1938, Adsorption of gases in multimolecular layers, *Journal American Chemical Society*, v. 60, p. 309-319.

Bryant, W.R. and Richardson, M.D., 1992, Permeability and porosity of clayey sediments in seismo-acoustics, *The Journal of the Acoustical Society of America*, v. 92, Issue 4, p. 2308.

Bujdak, J., Janek, M., Madejova, J. and Komadel, P., 1998, Influence of the layer charge density of smectites on the interaction with Methylene Blue, *Journal Chem. Society, Faraday Trans.*, v. 94, p. 3487-3492.

Bujdak, J. and Komadel, P., 1997, Interaction of Methylene Blue with reduced charge Montmorillonite, *Journal Physical Chemistry B*, v. 101, p. 9065-9068.

Bulat, J. and Stoker, S.J., 1987, Uplift determinations from interval velocity studies, UK southern North Sea, *in* Brooks, J. (editor): *Petroleum Geology of North West Europe*, p. 293-305.

Busenberg, E. and Clemency, C.V., 1973, Determination of the cation exchange capacity of clays and soils using an ammonia electrode, *Clays and Clay Minerals*, v. 21, p. 213-217.

Bush, D.C. and Jenkins, R.E., 1970, Proper Hydration of Clays for Rock Property Determinations, *Journal of Petroleum Technology*, July 1970, p. 800-804.

Bush, D.C. and Jenkins, R.E., 1977, CEC determinations by correlations with adsorbed water, *Society of Professional Well Analysts 18th Annual Logging Symposium*, 5-7 June 1977, paper I.

Byerlee, J., 1990, Friction, overpressure and fault normal compression, Geophysical Research Letters, v. 17, n. 12, p. 2109-2112.

Calvet, R., 1975, Dielectric properties of Montmorillonites saturated by bivalent cations, *Clays and Clay Minerals*, v. 23, p. 257-265.

Cannon, D.E., 1995, Shales: an alternate source for water resistivities, *Society of Professional Well Analysts 36th Annual Logging Symposium*, 26-29 June 1995, paper LLL.

Carcione, J.M. and Gang, A.F., 2000, Non-equilibrium compaction and abnormal pore-fluid pressures: Effects on rock properties, *Geophysical Prospecting*, v. 48, p. 521-537.

Carcione, J.M. and Tinivella, **U.,** 2001, The seismic response to overpressure: A modelling study based on laboratory, well and seismic data, *Geophysical Prospecting*, v. 49, p. 523-539.

Carnie, S.L. and Stell, G., 1982, Electrostriction and dielectric saturation in a polar fluid, *The Journal of Chemical Physics*, v. 77, issue 2, p. 1017-1026.

Carrique, F., Arroyo, F.J. and Delgado, A.V., 2002, Electrokinetics of concentrated suspensions of spherical colloidal particles with surface conductance, arbitrary zeta potential, and double-layer thickness in static electric fields, *Journal of Colloid and Interface Science*, v. 252, p. 126-137.

Carstens, H., 1978, Origin of abnormal formation pressures in central North Sea lower Tertiary clastics, *The Log Analyst*, March-April, p.24-28.

Carstens, H. and Dypvik, H., 1981, Abnormal formation pressure and shale porosity, *The American Association of Petroleum Geologists Bulletin*, v. 65, n. 2, p. 344-350.

Carrier, M. and Soga, K., 1999, A four terminal measurement system for measuring the dielectric properties of clay at low frequencies, *Engineering Geology, v. 53, p. 115-123.*

Caurie, M., 1981, Derivation of full range moisture sorption isotherms, In L.B. Rockland & G. F. Steward, *Water activity:Influences on food quality*, New York: Academic Press, p. 63-87.

Cerato, A.B. and Lutenegger, A.J., 2002, Determination of surface area of fine-grained soils by the Ethylene Glycol Monoethyl Ether (EGME) method, Geotechnical Testing Journal, v. 25, n. 3, paper ID# GTJ200210035_253.

Champion, A.R., Vaughan, R.W. and Drickamer, H.G., 1967, Effect of pressure on the Mossbauer resonance in ionic compounds of iron, *The Journal of Chemical Physics*, v. 47, n. 8, p. 2583-2590.

Chan, D.Y.C. and Horn, R.G., 1985, The drainage of thin liquid films between solid surfaces, *Journal of Chemical Physics*, v. 83, n. 10, p. 5311-5324.

Chang, F., Skipper, N.T. and Sposito, G., 1998, Monte Carlo and Molecular Dynamics simulations of electrical double-layer in potassium-montmorillonite hydrates, *Langmuir*, v. 14, p. 1201-1207.

Chavez-Paez, M., de Pablo, L. and de Pablo J.J., 2001a, Monte Carlo simulations of Wyoming sodium montmorillonite hydrates, *Journal of Chemical Physics*, v. 114, n. 3, p. 1405-1413.

Chelidze, T.L. and Guegen, Y. 1999, Electrical spectroscopy of porous rocks: a review – I. Theoretical models, *Geophysics Journal International*, v. 137, p. 1-15.

Chenevert, M.E. and Sharma, A.K., 1993, Permeability and Effective Pore Pressure of Shales, *Transactions American Institute of Mining Engineers*, v. 295. Reprinted in 1999 in *Society of Petroleum Engineers Reprint Series No. 49*, p. 71-77.

Cheng, L., Fenter, P., Nagy, K.L., Schlegel, M.L. and Sturchio, N.C., 2001, Molecular-scale density oscillations in water adjacent to a mica surface, *Physical Review Letters*, v. 87, n. 15.

Chilingar, G.V. and Knight, L., 1960, Relationship between pressure and moisture content of kaolinite, illite, and montmorillonite clays, *Bulletin of the American Association of Petroleum Geologists*, v. 44, no. 1, p. 101-106.

Chiou, C.T. and Rutherford, D.W., 1997, Effects of exchanged cation and layer charge on the sorption of water and EGME vapors on montmorillonite clays, *Clays and Clay Minerals*, v. 45, n. 6, p. 867-880.

Cho, W., Lee, J., and Kang, C., 2000, Influence of temperature elevation on the sealing performance of a potential buffer material for a high-level radioactive waste repository, *Annals of Nuclear Energy*, p. 1271-1284.

Churchman, G., Askary, M., Peter, P., Wright, M., Raven, M.D. and Self, P.G., 2002, Geotechnical properties indicating environmental uses for an unusual Australian bentonite, *Applied Clay Science*, v. 20, p. 199-209.

Clavier, C., Coates, G. and Dumanoir, J., 1984, The theoretical and experimental bases of the "dual water" model for the interpretation of shaly sands, *Society of Petroleum Engineering Journal*, April 1984, p. 153-168.

Cleveland, J.P., Schaffer, T.E. and Hansma, P.K., 1995, Probing oscillatory hydration potentials using thermal-mechanical noise in an atomic-force microscope, *Physical Review B*, v. 52, n. 12, p. 52.

Coelho, R., 1979, Physics of Dielectrics for the Engineer, *Elsevier Scientific Publishing Company*, Oxford.

Colten-Bradley, V.A., 1987, Role of pressure in smectite-dehydration – Effects on geopressure and smectite-to-illite transformation, *The American Association of Petroleum Geologists Bulletin*, v. 71, n. 11, p. 1414-1427.

Connolly, J.A.D. and Podladchikov, Y.Y., 2000, Temperature-dependent viscoelastic compaction and compartmentalization in sedimentary basins, *Tectonophysics*, v. 324, Issue 3, p. 137-168.

Connor, J.N. and Horn, R.G., 2001, Measurement of aqueous film thickness between charged mercury and mica surfaces: a direct experimental probe of the Poisson-Boltzmann distribution, *Langmuir*, v. 17, p. 7194-7197.

Courivaud, F., Hansen, E.W., Karlsson, A., Kolboe, S. and Stocker, M., 2000, Pulsed field gradient NMR study of the diffusion of n-hexane confined in hydroxylated and dehydroxylated MCM-41 of various pore diameters, Microporous and Mesoporous Materials, v. 35-36, p. 327-339

Coussot, P., 1998, Pore size NMR imaging, *Magnetic Resonance Imaging*, v. 16. n. 5/6, p. 621-623.

Cui, Y.J., Yahia-Aissa, M. and Delage, P., 2002, A model for the volume change behavior of heavily compacted swelling clays, *Engineering Geology*, v. 64, p. 233-250.

Danielewicz-Ferchmin, I. and Ferchmin, A.R., 1996, Water Density in the double layer, *Journal Physical Chemistry*, v. 100, p. 17,281-17,286.

Danielewicz-Ferchmin, I. and Ferchmin, A.R., 1998, Mass density in hydration shells of ions, *Physica B*, v. 245, p. 34-44.

Danielewicz-Ferchmin, I., Ferchmin, A.R. and Szlaferek, A., 1998, On the interrelation between charge and mass densities within a double layer, *Chemical Physics Letters*, v. 288. p. 197-202.

Das, S.K., Sharma, M.M. and Schechter, R.S., 1996, Solvation force in confined molecular fluids using Molecular Dynamics simulations, *Journal Physical Chemistry*, v. 100, p. 7122-7129.

David, F., Vokhim, V. and Ionova, G., 2001, Water characteristics depend on the ionic environment. Thermodynamics and modelisation of the aquo ions, *Journal of Molecular Liquids*, v. 90, p.45-62.

de Franco, R., 2001, Interval velocity and thickness estimate from wide-angle reflection data, *Geophysical Prospecting*, v. 49, p. 395-404.

Delage, P., Howat, M.D. and Cui, Y.J., 1998, The relationship between suction and swelling properties in a heavily compacted unsaturated clay, *Engineering Geology*, v. 50, p. 31-48.

de Lima, O.A.L. and Niwas, S., 2000, Estimation of hydraulic parameters of shaly sandstone aquifers from geoelectrical measurements, *Journal of Hydrology*, v. 235, p. 12-26.

Delville, A. and Letellier, M., 1996, ^{1}HMR study of the structure and dynamics of water confined between wetting solids, *Magnetic Resonance Imaging*, v. 14, n. 7/8, p. 975-977.

Delville, A. and Pellenq, R.J.-M., 1997, A Monto Carlo (N,V,T) study of the stability of charged interfaces: A simulation on a hypersphere, *Journal Chemical Physics*, v. 106, p. 7275-7285.

Delville, A., Gasmi, N., Pellenq R. J.-M., Caillol, J.M. and Van Damme, H., 1998, Correlation between the stability of charged interfaces and ionic exchange capacity: A Monte Carlo study, *Langmuir*, v. 14, 5077-5082.

Delville, A., 1999, (N,V,T) Monte Carlo simulations of the electrostatic interaction between charged colloids: Finite size effects, *Journal Physical Chemistry B*, v. 103, p. 8296-8300.

Demircan, G., Smith, J.R. and Bassiouni, Z., 2000, Estimation of shale cation exchange capacity using log data: Application to drilling optimisation, *Society of Professional Well Log Analysts 41st Annual Logging Symposium*, paper OO, 10 pages.

de Siqueira, A.V.C., Skipper, N.T., Coveney, P.V. and Boek, E.S., 1997, Computer simulation evidence for enthalpy-driven dehydration of smectite at elevated pressures and temperatures, *Molecular Physics*, v. 92. n. 1, p. 1-16.

de Siqueira, A.V., Lobban, C., Skipper, N.T., Williams, G.D., Soper, A.K., Done, R., Dreyer, J.W., Humphreys, R.J. and Bones, A.R., 1999, The structure of pore fluids in swelling clays at elevated pressures and temperatures, *Journal Physics: Condensed Matter*, v. 11, p. 9179-9188.

de Souza, E.F., Ceotto, G. and Teschke, O., 2001, Dielectric constant measurements of interfacial aqueous solutions using atomic force microscopy, *Journal of Modular Catalysis A: Chemical*, v. 167, p. 235.243.

Deutsch, W.L., Koerner, R.M. and Lord, A.E., 1989, Determination of pre-stress of in situ soils using acoustic emissions, *Journal of Geotechnical Engineering*, v. 115, n. 2, p. 228-245.

Dewan, J.T., 1983, Essentials of Modern Open-Hole Log Interpretation, *PennWell Books*, PennnWell Publishing Company, Tulsa, Oklahoma, U.S.A.

Dhinojwala, A. and Granick, S., 1997, Relaxation time of confined aqueous films under shear, *Journal American Chemistry Society*, v. 119, p. 241-242.

Dirksen, C. and Dasberg, S., 1993, Improved calibration of time domain reflectometry soil water content measurements, *Soil Science Society American Journal*, v. 57, p. 660-666.

Dollimore, D. and Heal, G.R., 1964, An improved method for the calculation of pore size distribution from adsorption data, *Journal Applied Chemistry*, v. 14, p. 109-114.

Drachman, S.R., Roch, G.E. and Smith, M.E., 1997, Solid state NMR characterisation of the thermal transformation of Fuller's earth, *Solid State Nuclear Magnetic Resonance*, v. 9, p. 257-267.

Drits, V.A. and Manceau, A., 2000, A model for the mechanism of Fe^{3+} to Fe^{2+} reduction in dioctahedral smectites, *Clays and Clay Minerals*, v. 48, n. 2, p. 185-195.

Du, Q., Freysz, E. and Shen, Y.R., 1994, Vibrational spectra of water molecules at quartz/water interfaces, *Physical Review Letters*, v. 72, n. 2. p. 238-241.

Dufreche, J.-F., Marry, V., Bernard, O. and Turq, P., 2001, Models for electrokinetic phenomena in montmorillonite, *Colloids and Surfaces, A: Physicochemical and Engineering Aspects*, v. 195, p. 171-180.

Dutta, N.C., 1986, Shale compaction, burial diagenesis and geopressures: A dynamic model, solution and some results, in Thermal Modeling in Sedimentary Basins edited by Jean Burrus, 1st IFP Exploration Research Conference, Carcans, France, June 3-7, 1985, Editions Technip (Paris), p. 149-172.

Dysthe, D.K. and Renard, F., 2002, Fluid in mineral interfaces – molecular simulations of structure and diffusion, *Geophysical Research Letters*, v. 29, n. 7, 4 pages.

Eaton, B.A., 1976, Graphical method predicts geopressures worldwide, *World Oil*, July 1976, p. 100-104.

Eberhart-Phillips, D., Han, D-H. and Zoback, M.D., 1989, Empirical relationships among velocity, effective pressure, porosity, and clay content in sandstone, *Geophysics*, v. 54, n. 1, p. 82-89.

Eberl, D.D., 1993, Three zones for illite formation during burial diagenesis and metamorphism, *Clays and Clay Minerals*, v. 41, n. 1, p. 26-37.

Engelhardt, W.V. and Gaida, K.H., 1963, Concentration changes of pore solutions during the compaction of clay sediments, *Journal of Sedimentary Petrology*, v. 33, n. 4, p. 919-930.

England, W.A., MacKenzie, A.S., Mann, D.M. and Quigley, T.M., 1987, The movement and entrapment of petroleum fluids in the subsurface, *Journal of the Geological Society, London*, v. 144, p. 327-437.

Evans, L.J., 1981, Cation exchange capacities and surface areas of humic Gleysolic Ap horizons southwestern Ontatio, *Canadian Journal of Soil Science*, v. 62, p. 291-296.

Faulkner, D.R. and Rutter, E.H., 2000, Comparisons of water and argon permeability in natural clay-bearing fault gouge under high pressure at 20º C, *Journal of Geophysical Research*, v. 105, n. B7, p. 16,415-16,426.

Fertl, W.H. and Timko, D.J., 1970, Occurrence of cemented reservoir roof rock and geopressure caprock and its implication in petroleum geology and geohydrology, *Paper 3085 presented at the 45th Annual Meeting of the Society of Petroleum Engineers,* 4-7 October, Houston, Texas, U.S.A., pp 7.

Fitts, T. and Brown, K.M., 1999, Stress-induced smectite dehydration: ramifications for patterns of freshening and fluid expulsion in the N. Barbados accretionary wedge, *Earth and Planetary Science Letters*, v. 172, p. 179-197.

Finney, C. and Kuhs, W.F., 2001, The phase diagram of water/ice and a new metastable phase of ice, from www.ill.fr/AR-97.

Franks, F., 1975, *Water, A Comprehensive Treatise, Vol. 5,* Plenum Press, New York.

Frink, L.J.D. and van Swol, F., 1994, Solvation forces and colloidal stability: A combined Monte Carlo and density functional theory approach, *Journal of Chemical Physics*, v. 100, n. 12, p. 9106-9116.

Fripiat, J.J., Chaussidon, J. and Touillaux, R., 1960, Study of dehydration of montmorillonite and vermiculite by infrared spectroscopy, *Journal of Physical Chemistry*, v. 64, p. 1234-1240.

Fripiat, J.J., Jelli, A., Poncelet, G. and Andre, J., 1965, Thermodynamic properties of adsorbed water molecules and electrical conduction in montmorillonites and silicas, *Journal of Physical Chemistry*, v. 69, p. 2185-2196.

Fröberg, J.C., Rojas, O.J. and Claesson, P.M., 1999, Surface forces and measuring techniques, *International Journal of Mineral Processing*, v. 56, p. 1-30.

Fukue, M., Minato, T., Horibe, H. and Taya, N., 1999, The micro-structure of clay given by resistivity measurements, *Engineering Geology*, v. 54, p. 43-53.

Gan, H. and Low, P.F., 1993, Spectroscopic study of ionic adjustments in the electric double layer of montmorillonite, *Journal of Colloid and Interface Science*, v. 161, n. 1, p.1-5.

Gao, J., LuedtkeW.D. and Landman, U., 1997, Layering transitions and dynamics of confined liquid films, *Physical Review Letters*, v. l79, n. 4, p. 705-708.

Garrouch, A.A. and Sharma, M.M., 1994, The influence of clay content, salinity, stress, and wettability on the dielectric properties of brine-saturated rocks: 10Hz to 10 MHz, *Geophysics*, v. 59, n. 6, p. 909-917.

Gates, W.P., Wilkison, H.T. and Stucki, J.W., 1993, Swelling properties of microbially reduced ferruginous smectite, *Clays and Clay Minerals*, v. 41,. N. 3, p. 360-364.

Gemeay, A.H., El-Sherbiny, A.S. and Zaki, A.B., 2002, Adsorption and kinetic studies of the intercalation of some organic compounds onto Na-Montmorillonite, *Journal of Colloid and Interface Science*, v. 245, p. 116-125.

Ghassemi, A. and Diek, A., 2002, Porothermoelasticity for swelling shales, *Journal of Petroleum Science and Engineering*, v. 34, p.123-135.

Gier, S and Johns, W.D., 2000, Heavy metal-adsorption on micas and clay minerals studied by X-ray photoelectron spectroscopy, *Applied Clay Science*, v. 16, p. 289-299.

Giese, R.F. and Oss, C.J., 2002, Colloid and surface properties of clays and related minerals, *Marcel Dekker, Inc*., New York.

Glover, P.W.J., Meredith, P.G., Sammonds, P.R. and Murrell, S.A.F., 1994, Ionic surface electrical conductivity in sandstone, *Journal of Geophysical Research*, v. 99, n. B11, p. 21,635-21,650.

Glover, P.W.J., Hole, M.J. and Pous, J., 2000, A modified Archie's law for two conducting phases, *Earth and Planetary Science Letters, v. 180*, p. 369-383.

Gomaa, M.M., Hussain, S.A., El-Diwany, E.A., Bayoumi A.E. and Ghobashy, M.M., 2001, A.C. electrical properties of kaolinite under pressure-pseudo random network modeling, *EAGE 63rd Conference and Technical Exhibition – Amserdam, The Netherlands*, 11-15 June 2001.

Goode, P.A. and Sen, P.N., 1988, Charge density and permeability in clay-bearing sandstones, *Geophysics*, v. 53, n. 12, p. 1610-1612.

Goode, P.A., Pietsch, A.P., Williams, N.V. and Sibbit, A.M., 1995, Determination of petrophysical parameters using wireline logs in low salinity reservoirs, *Society of Petroleum Engineers Asia Pacific Oil and Gas Conference held in Kuala Lumpur, Malaysia*, 20-22 March 1995.

Gordon, J.G., Melroy, O.R. and Toney, M.F., 1995, Structure of metal-electrolyte interfaces: copper on gold(111), water on silver(111), *Electrochimica Acta*, v. 40, no. 1, p. 3-8.

Graham, J., Yuen, K. Goh, T.B. Janzen, P. and Sivakumar, J.V., 2001, Hydraulic conductivity and pore fluid chemistry in artificially weathered plastic clay, *Engineering Geology*, v. 60, p. 69-81.

Graham, J., Halayko, K.G., Hume, H., Kirkham, T., Gray, M. and Oscarson, D., 2002, A capillarity-advective model for gas break-through in clays, *Engineering Geology*, v. 64, p. 273-286.

Gravestock, D.J., 1991, Behavior of Waxman-Smits Parameter 'B' in high Rw, high temperature reservoirs, *The Log Analyst*, September-October, 1991, p. 596-601.

Greathouse, J.A., Refson, K. and Sposito, G., 2000, Molecular dynamics simulation of water mobility in magnesium-smectite hydrates, *Journal American Chemical Society*, v. 122, p. 11, 459-11,464.

Green, M.E. and Lu, J., 1995, Monte-Carlo simulation of the effects of charges on water and ions in a tapered pore, *Journal of Colloid and Interface Science*, v. 171, p. 117-126.

Green, M.E. and Lu, J., 1997, Simulation of water in a small pore: effect of electric field and density, *Journal Physical Chemistry* B, v. 101. p. 6512-6524.

Greenspan, L., 1977, Humidity fixed point of binary saturated aqueous solutions, *Journal of Research National Bureau of Standards A: Physics and Chemistry*, v. 81, p. 89-96.

Grim, R.E., 1953**,** *Clay Mineralogy*, McGraw Hill, London, p. 139 and p. 171.

Guarnieri, F. and Mezei, M., 1996, Simulated annealing of chemical potential: A general procedure for location bound waters. Application to the study of the differential hydration propensities of the major and minor grooves of DNA, *Journal of American Chemistry Society*, v. 118, p. 8493-8494.

Guggenheim, S. and Van Groos, A.F.K., 2001, Baseline studies of the clay minerals society source clays: Thermal analysis, *Clays and Clay Minerals*, v. 49, n. 5, p. 433-443.

Guidelli, R. and Schmickler, **W.,** 2000, Recent developments in models for the interface between a metal and an aqueous solution, *Electrochimica Acta*, v. 45, p. 2317-2338.

Gur, Y., Ravina, I. and Babchin A.J., 1978, On the electrical double layer theory. II. The Poisson-Boltzmann equation including hydration forces, *Journal of Colloid and Interface Science*, v. 64, Issue 2, p. 333-341.

Gurevich, A.E. and Chilingarian, G.V., 1997, Notes on the origin of formation fluid pressure: Well logging methods aspect, *Journal of Petroleum Science and Engineering*, v. 17, p. 321-330.

Halley, J.W., Mazzolo, A., Zhou, Y. and Price, D., 1998, First-principles simulations of the electrode|electrolyte interface, *Journal of Electroanalytical Chemistry*, v. 450, p. 273-280.

Ham, H.H., 1966a, A method of estimating formation pressures from Gulf Coast well logs, *Transactions – Gulf Coast Association of Geological Societies*, v. XVI, p. 185-187.

Ham, H.H., 1966b, New charts help estimate formation pressures, the Oil and Gas Journal, December 19, 1966, p.58-63.

Hansen, E.W., Schmidt, R. and Stocker, M., 1996, Pore structure characterization by ^{1}H NMR using water, benzene, and cyclohexane as probe molecules, *Journal Physical Chemistry*, v. 100, p. 11,396-11,401.

Hansen, E.W., Stocker, M. and Schmidt, R., 1996, Low-temperature phase transition of water confined in mesopores probed by NMR influence on pore size distribution, *Journal Physical Chemistry*, v. 100, p. 2195-2200.

Hansen, S., 1996, A compaction trend for Cretaceous and Tertiary shales on the Norwegian shelf based on sonic transit times, *Petroleum Geoscience*, v. 2. p. 159-166.

Harrold, W.D., Swarbrick, R.E. and Goulty, N.R., 1999, Pore Pressure Estimation from Mudrock Porosities in Tertiary Basins Southeast Asia, The *American Association of Petroleum Geologists Bulletin*, v. 83, n. 7, p. 1057-1067.

Hartnig, C., Witschel, W. and Spohr, E., 1998, Molecular dynamics study of the structure and dynamics of water in cylindrical pores, *Journal Physical Chemistry*, v. 102, p. 1241-1249.

Hawkins, R.K. and Elgelstaff, P.A., 1980, Interfacial water structure in montmorillonite from neutron diffraction experiments, *Clays and Clay Minerals*, v. 28, n. 1, p. 19-28.

Headley, L.C., 1970, Fluid flow in channels, capillaries, and porous media under the influence of an electric field, Report 7342 U.S. Department of the Interior, Bureau of Mines.

Hearst, J.R. and Nelson, P.H., 1985, *Well Logging for Physical Properties*, McGraw Hill Book Company, New York, 571 pages.

Heasler, H.P. and Kharitonova, N.A., 1996, Analysis of sonic well logs applied to erosion estimates in the Bighorn basin, Wyoming, The *American Association of Petroleum Geologists Bulletin*, v. 80, n. 5, p. 630-646.

Hedberg, W.H., 1967, Pore-water chlorinities of subsurface shales, Ph.D Dissertation, The University of Wisconsin, Supervisors: Dr. Ivan Milne and Professor Lewis Cline.

Heinbuch, U. and Fischer, J., 1989, Liquid flow in pores: Slip, no-slip, or multiplayer sticking, *Physical Review A*, v. 40, n. 2, p. 1144-1146.

Heller-Kallai, L., 2001, Protonation-deprotonation of dioctahedral smectites, *Applied Clay Science*, v. 20, p. 27-38.

Henniker, J.C., 1949, The depth of the surface zone of a liquid, *Reviews of Modern Physics*, v. 21, n. 2, p. 322-341.

Henry F., Gaudillat, M., Costa L.C. and Lakkis, 2002, Free and/or bound water by dielectric measurements, *2nd Internaltional Workshop on Water in Food*, 26-27 March, Reims France.

Henry, P., 1997, Relationship between porosity, electrical conductivity, and cation exchange capacity in Barbados wedge sediments, *in* Shipley, T.H., Ogawa, Y., Blum, P. and Bahr, J.M. (editors): *Proceedings of the Ocean Drilling Program, Scientific Results*, v. 156, p. 137-149.

Hensen, E.J.M., Tambach, T.J., Bliek, A. and Smit B., 2001, Adsorption isotherms in Li-, Na-, K-montmorillonite by molecular simulation, *Journal of Chemical Physics*, v. 115, v. 7, p. 3222-3329.

Heppard, P.D., Cander, H.S. and Eggertson, E.B., 1998, Abnormal pressure and the occurrence of hydrocarbons in offshore eastern Trinidad, West Indies. *in* Law, B.E., Ulmishek, G.F, and Salvin, V.I. (editors): *Abnormal Pressures in Hydrocarbon Environments: The American Association of Petroleum Geologists Memoir 70*, p. 215-246.

Hermanrud, C., Wensaas, L., Teige, T.M.G., Nordgård Bolås, H.M., Hansen, S. and Vik, E., 1998, Shale porosities from well logs Haltenbanken (Offshore Mid-Norway) show no influence of overpressuring, *in* Law, B.E., Ulmishek, G.F, and Salvin, V.I. (editors): *Abnormal Pressures in Hydrocarbon Environments: The American Association of Petroleum Geologists Memoir 70*, p. 65-85.

Herrera-Gomez, A., Velazquez-Cruz, G. and Martin-Polo, M.O., 2001, Analysis of the water bound to a polymer matrix by infrared spectroscopy, *Journal of Applied Physics*, v. 89, n. 10, p. 5431-5437.

Heuberger, M., Zach, M. and Spencer, 2001, Density fluctuations under confinement: When is a fluid not a fluid?, *Science*, v. 292, p. 905-908.

Hill, H.J., Shirley, O.J. and Klein, G.E. (Edited by W.H. Waxman and E.C. Thomas), 1979, Bound water in shaly sands – its relation to Q_v and other formation properties, *The Log Analyst*, May-June, 1979, p. 3-19.

Hill, N.E., Vaughan, W.E., Price, A.H., and Davies, M., 1969, *Dielectric Properties and Molecular Behaviour*, van Nostrand Reinhold Company, London., p. 428-431.

Hirama, Y., Takahashi, T., Hino, M. and Sato, T., 1996, Studies of water adsorbed in porous Vycor glass, *Journal of Colloid and Interface Science*, v. 184, p. 349-359.

Holbrook, P.W., 1999, A simple closed form balanced solution for pore pressure, overburden and the principal effective stresses in the Earth, *Marine and Petroleum Geology*, v. 16, p. 303-319.

Holt, R.M., Furre, A.-K. and Horsrud, P., 1997, Stress dependent wave velocities in sedimentary rock cores: Why and why not?, *International Journal Rock Mechanics Minerals Science*, v. 34, n. 3, paper number 128, p. 399.

Horn, R.G., Smith, D.T. and Haller, 1998, Surface forces and viscosity of water measured between silica sheets, *Chemical Physics Letters*, v. 162, n. 4,5, p. 404-407

Hottman, C.E. and Johnson, R.K., 1965, Estimation of Formation Pressures from Log-Derived Shale Properties, J*ournal of Petroleum Engineering*, June 1965, p. 717.

Hrubesh, L.W., Keene, L.E. and Latorre, V.R., 1993 Dielectric properties of aerogels, *Journal of Materials Research*, v. 8, n. 7, p. 1736.

Hsieh, P.A., Tracy, J.V., Neuzil, C.E., Bredehoeft, J.D. and Silliman, S.E., 1981, A transient laboratory method for determining the hydraulic properties of 'tight' rocks – Theory, *International Journal Rock Mechanics Minerals Science and Geomechanics Abstracts*., v. 18, p. 245-252.

Hu, J., Xiao, X-D., Ogletree, D.F. and Salmeron, M., 1995, Imaging the condensation and evaporation of molecularly thin films of water with nanometer resolution, *Science*, v. 268, p. 267269.

Iiyama, T. Ruike, M. and Kaneko, K., 2000, Structural mechanism of water adsorption in hydrophobic micropores from in situ small angle X-ray scattering, *Chemical Physics Letters*, p. 395-364.

Ishida, T. and Makino, T., 1999a, Microwave dielectric relaxation of bound water to silica, alumina, and silica-alumina gel suspensions, *Journal of Colloid and Interface Science*, v. 212, p. 144-151.

Ishida, T. and Makino, T., 1999b, Effects of pH on dielectric relaxation of montmorillonite, allophane, and imogolite suspensions, *Journal of Colloid and Interface Science*, v. 212, p. 152-161.

Ishikiriyama, K., Todoki, M. and Motomura, K., 1995, Pore size distribution measurements of silica gels by means of differential scanning calorimetry, I. Optimization for determination of PSN, *Journal of Colloid and Interface Science*, v. 171, p. 92-103.

Ishikiriyama, K. and Todoki, M., 1995a, Pore size distribution measurements of silica gels by means of differential scanning calorimetry, II. Thermoporosimetry, *Journal of Colloid and Interface Science*, v. 171, p. 103-111.

Ishikiriyama, K. and Todoki, M.,1995b, Evaluation of water in silica pores using differential scanning calorimetry, *Thermochimica Acta*, v. 256, p. 213-226.

Islam, K.R., Weil, R.R., Mulchi, C.L. and Glenn, S.D., 1997, Freeze-dried soil extraction method for the measurement of microbial biomass C, *Biol Fertil Soils*, v. 24, p. 205-210.

Israelachvili, J., 1991, *Intermolecular and Surface Forces*, Academic Press.

Israelachvili, J. and Gourdon, D., 2001, Putting liquids under molecular-scale confinement, *Science*, v. 292, p. 867-868.

Israelachvili, J., McGuiggan, P., Gee, M., Homola, A., Robbins, M, and Thompson, P., 1990, Liquid dynamics in molecularly thin films, Journal Physics: Condensed Matter, v. 2, p. SA89-SA98.

Israelachvili, J. and Pashley, R.M., 1983, Molecular layering of water at surfaces and origin of repulsive hydration forces, *Nature*, v. 306, p. 249-250.

Israelachvili, J. and Wennerstrom, H., 1996, Role of hydration and water structure in biological and colloidal interactions, *Nature*, v. 379, p. 219-225.

Issler, D.R., 1992, A new approach to shale compaction and stratigraphic restoration, Beaufort-Mackenzie basin and Mackenzie corridor, northern Canada, *The American Association of Petroleum Geologists Bulletin*, v. 76, n. 8, p. 1170-1189.

Issler, D.R. and Katsube, T.J., 1994, Effective porosity of shale samples from the Beaufort-Mackenzie basin, northern Canada, Geological Survey of Canada, Research 1994-B, p. 19-26.

Johari, G.P., 2000, On the origin of heat capacity feature of annealed ices and ice clathrates, and interpreting water's diffusivity in terms of the entropy, *Chemical Physics*, v. 258, p. 277-290.

Johnson, W.L. and Linke, W.A., 1978, Some practical applications to improve formation evaluation of sandstones in the Mackenzie Delta, *Society of Professional Well Log Analysts 19th Annual Logging Symposium*, 13-16 June 1978, Paper C.

Johnson, D.L., Koplik, J. and Schwartz, L.M., 1986, New pore-size parameter characterizing transport in porous media, *Physical Review Letters*, v. 57, n. 20, p. 2564-2567.

Johnson, D.L. and Sen, P.N., 1988, Dependence of the conductivity of a porous medium on electrolyte conductivity, *Physical Review B*, v. 37, n. 7, p. 3502-3510.

Johnston, D.H., 1987, Physical properties of shale at temperature and pressure, *Geophysics*, v. 52, n. 10, p. 1391-1401.

Jones, L.E.A. and Wang, H.F., 1981, Ultrasonic velocities in Cretaceous shales from the Williston Basin, *Geophysics*, v. 46, n. 3, p. 288-297.

Jones, P.H., 1967, Hydrology of Neogene Deposits in the Northern Gulf of Mexico Basin, *in* Ferrell, R.E. and Hise, B.R. (editors): *Proceedings of the First Symposium on Abnormal Surface Pressure*, Louisiana State University, 28 April 1967, p. 91-205.

Jones, S.B. and Friedman, S.P., 2000, Particle shape effects on the effective permittivity of anisotropic or isotropic media consisting of aligned or randomly oriented ellipsoidal particles, *Water Resources Research*, v. 36, Issue 10, p. 2821-2833.

Jones, S.B. and Or, D., 2002, Surface area, geometrical and configurational effects on permittivity of porous media, *Journal of Non-Crystalline Solids*, v. 305, p. 247-254.

Jorgensen, D.G., *1988,* Estimating permeability in water-saturated formations, *The Log Analyst,* November-December, 1988, p. 401-409.

Juhasz, I., 1979, The central role of Q_v and formation-water salinity in the evaluation of shaly formations, *Society of Professional Well Logging Analysts 20th Annual Logging Symposiurm*, 3-6 June, 1979, Paper AA.

Jumikis, A.R., 1962, *Soil Mechanics*, Van Nostrand Company, Inc., Princeton, New Jersey, p. 179-181.

Kagunya, W.W., 1996, Properties of water adsorbed in anionic clays: A neutron scattering study, *Journal Physical Chemistry*, v. 100, p. 327-330.

Kahr, G. and Madsen, F.T., 1995, Determination of the cation exchange capacity and the surface area of bentonite, Illite and kaolinite by methylene blue adsorption, *Applied Clay Science*, v. 9, p. 327-336.

Kan, T.K., Kilsdonk, B. and West, C.L., 1999, 3-D geopressure analysis in the deepwater Gulf of Mexico, *The Leading Edge*, April 1999, p. 502-508.

Kan, T.K. and Swan, H.W., 2001, Geopressure prediction from automatically-derived seismic velocities, *Geophysics*, v. 66, p. 1937-1946.

Karlsson, L.E., Wesslen, B. and Jannasch, P., 2002, Water absorption and proton conductivity of sulfonated acrylamide copolymers, *Electrochimica Acta*, v. 47, Issue 20, p. 3269-3275.

Katsube, T.J,, 1993, Nano pore transport mechanism of tight shales from the Scotian shelf. In Current Research, Part D, Geological Survey of Canada, Paper 93-1D, p. 121-127.

Katsube, T.J., 2000, Shale permeability and pore-structure evolution characteristics, In Current Research, Paper 2000-E15, p. 1-8.

Katsube, T.J., Mudford, B.S. and Best, M.E., 1991, Petrophysical characteristics of shales from the Scotian shelf, *Geophysics*, v. 56, n. 10, p. 1681-1698.

Katsube, T.J. and Issler, D.R., 1993, Pore-size distribution of shales from the Beaufort-Mackenzie basin, northern Canada. In Current Research, Part E, Geological Survey of Canada, Paper 93-1E, p. 123-132.

Katsube, T.J. and Williamson, M.A., 1994, Effects of diagenesis on shale nano-pore structure and implications for sealing capacity, *Clay Minerals*, v. 29, p. 451-461.

Katsube, T.J., Issler, D.R. and Coyner, K., 1996, Petrophysical characteristics of shale from the Beaufort-Mackenzie Basin, northern Canada: permeability, formation factor, and porosity versus pressure, Geological Survey of Canada, in Current Research 1966-B, p. 45-50.

Katsube, T.J., Scromeda, N., and Connell, S., 2000, Thicknesses of adsorbed water layers on sediments from the JAPEX/JNOC/GSC Mallik 2L-38 gas hydrate research well, Northwest Territories, Geological Survey of Canada, in Current Research 2000-E5, p. 1-6.

Katsube, T.J., Scromeda, N. and Williamson, M., 1992, Effective porosity of tight shales from the Venture Gas Field, offshore Nova Scotia, in Current Research, Part D, Geological Survey of Canada, Paper 92-1D. p. 111-119.

Katz, A.J. and Thompson, A.H., 1986, Quantitative prediction of permeability in porous rock, *Physical Review B*, v. 34, n. 11, p. 8129-8181.

Kaviratna. P.D., Pinnavalia, T.J. and Schroeder, P.A., 1996, Dielectric properties of smectite clays, *Journal Physical Chem. Solids*, v. 57, n. 12, p. 1897-1906.

Keijzer, T.J.S., Kleingeld, P.J. and Loch, J.P.G., 1999, Chemical osmosis in compacted clayey material and the prediction of water transport, *Engineering Geology*, v. 53, p. 151-159.

Kendall, H.A. and Norton, P., 1974, Clay mineralogy and solutions to the clay problems in Norway, *Journal of Petroleum Technology*, January 1974, p. 25-32.

Kerimov, K.M., Chilingar, G.V. and Katz, S.A., 1996, Estimation of sonic velocity in shales in abnormally-pressured formations from resistivity data, *Journal of Petroleum Science and Engineering*, v. 15, p. 375-377.

Kern, J.W., Hoyer, W.A. and Spann, M.M., 1976, Low porosity gas sand analysis using cation exchange and dielectric constant data, *Society of Professional Well Log Analysts 17th Annual Logging Symposium*, 9-12 June 1976, paper PP.

Khaksar, A. and Griffiths, C.M., 1999, Influence of effective stress on the acoustic velocity and log-derived porosity, *Society of Petroleum Engineers, Reservoir Evaluation and Engineering*, v. 2, February 1999, p. 69-73.

Khaled, E.M. and Stucki, J.W., 1991, Iron oxidation state effects on cation fixation in smectites, *Soil Science Society American Journal*, v. 55, p. 550-553.

Khalfi, A. and Blanchart, P., 1999, Desorption of water during the drying of clay minerals. Enthalpy and entropy variation, *Ceramics International*, v. 25, p. 409-414.

Khatchikian, A., 2001, A novel method of estimation static bottomhole temperature using array induction logs, *Society of Petroleum Engineers Latin American and Caribbean Petroleum Engineering Conferenc,* Buenos Aires, Argentina, 25-28 March 2001, Paper 69605.

Klein, J. and Kumacheva, E., 1998a, Liquid-to-solid transitions in thin liquid films induced by confinement, *Physica A*, v. 249, p. 206-215.

Klein, J. and Kumacheva, E., 1998b, Simple liquids confined to a molecularly thin layers. I. Confinement-induced liquid-to-solid phase transitions, *Journal of Chemical Physics*, v. 108, n. 16, p. 6996-7009.

Kocherginsky, N.M. and Stucki, J.W., 2000, Sorption, diffusion, and desorption of Alachlor in oxidized and reduced smectite membranes, *Environmental Science Technology* v. 34, p. 3574-3578.

Kostka, J.E., Wu, J., Nealson, K.H. and Stucki, J.W., 1999, The impact of structural Fe(III) reduction by bacteria on the surface chemistry of smectites clay minerals, *Geochimica et Cosmochimica Acta*, v. 63, n. 22, p. 3705-3713.

Krooss, B.M., Schlömer, S. and Ehrlich, R., 1995, Experimental investigation of fluid flow in unfaulted and faulted pelitic rocks, *in* Jones, G. and Knipe, R. (editors): *Sealing and Fluid flow in Hydrocarbon Reservoirs,* University of Leeds, 23-25 September 1995.

Kwon, O., Kronenberg, A.K., Gangi, **A.F. and Johnson, B.,** 2001, Permeability of Wilcox shale and its effective pressure law, *Journal of Geophysical Research*, v. 106, n. B9, p. 19,339-19,353.

Lade, P.V. and De Boer, R., 1997, The concept of effective stress for soil, concrete and rock, *Geotechnique*, v. 47, n. 1, p. 61-78.

Laird, D.A., 1999, Layer charge influences on the hydration of expandable 2:1 phyllosilicicates, *Clays and Clay Minerals*, v. 47, n. 5, p. 630-636.

Laird, D.A., Shang, C. and Thompson, M.L., 1995, Hysteresis in crystalline swelling of smectites, *Journal of Colloid and Interface Science*, v. 171, p. 240-245.

Lahann, R.W., McCarty, D.K. and Hsieh, J.C.C., 2001, Influence of clay diagenesis on shale velocities and fluid-pressure, Offshore Technology Conference held in Houston, Texas, 30 April – 3 May, 2001, Paper OTC 13046.

Lambe, T. and Whitman, R. 1979, *Soil Mechanics*, SI Version, John Wiley and Sons. P. 53-55.

Lane, R.A. and Macpherson, L.A., 1976, A review of geopressure evaluation from well logs – Louisiana Gulf Coast, *Journal of Petroleum Technology*, September 1976, p. 963-971.

Lang, W.J., 1967, The influence of pressure on the electrical resistivity of clay-water systems, *Proceedings of the 15th National Conference of Clays and Clay Minerals*, Pergamon Press (New York), p. 455-468.

Lauer-Leredde, C., Pezard, P.A., Robert, C. and Dekeyser, I., 1998, Mineralogical association and physical properties of sediments with palaeoclimatic implications (ODP Site 798B, Japan Sea): a comparative study from core and downhole measurements, *Marine Geology*, v. 150, p. 73-98.

Lebedev, K., Mafe, S., Alcaraz, A. and Ramirez, P., 2000, Effects of water dielectric saturation on the space-charge junction of a fixed-charge bipolar membrane, *Chemical Physics Letters*, v. 326, p. 87-92.

Lee, C.Y., McCammon, J.A. and Rossky, P.J., 1984, The structure of liquid water at an extended hydrophobic surface, *Journal of Chemistry Physics*, v. 80, n. 9, p. 4448-4455.

Lee, H.T, 1980, Compressibility and permeability of clay at high pressure, *Master of Science Thesis, Texas A and M University, College Station, Texas*, 142 pages.

Lee, S.H. and Rasaiah, J.C., 1986, Molecular dynamics study of a dipolar fluid between charged plates, *Journal of Chemical Physics*, v. 85, n. 9, p. 5232-5237.

Lele, A.K., Hirve, M.M., Badiger, M.V. and Mashelkar, R.A., 1997, Predictions of bound water content in poly (N-isopropylacrylamide) gel, *Macromolecules*, v. 30, p. 157-159.

Leote de Carvalho, R.J.F. and Skipper, N.T., 2001, Atomistic computer simulation of the clay-fluid interface in colloidal laponite, *Journal of Chemical Physics*, v. 114, n. 8, p. 3727-3733.

Letellier, M., 1998, Freezing D_2O clay gels, *Magnetic Resonance Imaging*, v. 16, n. 5-6, p. 505-510.

Li, D., 2001, Electro-viscous effects on pressure-driven liquid flow in microchannels, *Colloids and Surfaces A: Physicochemical and Engineering Aspects*, v. 195, p. 35-57.

Li, J.-C., and Ross, D.K. and Benham, 1991, Small-angle neutron scattering studies of water and ice in porous Vycor glass, *Journal Applied Cryst*., v. 24, p. 794-802.

Liltorp, K., Jakobsen, K.L., Nielsen, O.F., Ramlov, H. and Westh, P., 2001, Bound water and cryptobiosis: thermodynamic properties of water at biopolymer surfaces, *Zoologischer Anzeiger*, v. 240, no. 3-4, p. 557-562.

Littleton, R., Cody, R., Landreth, J., and Greve, J., 2002, Pre-drill seismic predictions platform (pore pressure, fracture gradient, lithology, and pore fluids) effectively used as a well planning tool by a multi-discipline deepwater operations team, presented at the International Association of Drilling Contractors and the Society of Petroleum Engineers Drilling Conference in Dallas, Texas, 26-28,. Paper IADC/SPE 74487.

Liu L. and Buckley, J.S. 1999, Alteration of wetting of mica surfaces, *Journal of Petroleum Science and Engineering*, v. 24, p. 75-83.

Liu, W.G. and Yao, K.D., 2001, What causes the unfrozen water in polymers: hydrogen bonds between water and polymer chains?, *Polymer*, v. 42, p. 3943-3947.

Lockhart, D.J. And Kim, P.S., 1992, Internal stark effect measurements of the electric field at the amino terminus of an α helix, *Science*, v. 257, Issue 5072, p. 947-951.

Logsdon, S.D. and Laird, D.A., 2002, Dielectric spectra of bound water in hydrated Ca-smectite, *Journal of Non-Crystalline Solids*, v. 305, p. 243-246.

Lomba, R.F.T., Chenevert, M.E. and Sharma, M.M., 2000, The ion-selective membrane behavior of native shales, *Journal of Petroleum Science and Engineering*, v. 25, p. 9-23.

Lomba, R.F.T., Chenevert, M.E. and Sharma, M.M., 2000, The role of osmotic effects in fluid flow through shales, *Journal of Petroleum Science and Engineering*, v. 25, p. 25-35.

Low, P.L, 1980, The swelling of clay: II. Montmorillonites, *Soil Science Society of America Journal*, v. 44, n. 4, p. 667-676.

Lu, J. and Green M.E., 1999, Simulation of water in a small pore: effect of electric field and Density II: Immobilized molecules, *Journal Physical Chemistry B*, v. 103, p. 2776-2780.

Lutenegger, A.J., Cerato, A.B. and Harrington, N., 2003, Some physical and chemical properties of some Piedmont residual soils, *Proceeding of the 12th Panamerican Conference on Soil Mechanics and Geotechnical Engineering and the 39th U.S. Rock Mechanics Symposium*, v. 1, p. 775-782.

Mackenzie, R.C., 1958, Density of water sorbed on montmorillonite, *Nature*, v. 181, p. 334.

Madejova, J., Janek, M., Komadel, P., Hebert, H.-J. and Moog, H.C., 2002, FTIR analyses of water in MX-80 bentonite compacted from high salinity salt solution systems, *Applied Clay Science*, v. 20, p. 255-271.

Madsen, F.T. and Müller-Vonmoos, M., 1985, Swelling pressure calculated from mineralogical properties of a Jurassic Opalinum shale, Switzerland, *Clays and Clay Minerals*, v. 33, n. 6, p. 501-509.

Maftuleac, A., Dranca, I. and Lupascu, T., 2002, Study of interlayer water on the active sites of mineral sorbent, *Journal of Thermal Analysis and Calorimetry*, v. 69, n. 2, p. 589-598.

Magara, K., 1968, Compaction and migration of fluids in Miocene mudstones, Nagaoka plain, Japan, *The American Association of Petroleum Geologists Bulletin*, v. 52, n. 12, p. 2466-2501.

Magara, K., 1986, Porosity-depth relationship during compaction in hydrostatic and non-hydrostatic cases in Thermal Modeling in Sedimentary Basins, *in* Burrus, J. (editor): 1st IFP Exploration Research Conference, Carcans, France, June 3-7, 1985, Editions Technip (Paris), p. 149-172.

Mammar, N., Rosanne, M., Prunet-Foch, B., Thovert, J.-F., Tevissen, E., and Adler, P.M., 2001, Transport properties of compact clays, *Journal of Colloid and Interface Science*, v. 240, p. 498-508.

Manning, G.S., 1996, Counterion condensation theory constructed from different models, *Physica A*, p. 236-253.

Marcial, D., Delage, P. and Cui, Y.J., 2002, On the high stress compression of bentonites, *Canadian Geotechnicial. Journal*, v. 39, p. 812-820.

Martin, R.T., 1960, Water vapor sorption on kaolinite: entropy of adsorption, *in* Ingerson, E. (editor): *Clays and Clay Minerals*, Monograph No. 9, Pergamon Press, London, p. 102-113.

Martin, R.T., 1962, Adsorbed water on clay: a review, in *Clays and Clay Minerals* Monograph No. 2, Pergamon Press, London, p. 28-53.

Martinez, G. and Davis, L.A., 2000, Petrophysical measurements on shales using NMR, *Society of Petroleum Engineers and the American Association of Petroleum Geologists Western Regional Meeting, L*ong Beach, California, 19-23 June 2000, Paper SPE 62851.

Meglis, I. and Schmitt, D.R., 1999, Shale velocities from the western Canadian Basin: Laboratory determinations of elastic properties, *Canadian Society of Economic Geophysicists Annual Meeting*, 1999.

Mello, U.T., Karner, G.D. and Anderson, R.N., 1994, A physical explanation for the positioning of the depth to the top of overpressure in shale-dominated sequences in the Gulf Coast basin, United States, *Journal of Geophysical Research*, v. 99, Issue B2, p. 2775-2790.

Mermut, A.R. and Lagaly, M. G., 2001, Baseline studies of the clay minerals society source clays: Layer-charge determination and characteristics of those minerals containing 2:1 layers, *Clays and Clay Minerals*, v. 49, n. 5, p. 393-397.

Meyer, S., Levitz, P. and Delville, A., 2001, A (N,V,T) Monte Carlo study of the long-range electrostatic coupling between a large collection of charged colloidal platelets, *Journal Physical Chemistry B*, vl 105, p. 9595-9602.

Meziani, M., Zajac, J., Douillard, J.-M., Jones, D.J., Partyka, S. and Roziere, J., 2001, Evaluation of surface enthalpy of porous aluminosilicates of the MCM-41 type using immersional calorimetry: Effect of pore size and framework Si:Al ratio, *Journal of Colloid and Interface Science*, v. 233, p. 219-226.

Miller, R.J. and Low, P.F., 1963, Threshold gradient for water flow in clay systems, *Soil Science Society of America Proceedings*, v. 27, n. 6, p. 605-609.

Miranda, P.D., Xu, L., Shen, Y.R. and Salmeron, M., 1998, Icelike water monolayer adsorbed on mica at room temperature, *Physical Review Letters*, v. 81, n. 26, p. 5876-5879.

Mitchell, J., 1993, *Fundamentals of Soil Behavior*, 2nd Edition, John Wiley and Sons. p. 107-114.

Mohan, K.K. and Fogler, H.S., 1997, Effect of pH and layer charge on formation damage in porous media containing swelling clay, *Langmuir*, v. 13, p. 2863-2872.

Moore, J.C. and Tobin, H., 1997, Estimated fluid pressures of the Barbados accretionary prism and adjacent sediments, Shipley, *in* Ogawa, T.H. and Bahr, J.M. (editors): *Proceedings of the Ocean Drilling Program*, v. 156, p. 229-237.

Morishige, K. and Nobuoka, K., 1997, X-ray diffraction studies of freezing and melting of water confined in a mesoporous adsorbent (MCM-41), *Journal of Chemical Physics*, v. 107, n. 17, p. 6965-6968.

Morishige, K. and Kawano, K., 1999, Freezing and melting of water in a single cylindrical pore: The pore-size dependence of freezing and melting behavior, *Journal of Chemical Physics*, v. 110, n.10, p. 4867-4872.

Mudford, B.S. and Best, M.E., 1989, Venture gas field, offshore Nova Scotia: Case study of overpressuring in region of low sedimentation rate, *The American Association of Petroleum Geologist Bulletin*, v. 73, n. 11, p. 1383-1396.

Muller-Plathe, F., 1998, Different states of water in hydrogels*?, Macromolecules*, v. 31, p. 6721-6723.

Murad, M.A. and Cushman, J.H., 1996, Multiscale flow and deformation in hydrophilic swelling porous media, *International Journal of Engineering Science*, v. 34, n. 3, p. 343-338.

Murad, M.A. and Cushman, J.H., 2000, Thermomechanical theories for swelling porous media with microstructure, *International Journal of Engineering Science*, v. 38, p. 517-564.

Nakamura, M., Endo, O., Ohta, T., Ito, M. and Yoda, Y., 2002, Surface X-ray diffraction study of Cu UPD on Au(111) electrode in 0.5 M H_2SO_4 solution: The coadsorption structure of UPD copper, hydration water molecule and bisulfate anion on Au(111), *Surface Science*, v. 514, p. 227-233.

Neuzil, C.E., 1986, Groundwater flow in low-permeability environments, *Water Resources Research*, v. 22, n. 8, p. 1163-1195.

Neuzil, C.E., 1994, How permeable are clays and shales?, *Water Resources Research*, v. 30, n. 2. p. 145-150.

Neuzil C.E., 2000, Osmotic generation of 'anomalous' fluid pressures in geological environments, *Nature*, v. 403, Issue 6766, p. 182-184.

Newman, A.C.D., 1983, The specific surface of soils determined by water sorption, *Journal of Soil Science*, v. 34, p. 23-32.

Newman. A.C.D., 1987, *Chemistry of Clays and Clay Minerals*, Longman Scientific & Technical, Mineralogical Society, Mineralogical Society Monograph No. 6, p.242.

Odelius, M., Bernasconi, M. and Parrinello, M., 1997, Two dimensional ice adsorbed on mica surface, *Physical Review Letters*, v. 78, n. 14, p. 2855-2858.

Osman, M.A. and Suter, U.W., 2000, Determination of the cation-exchange capacity of muscovite mica, *Journal of Colloid and Interface Science*, v. 224, p. 112-115.

Overloop, K. and Van Gerven, L., 1993, Freezing phenomena in adsorbed water as studied by NMR, *Journal of Magnetic Resonance, Series A*, v. 101, p. 179-187.

Padmanabhan, E. and Mermut, A.R., 1995, The problem of expressing the specific surface areas of clay fractions, *Clays and Clay Minerals*, v. 43, n. 2, p. 237-245.

Palmer, L.S., Cunliffe, A. and Hough, J.M., 1952, Dielectric constant of water films, *Nature*, v. 170, p. 796.

Papelis, C. and Hayes, K.F., 1996, Distinguishing between interlayer and external sorption sites of clay minerals using X-ray absorption spectroscopy, *Colloids and Surfaces A: Physicochemical and Engineering Aspects*, v. 107, p. 89-96.

Park, S.H. and Sposito, G., 2000, Monte Carlo simulation of total radial distribution functions for interlayer water in Li-, Na-, and K-montmorillonite hydrates, *Journal Physical Chemistry B*. v. 104, p. 4642-4648.

Patchett, J.G., 1975, An investigation of shale conductivity, *The Log Analyst*, December-November 1975. p. 3-10.

Pauling, L., 1953, *General Chemistry*, Second Edition, W. H. Freeman and Company, San Francisco and London.

Paunov, V.N., Dimova, R.I., Kralchevski, A., Broze, G. and Mehreteab, A., 1996, The hydration repulsion between charged surfaces as an interplay of volume exclusion and dielectric saturation effects, *Journal of Colloid and Interface Science*, v. 182, p. 239-248.

Peng, C., 2001, 3-D pre-stack depth migration in anisotropic media: A case study at the Lodgepole reef play in North Dakota, *The Leading Edge*, May 2001, p. 524-527.

Pengra, D.B., 1999, Determination of rock properties by low-frequency AC electrokinetics, *Journal of Geophysical Research*. V. 104, n. B12, p. 29,485-29,508.

Peric, D. and Ayari, M.A., 2002, Influence of Lode's angle on the pore pressure generation in soils, *International Journal of Plasticity*, v. 18, p. 1039-1059.

Philen, O.D., Weed, S.B. and Weber, J.B., 1970, Estimation of surface charge density of mica and vermiculite by competitive adsorption of diquat and paraquat, *Soil Science Society of America, Proceedings*, v. 34, p. 527-531.

Philen, O.D., Weed, S.B. and Weber, J.B., 1971, Surface charge characterization of layer silicates by competitive adsorption of two organic divalent cations, *Clays and Clay Minerals*, v. 19, p 295-302.

Pitteloud, C., Powell, D.H., Soper, A.K. and Benmore, C.J., 2000, The structure of interlayer water in Wyoming montmorillonite studied by neutron diffraction with isotopic substitution, *Physica B*, p. 236-237.

Poinsignon, C., 1997, Protonic conductivity and water dynamics in swelling clays, *Solid State Ionics*, v. 97. p. 399-407.

Porter, J.D. and Zinn, A.S., 1993, Ordering of liquid water at metal surfaces in tunnel junction devices, *Journal of Physical Chemistry*, v. 97, p. 1190-1203.

Powell, D.H., Tongkhao, K., Kennedy, S.J. and Slade, P., 1998, Interlayer water structure in Na- and Li-montmorillonite clays, *Physica B.* v. 241, p. 387-389.

Prost, R., Koutit, T., Benchara, A. and Huard, E., 1998, State and location of water adsorbed on clay minerals: consequences of the hydration and swelling-shrinkage phenomena, *Clays and Clay Minerals*, v. 46, n. 2, p. 117-131.

Rao, S.N. and Mathew, P.K., 1995, Effects of exchangeable cations on hydraulic conductivity of a marine clay, *Clays and Clay Minerals*, v. 43, n. 4, p. 433-457.

Rask, J.H., Bryndzia, L.T., Braunsdorf, N.R and Murray, T.E., 1997, Smectite illitization in Pliocene-age Gulf of Mexico mudrocks, *Clays and Clay Minerals*, v. 45, n.1, p. 99-109.

Rasmusson, M., Rowlands, W., O'Brien, R.W., and Hunter, R.J., 1997, The dynamic mobility and dielectric response of sodium bentonite, *Journal of Colloid and Interface Science*, v. 189, p. 92-100.

Raviv, U. and Klein, J., 2001, Fluidity of water-confined to subnanometre films, *Nature*, v. 413, p. 51-54.

Raviv, U. and Klein, J. 2002, Fluidity of bound hydration layers, *Science*, v. 297, p. 1540-1543.

Rempe, S. and Pratt, R., *2001*, The hydration number of Na+ in liquid water, *Fluid Phase Equilibria*, v. 183-184, p. 121-132.

Renard, F. and Ortoleva, P., 1997, Water films at grain-grain contacts: Debye-Huckel, osmotic model of stress, salinity, and mineralogy dependence, *Geochimical et Cosmochimica Acta*, v. 61, n.10, 1963-1970.

Revil, A. and Cathles III, L.M., 1999, Permeability of shaly sands, *Water Resources Research*, V. 35, n. 3, p. 651-662.

Revil, A., Cathles III, L.M. and Losh, S., 1997, Electrical conductivity in shaly sands with geophysical application, *Journal of Geophysical Research*. ???

Revil, A. and Glover, P.W.J., 1997, Theory of ionic-surface electrical conduction in porous media, *Physical Review B*, v. 55, n. 3, p. 1757-1773.

Revil, A., Glover, P.W.J., Pezard, P.A., and Zamora, M., 1999, Electrical conductivity, permeability, streaming potential and electro-osmosis in granular porous media: A unified approach, *Journal of Geophysical Research Solids Earth*, v. 104, no. 9, p. 20,033.

Robinson, D.S., Cooper, J.D. and Gardner, C.M.K., 2002, Modelling the relative permittivity of soils using soil hygroscopic water content, *Journal of Hydrology*, v. 255, p. 39-49.

Rojas, O.J., Ernstsson, M., Neuman, R.D. and Claesson, P.M., 2002, Effect of polyelectrolyte charge density on the adsorption behavior on mica, *Langmuir*, v. 18, p. 1604-1612.

Romero, E. and Lloret, A.G., 1999, Water permeability, water retention and microstructure of unsaturated compacted Boom clay, *Engineering Geology*, v. 544, p. 117-127.

Rough, S.L., Bridgwater, J. and Wilson, D.I., 2002, In situ measurement of porosities and permeabilities of alumina pastes, *Powder Technology*, v. 122, p. 262-274.

Rutter, E.H., 1983, Pressure solution in nature, theory and experiment, *Journal Geological Society of London*, v. 140, p. 725-740.

Saarenketo, T., 1998, Electrical properties of water in clay and silty soils, *Journal of Applied Geophysics*, v. 40, p. 73-88.

Sadek, O.M. and Mekhemer, W.K., 2001, Na-montmorillonite clay as thermal energy storage material, *Thermochimica Acta*, v. 370, p. 57-63.

Salem, H. and Chilingarian, **G.,** 1999, Determination of specific surface area and mean grain size from well-log data and their influence on the physical behavior of offshore reservoirs, *Journal of Petroleum Engineering*, v. 22, p. 241-252.

Sato, T., Murakami, T. and Watanabe, T., 1996, Charge in layers charge of smectites and smectite layers in illite/smectite during diagenetic alteration, *Clays and Clay Minerals*, v. 44, n. 4, p. 460-469.

Schafer, L., Yu C.-H., Newton, S.Q., Norman, M.A., Miller, D.M. and Teppen, B.J., 2000, Molecular dynamics simulations of the sorption of organic compounds at the clay mineral/aqueous solution interface, *European Congress on Computational Methods in Applied Sciences and Engineering*, Barcelona, 11-14 September 2000. 14 pages.

Schlegel, M.L., Nagy, K.L., Fenter, P., Cheng, L. and Sturchio, N.C., 2001, X-ray reflectivity of the muscovite-water interface in $CaCl_2$ and $BaCl_2$ solutions: Mechanism of cation sorption, 11th Annual V.M. Goldschmidt Conference, 2001.

Schmidt, R., Hansen, E.W., Stöcker, M., Akporiaye, D. and Ellestad, O.H., 1995, Pore size determination of MCM-41 mesoporous material by means of ^{1}H NMR, N_2 adsorption, and HREM: a preliminary study, *Journal of American Chemistry Society*, v. 117, p. 4049-4056.

Schlömer, S. and Krooss, B.M., 1997, Experimental characterisation of the hydrocarbon sealing efficiency of cap rocks, *Marine and Petroleum Geology*, v. 14, n. 5, p. 565-580.

Schmitz, K.S., 1999, Distribution of water and counterions in vermiculite clays, *Journal Physical Chemistry B*, v. 103. p. 8882-8887.

Schneider, F., Bouteca, M. and Vasseur, G., 1994, Validity of the porosity/effective-stress concept in sedimentary basin modelling, *First Break*, v. 12, n. 6, p. 321-325.

Schofield, R.K., 1947, Calculation of surface areas from measurements of negative adsorption, *Nature*, v. 160, p. 408410.

Schulz, J. and Warr, **G.G.,** 2000, Adsorbed layer structure of cationic surfactants on clays (mica is NOT a typical substrate for adsorption studies), *Langmuir*, v. 16, p. 2995-2996.

Schwartz, L.M., Sen, P.N. and Johnston, D.L., 1989, Influence of rough surfaces on electrolytic conduction in porous media, *Physical Review B*, v. 40, n. 4, p. 24502458.

Schweighofer, K.J., Xia, X. and Berkowitz, M.L., 1996, Molecular dynamics study of water next to electrified Ag(111) surfaces, *Langmuir*, v. 12, no. 12, p. 3747-3752.

Scott D. and Thomsen, L.A., 1993, A Global algorithm for pore pressure prediction, *Society of Petroleum Engineers Middle Eas Oil Technical and Exhibition in Bahrain*, 3-6 April 1993, Paper SPE 25674, p. 645-653.

Sen, P.N., 1989, Influence of microgeometry on membrane potential of shale sands, *Geophysics*, v. 54, n. 12, p. 1543-1553.

Sen, P.N. and Goode, P.A., 1992, Influence of temperature on electrical conductivity in shaly sands, *Geophysics*, v. 57, n. 1, p. 89-96.

Sen, P.N., Straley, C., Kenyon, W.E. and Whittingham, M.S., 1990, Surface-to-volume ratio, charge density, nuclear magnetic relaxation, and permeability in clay-bearing sandstones, *Geophysics*, v. 55, n. 1, p. 61-69.

Senapati, S. and Chandra, A., 1998, Computer simulations of dipolar liquids near charged solid surfaces: electric-field-induced modifications of structure and dynamics of interfacial solvent, *Journal of Molecular Structure (Theochem),* v. 455, p. 1-8.

Senapati, S. and Chandra, A., 2000, Surface charge induced modification of the structure and dynamics of mixed dipolar liquids at solid-liquid interfaces: A molecular dynamics simulation study, *Journal of Chemical Physics*, v. 113, n. 19, p. 8817-8826.

Shainberg, I., Alperovitch, N.I. and Keren, R., 1987, Charge density and Na-K-Ca exchange on smectites, *Clays and Clay Minerals*, v. 35, n. 1, p. 68-73.

Shapovalov, V., Truong, T.N., Kovalenko, A. and Hirata, F., 2000, Liquid structure at metal oxide – water interface: Accuracy of a three-dimensional RISM methodology, *Chemical Physics Letters*, v. 320, p. 186-193.

Shelley, J.C., Patey, G.N., Bérard, D.R. and Torrie, G.M., 1997, Modeling and structure of mercury-water interfaces, Journal Chemical Physics, n. 8, p. 2122-2141.

Sherwood, J.D., 1994, Model for the flow of water and ions into swelling shale, *Langmuir,* v. 10, Issue 7, p. 2480-2486.

Sherwood, J.D., 1995, Ionic transport in swelling shale, *Advances in Colloid and Interface Science*, v. 61, p. 51-64.

Shi Y. and Wang C.-Y., 1986, Pore pressure generation in sedimentary basins: overloading versus aquathermal, *Journal of Geophysical Research*, v. 91. p. 2153-2162.

Shubin, V.E., Hunter, R.J. and O'Brien, R.W., *1993,* Electroacoustic and dielectric study of surface conduction, *Journal of Colloid and Interface Science*, v. 159, p. 174-183.

Sigal, R., 2002a, Coates and SDR permeability: Two variations on the same theme, *Petrophysics*, v. 43, n. 1, p. 38-46.

Sigal, R., 2002b, The pressure dependence of permeability, *Petrophysics*, v. 43, n. 2, p. 92-102.

Singh, R.R.B., Rao, K.H., Anjaneyulu, A.S.R. and Patil, **G.R.,** 2001, Moisture sorption properties of smoked chicken sausages from spent hen meat, *Food Research International*, v. 34, p. 143-148.

Skipper, N.T., 1995, Monte Carlo simulation of interlayer molecular structure in swelling clay minerals. 2. Monolayer hydrates, *Clays and Clay Minerals*, v. 43, n. 3, p. 294-303.

Skipper, N.T., Chang, F-R.,C. and Sposito, G., 1995, Monte Carlo simulation of interlayer molecular structure in swelling clay minerals. 1. Methodology, *Clays and Clay Minerals*, v. 43, n. 3, p. 285-293.

Skipper, N.T., Smalley, M.V., Williams, G.D., Soper, A.K. and Thompson, C.H., 1995, Direct measurement of the electric double-layer structure in hydrated lithium vermiculite clays by neutron diffraction, *Journal of Physical Chemistry*, v. 99, n. 39, p. 14,201-14,204

Skipper, N.T., Refson, K. and McConnell D.C, 1991, Computer simulation of interlayer water in 2:1 clays, *Journal of Chemical Physics*, v. 94, n. 11, p. 7434-7445.

Skipper, N.T., Soper, A.K. and McConnell, D.C., 1991,The structure of interlayer water in vermiculite, *Journal of Chemical Physics*, v. 94, n. 8, p. 5751-5760.

Skipper, N.T., Soper, A.K. and Smalley, M.V., 1994, Neutron diffraction study of calcium vermiculite: Hydration of calcium ions in a confined environment, *Journal Physical Chemistry*, v. 98, n. 3, p. 942-945.

Skipper, N.T., Williams, G.D., de Siqueira, A.V.C., Lobban, C. and Soper, A.K., 2000, Time-of-flight neutron diffraction studies of clay-fluid interactions under basin conditions, *Clay Minerals*, v. 35, p. 283-290.

Sliwinska-Bartkowiak, M., Dudzisak, G., Sikorski, R., Gras, R., Radhakrishnan, R. and Gubbins, K.E., 2001, Melting/freezing behavior of a fluid confined in porous glasses and MCM-41: Dielectric spectroscopy and molecular simulation, *Journal of Chemical Physics*, v. 114, n. 2, p. 950-961.

Smirnov, K.S. and Bougeard, D., 1999, A molecular dynamics study of structure and short-time dynamics of water in kaolinite, *Journal of Physical Chemistry B*, v. 103, p. 5266-5273.

Smith, J.E., 1973, Shale Compaction, *Society of Petroleum Engineers Journal*, February 1973, p. 12-22.

Smith, G.N. and Smith I.G.N., 1998, *Elements of Soil Mechanics – Seventh Edition*, Blackwell Science, Oxford.

Sokhan, V.P., Nicholson, D. and Quirke, N., 2001, Fluid flow in nanopores: An examination of hydrodynamic boundary conditions, *Journal of Chemical Physics*, v. 115, n. 8, p. 3878-3887.

Spohr, E., 2002, Molecular dynamics simulations of water and ion dynamics in the electrochemical double layer, *Solid State Ionics*, v. 150, p. 1-12.

Sposito, G., 1998, On points of zero charge, *Environmental Science and Technology*, v. 32, n. 19, p. 2815-2819.

Sridharan, A., Abraham, B.M. and Jose, B.T., 1991, Improved technique for estimation of preconsolidation pressure, *Geotechnique*, v. 41, n. 2, p. 263-268.

Stapf, S. and Kimmich, R., 1995, Molecular dynamics in confined monomolecular layers. A field-cycling nuclear magnetic resonance relaxometry study of liquids in porous glass, *Journal of Chemical Physics*, v. 103, n. 6, p. 2247-2250.

Street, N., 1961, Electrokinetics III. – Surface conductance and the conductive solids effect, *Illinois State Geological Survey*, Urbana, Illinois, Circular 315.

Stucki, J.W. and Roth, C.B., 1977, Oxidation-reduction mechanism for structural iron in nontronite, *Soil Science Society of American Journal*, v. 41, p. 808-813.

Sultan, N., Delage, P. and Cui, Y.J., 2002, Temperature effects on the volume change behaviour of Boom clay, *Engineering Geology*, Uncorrected Proof.

Stump, B.B. and Flemings, P.B., 2002, Consolidation State, Permeability, and Stress Ratio as Determined from Uniaxial Experiments on Mud Samples from the Eugene Island 330 Area, Offshore Louisiana, *in* Huffman, A.R. and Bowers, G.L. (editors): *Pressure Regimes in Sedimentary Basins and Their Prediction: The American Association of Petroleum Geologists Memoir 76*, p. 131-144.

Sutmann, G., 1998, Structure formation and dynamics of water in strong external electric fields, *Journal of Electroanalytical Chemistry*, v. 450, p. 289-302.

Sutton, R. and Sposito, G., 2001, Molecular Simulation of interlayer structure and dynamics in 12.4 A Cs-Smectite hydrates, *Journal of Colloid and Interface Science*, v. 237, p. 174-184.

Svergun, D.I., Richard, S., Koch, M., H.J., Sayers, Z., Kuprin, S. and Zaccai, G., 1998, Protein hydration in solution: Experimental observation by x-ray and neutron scattering, *Proc. Natl. Acad. Sci. USA*, Biophysics, v. 95,p. 2267-2272.

Svishchev, I.M. and Kusalik, P. G., 1994, Crystallization of liquid water in a molecular dynamics simulation, *Physical Review Letters*, v. 73, n. 7, p. 975-978.

Swanson, B.F., 1981, A simple correlation between permeabilities and mercury capillary pressures, *Journal of Petroleum Technology*, December 1981, p. 2498-2504.

Swarbrick, R.E., Osborne, M.J. and Yardley, G.S., 2002, Comparison of Overpressure Magnitude Resulting from the Main Generating Mechanisms, *in* Huffman,

A.R. and Bowers, G.L. (editors): *Pressure Regimes in Sedimentary Basins and Their Prediction: The American Association of Petroleum Geologists Memoir 76*, p. 1-12.

Swenson, J., Bergman, R. and Howells, W.S., 2000, Quasi-elastic neutron scattering of two-dimensional water in a vermiculite clay, *Journal of Chemical Physics*, v. 113, n. 7, p. 2873-2879.

Swenson, J., Bergman, R. and Longeville, S., 2002, Experimental support for a dynamic transition of confined water, *Journal of Non-Crystaline Solids*, v. 307-310, p. 573-578.

Swenson, J., Bergman, R., Longeville, S. and Howells, W.S., 2001, Dynamics of 2D-water as studied by quasi-elastic neutron scattering and neutron resonance spin-echo, *Physica B*, v. 301, p. 28-34.

Swenson, J., Smalley, M.V., Thomas, R.K. and Crawford, R.J., 1998, Uniaxial stress and sol concentration dependence of the structure of a dressed macroion in a dilute electrolyte solution, *Journal Physical Chemistry B*, v. 102, p. 5823-5829.

Swenson, J., Smalley, M.V., Thomas, R.K., Crawford, R.J. and Braganza, L.F., 1997, Intermediate interlayer structure in butylammonium vermiculites, *Langmuir*, v. 13, p. 6654-6657.

Takamuku, T., Yamagami, M., Wakita, H., Masuda, Y. and Yamaguchi, T., 1997, Thermal property, structure, and dynamics of supercooled water in porous silica by calorimetry, neutron scattering, and NMR relaxation, *Journal Physical Chemistry B*, v. 101, p. 5730-5739.

Tang, Z., Scriven, L.E. and Davis, H.T., 1992, A three-component model of the electrical double layer, *Journal Chemical Physics*, v. 97, n. 1, p. 494-503.

Tao, R., Woestman, J.T. and Jaggi, N.K., 1989, Electric field induced solidification, *Applied Physics Letters*, v. 55, n. 18, p. 1844-1946.

Teew, D., 1971, Prediction of formation compaction from laboratory compressibility data, *Society of Petroleum Engineers Journal*, September 1971, p. 263-271.

Teige, G.M.G., Hermanrud, C., Wensaas, L. and Norgård Bolås, H.M., 1999, The lack of relationship between overpressure and porosity in North Sea and Haltenbanken shales**,** *Marine and Petroleum Geology*, v. 16, Issue 4, p. 321-335.

Teppen, B.J., Rasmussen, K., Bertsch, P.M., Miller, D.M. and Shafer, L., 1997, Molecular Dynamics modelling of clay minerals. 1. Gibbsite, kaolinite, pyrophyllite, and beidellite, *Journal Physical Chemistry B*, v. 101, p. 1579-1587.

Teschke, O., Ceotto, G. and de Souza, E.F., 2001, Rupture force of adsorbed self-assembled surfactant layers effect of the dielectric exchange force, *Chemical Physics Letters*, v. 344, p. 429-433.

Thompson, L.J., Chen, R.H. and Bryant, W.R., 1977, Overpressured Marine Sediments, *Texas A and M University Research Foundation*, Project Number 3249, College Station, Texas, 91 pages.

Thompson, P.A. and Grest, G.S., 1992, Phase transitions and universal dynamics in confined films, *Physical Review Letters*, v. 68, n. 23, p. 3448-3451.

Thompson, P.A. and Robbins, M.O., 1990, Shear flow near solids: Epitaxial order and flow boundary conditions, *Physical Review A*, v. 41, n. 12, 6830-6837.

Tiab, D. and Donaldson, E.C., 1996, Petrophysics: Theory and Practice of Measuring Reservoir Rock and Fluid Transport Properties, *Gulf Publishing Company*, Houston, Texas.

Titiloye, J.O. and Skipper, N.T., 2000, Computer simulation of the structure and dynamics of methane in hydrated Na-smectite clay, *Chemical Physics Letters*, v. 329, p. 23-28.

Titiloye, J.O. and Skipper, N.T., 2001, Molecular dynamics simulation of methane in sodium montmorillonite clay hydrates at elevated pressures and temperatures, *Molecular Physics*, v. 99, n. 10, p. 899-906.

Tittman, W., 1965, Physical fundamentals of formation density logging (Gamma Gamma), *Geophysics*, n. 2, p. 284-294.

Toney, M.F., Howard, J.N., Richer, J., Borges, G.L., Gordon, J.G., Melroy, O.R., Wiesler, D.G., Yee, D. and Sorensen, L.B., 1994, Voltage-dependent ordering of water molecules at an electrode-electrolyte interface, *Nature*, v. 368, p. 444-446.

Toney, M.F., Howard, J.N., Richer, J., Borges, G.L., Gordon, J.G., Melroy, O.R., Wiesler, D.G., Yee, D. and Sorensen, L.B., 1995, Distribution of water molecules at Ag(111)/ electrolyte interface as studied with surface X-ray scattering, *Surface Science*, v. 335, p. 326-332.

Tosaya, C. and Nur, A., 1982, Effects of diagenesis and clays on compressional velocities in rocks, *Geophysical Research Letters*, v. 9, n. 1, p. 5-8.

Traugott, M., 1982, Rock mechanics, petrophysics, and stratigraphy of the Tuscaloosa trend, *Journal of Petroleum Technology*, February 1982.

Traugott, M., 1997, Pore/fracture pressure determinations in deep water, Deepwater Technology supplement to *World Oil*, August 1997, p. 68-70.

Traugott, M. and Swarbrick, R., 2002, Dimensionless Gradients Applied to Pore Pressure Prediction – A New Standard, *Recorder, Canadian Society of Exploration Geophysics*, September, p. 7980.

Travis, K.P., Todd, B.D and Evans, D.J., 1997, Departure from Navier-Stokes hydrodynamics in confined liquids, *Physical Review E*, v. 55, n. 4, p. 4288-4295.

Travis, K.P. and Gubbins, K.E., 2000, Poiseuille flow of Lennard-Jones fluids in narrow slit pores, *Journal of Chemical Physics*, v. 112, n. 4, p. 1984-1994.

Trimmer, D., 1980, Effect of Pressure and Stress on Water Transport in Intact and Fractured Gabbro and Granite, *Journal of Geophysical Research*, v. 85, p. 7059-7071.

Truman, R.B., Howard, W.E. and Luffel, D.L., 1989, Shale Porosity – Its impact on well log modelling and interpretation, *Society of Professional Well Analysts 30th Annual Logging Symposium*, 11-14 June 1989, paper Q.

Turov, V.V., Chodorowski, S., Leboda, R., Skubiszewska-Zieba, J., and Brei, V.V., 1999, Thermogravimetric and ^{1}H NMR spectroscopy studies of water on silicalites, *Colloids and Surfaces A: Physicochemical and Engineering Aspects*, v. 158, p. 363-373.

Turov, V.V. and Leboda, R., 1999, Application of ^{1}H NMR spectroscopy method for determination of characteristic of thin layers of water adsorbed on the surface of dispersed and porous adsorbents, *Advances in Colloid Interface Science*, v. 79, p. 173-211.

Uffindell, C.H., Kolesnikov, A.I., Li, J-C. and Mayers, J., 2000, Inelastic neutron scattering study of water in the sub- and supercritical region, *Physica B*, v. 276/278, p. 444-445.

Valckenborg, R.M.E., Pel, L. and Kopinga, K., 2001, NMR relaxation and diffusion measurements on iron(III)-doped kaolin clay, *Journal of Magnetic Resonance*, v. 151, p. 291-297.

van Alsten, J. and Granick, S., 1988, Molecular tribometry of ultrathin liquid films, *Physical Review Letters*, v. 61, n. 22, p. 2570-2573.

van Olphen, H., 1963, Compaction of clay sediments in the range of molecular particle distances, *in* Bradley, W.F. (editor): Clays and Clay Minerals Proceedings of the 11th National Conference on Clays and Clay Minerals, Ottawa, Ontario, Canada, August 13-17, 1962, Pergamon Press, Oxford, p. 178-187.

van Olphen, H and Fripial, J., 1979, Data Handbook for Clay Materials and Non-Metallic Minerals, *Pergamon Press*, New York. 346pp.

Vasseur, G. Djeran-Maigre, I., Grunberber, D., Rousset, G., Tessier, D. and Velde, B., 1995, Evolution of structural parameters of clays during experimental compaction, *Marine and Petroleum Geology*, v. 12, n. 8, p. 941-954.

Vernik, L., 1998, Acoustic velocity and porosity systematics in siliciclastics, *The Log Analyst*, July-August 1998, p. 27-35.

Vernik, L. and Liu, X., 1997, Velocity anisotropy in shales: A petrophysical study, *Geophysics*, v. 62, n. 2, p. 521-532.

Vigil, G., Xu, Z., Steinberg, S. and Israelachvili, J., 1994, Interactions of silica surfaces, *Journal of Colloid and Interface Science*, v. 165, p. 367-385.

Vinegar, H.J. and Waxman, M.H., 1984, Induced polarization of shaly sands, *Geophysics*, v. 49, n. 8, p. 1267-1287.

Wallacher, D. and Knorr, K., 2001, Melting and freezing of Ar in nanopores, *Physical Review B*, v. 63, Issue 10, 9 pages.

Wang, F., Chen, J., Chen, J. and Forsling, W., 1997, Surface properties of natural aquatic sediments, *Water Resources*, v. 31, n. 7, p. 1796-1800.

Wang, P. and Anderko, A., 2001, Computation of dielectric constants of solvent mixtures and electrolyte solutions, *Fluid Phase Equilibria*, v. 186, p. 103-122.

Wangen, M., 2000, Generation of overpressure by cementation of pore space in sedimentary rocks, *Geophysical Journal International*, v. 143, p. 608-620.

Warne, M.R., Allan, N.L. and Cosgrove, T., 2000, Computer simulation of water molecules at kaolinite and silica surfaces, Published on the Web 25th July, 2000.

Watanabe, M., Brodsky, A.M. and Reinhardt, W.P., 1991, Dielectric properties and phase transitions of water between conducting plates, *Journal of Physical Chemistry*, v. 95, p. 4593-4596.

Watanabe, K. and Mizoguchi, M., 2002, Amount of unfrozen water in frozen porous media saturated with solution, *Cold Regions Science and Technology*, v. 34, p. 103-110.

Waxman, M.H. and Smits, L.J.M., 1968, Electrical conductivities in oil-bearing shaly sands, *Society of Petroleum Engineers Journal*, June 1968, p. 107-122.

Waxman, M.H. and Thomas, E.C., 1974, Electrical Conductivities in shaly sands. II. The temperature coefficient of electrical conductivity. *Journal of Petroleum Technology*, February, 1974, p. 213-225.

Whitworth, T.M. and Gu, C., 2001, Hyperfiltration-induced precipitation of sodium chloride, Technical Report 01423959, Departmental of Environmental Engineering, New Mexico Tech, USA.

Williams, G.D., Soper, A.K., Skipper, N.T. and Smalley, M.V., 1998, High-resolution structural study of an electrical double layer by neutron diffraction, *Physical Chemistry B*, v. 102, n. 45, p. 8945-8949.

Withers, A., Kohn, S.C., Brooker, R.A. and Wood, B.J., 2000, A new method for determining the P.V.T properties of high-density H_2O using NMR: Results at 1.4 – 4 Gpa and 700-1100 C, *Geochimica et Cosmochimica Acta*, v. 64, n. 6, p. 1051-1057.

Woelki, S. and Kohler, H-H., 2000, A modified Poisson-Boltzmann equation II. Models and solutions, *Chemical Physics*, v. 261, p. 421-438.

Wojtanowicz, A.K., Bourgoyne Jr., A.T., Zhou, D. and Bender, K., 2000, Strength and fracture gradients for shallow marine sediments, Submitted to US Department of Interior, Minerals Management Service, 108 pages.

Wolf, A.V., Brown, M.G. and Prentiss, P.G., 1985, Concentrative Properties of Aqueous Solutions, *in* Weast, R.C. (editor): *CRC Handbook of Chemistry*, 66, CRC Press, Inc., Boca Raton, Florida, U.S.A., p. 219.

Wong, R.C.K. and Wang, E.Z., 1997, Three-dimensional anisotropic swelling model for clay shale – a fabric approach, *International Journal Rock Mechanics Minerals Science*, v. 34, n. 2, p. 187-198.

Wu, C.C., Huang, C. and Lee, D.J., 1997, Effects of polymer dosage on alum sludge dewatering charactertics and physical properties, *Colloids and Surfaces A: Physicochemical and Engineering Aspects*, v. 122, p. 89-96.

Xia, X. and Berkowitz M.L., 1995, Electric-field induced restructuring of water at a platinum-water interface: A molecular dynamics computer simulation, *Physical Review Letters*, v. 74, n. 16. p. 3193-3196.

Yan, L., Low, P.F., and Roth, C.B., 1996, Swelling pressure of montmorillonite layers versus H-O-H bending frequency of the interlayer water, *Clays and Clay Minerals*, v. 44, n. 67, p. 749-756.

Yan, L., Roth, C. and Low, P.F., 1996, Effects of monovalent, exchangeable cations and electrolytes on the infrared vibrations of smectite layers and interlayer water, *Journal of Colloid and Interface Science*, v. 184, p. 663-670.

Yan, L. and Stucki, J., 1999, Effects of structural Fe oxidation state on the coupling of interlayer water and structural Si-O stretching vibrations in montmorillonite, *Langmuir*, v. 15, p. 4648-4657.

Yang, C. and Li, D., 1997, Electrokinetic effects on pressure-driven flows in rectangular micochannels, *Journal of Colloid and Interface Science*, v. 194, v. 1.

Yang, Y. and Aplin, A.C., 1998, Influence of lithology and compaction on the pore size distribution and modelled permeability of some mudstones from the Norwegian margin, *Marine and Petroleum Geology*, v. 15, p. 163-175.

Yang, Y., Aplin, A.C, and Larter, S.R., 2002, Quantification, Permeability and Compaction of Mudstones: Some Applications to Basin Modelling and Pore Pressure Estimation, *American Association of Petroleum Geologists Annual Meeting,* March 10-13, 2002, Houston, Texas.

Yeh, I-C. and Berkowitz, M.L. 1998, Structure and dynamics of water at water|Pt interface as seen by molecular dynamics computer simulations, *Journal of Electroanalytical Chemistry*, v. 450, p. 313-325.

Yeh, I-C. and Berkowitz, M.L., 1999a, Aqueous solution near charged Ag(111) surfaces: comparison between a computer simulation and experiment, *Chemical Physics Letters*, v. 301. p. 81-86.

Yeh, I-C. and Berkowitz, M.L., 1999b, Dielectric constant of water at high electric fields: Molecular dynamics study, *Journal of Chemical Physics*, v. 110, n. 16., p. 7935-7942.

Yeh, I-C. and Berkowitz, M.L., 2000, Effects of the polarizability and water density constraint on the structure of water near charged surfaces: Molecular dynamics simulations, Journal of Chemical Physics, v. 112, n. 23, p. 10,491-10,495.

Yen, P.S. and Lee, D.J., 2001, Errors in bound water measurements using centrifugal settling method, *Water Resources*, v. 35, n. 16, p. 4004-4009.

Yu, C-J., Richter, A.G., Kmetko, J., Dugan, S.W., Datta, A. and Dutta, P., 2001, Structure of interfacial liquids: X-ray scattering studies, *Physical Review E*, v. 63, 8 pages.

Zhmud, B.V., Sonnefeld, J. and House, W.A., 1997, Role of ion hydration in the charge regulation at the surface of porous silica gel, *Journal Chemical Society, Faraday Transactions*, v. 93, n. 17, p. 3129-3136.

Zhu, Y. and Granick, S., 2001, Viscosity of interfacial water, *Physical Review Letters*, v. 87, n. 9, p. 4 pages.

Zou, Y., 1996, A non-linear permeability relation depending on the activation energy of pore liquid, *Geotechnique*, v. 46, n. 4, p. 769-774.

Appendix: Total Surface Area Determination

(from Cerato, A.B. and Lutenegger, A.J., 2002, Determination of surface area of fine-grained soils by the ethylene glycol monoethyl ether (EGME) method, Geotechnical Testing Journal, v. 25, n. 3, paper ID# GTJ200210035_253.)

Place about 1 g of crushed oven-dried sample passing a #40 sieve in the bottom of a clean, dry aluminum or glass tare having dimensions of approximately 76 mm in diameter by 20 mm in height. Determine the mass of the soil to the nearest 0.001 g.

Using a small pipette, gently place approximately 3 mL of laboratory grade EGME over the soil. Gently mix the soil and EGME together using a slow swirling motion of the hand until the mixture forms a slurry and the appearance of the slurry is uniform. It is important not to place a stirrer in the mixture, as any loss of soil would directly affect the surface area measurement. Swirling the mixture in the aluminum tare with a circular hand motion allows for no soil loss and a uniform coverage of all soil particles by the EGME.

Place the tare into a vacuum desiccator and place a small plexiglass lid over the tare, leaving a gap of 2–3 mm between the lid and the tare. Attach the lid of the desiccator to a vacuum pump and begin evacuating using a vacuum of at least 635 mm Hg. After 8 to 10 hours, remove the tare and determine the mass of the soil/EGME mixture. Repeat this step again at approximately 18 hours and again at 24 hours. The weight of the mixture should not vary more than 0.001 g. If it does, place the tare back in the desiccator and weigh it again in approximately 4 h.

Calculate SSA as $W_a/(0.000286 \times W_s)$ where

SSA = specific surface area in m^2/g

W_a = weight EGME retained by the sample in grams (final slurry weight – W_s)

0.000286 = weight of EGME required to form a monomolecular layer on a square meter of surface (g/m^2)

W_s = weight of soil added initially (g)

Example:
Initial Tin Weight: 30.0485 g
Initial Soil Weight (Ws): 1.0030 g
18 h tare + slurry weight: 31.0634 g
18 h slurry weight: 31.0634 – 30.0485 = 1.0149 g
24 h tare + slurry weight: 31.0625 g
24 h slurry weight: 31.0625 – 30.0485 = 1.014 g
$W_s = 1.014 – 1.0030 = 0.011$ g
$SSA = 0.011/(1.0030 \times 0.000286) = 38\ m^2/g$